ELOFF, C C

ADSORPTION MECHANISM OF ORGANO-S-COMPOUNDS ON
ACTIVATED CARBON IMPREGNATED INTO TEXTILES

PhD   UP   1998

Adsorption mechanism of organo-S-compounds on activated carbon impregnated into textiles

by

CORNELIA C. ELOFF

Adsorption mechanism of organo-S-compounds on activated carbon impregnated into textiles

by

Cornelia Carolina Eloff

A thesis submitted in partial fulfilment of the prerequisites for the degree

DOCTOR IN PHILOSOPHY

in the Faculty of Science

University of Pretoria

Pretoria

April 1998

Declaration

I hereby declare that this thesis which is submitted for the degree of Doctor Philosophiae at the University of Pretoria, has not been submitted for a degree at any other University and that it is my own work.

<div style="text-align: right;">

CC Eloff (signature)

CC ELOFF

</div>

ACKNOWLEDGEMENTS

I wish to express my sincere thanks and appreciation to Professor J F van Staden for his patience, encouragement and friendliness throughout this study.

Special thanks are extended to Mrs Melissa Papenfus for her valuable assistance with the experimental work.

I am also grateful to Dr P Harris for his valuable discussion and review of this work.

ii

SAMEVATTING

"Adsorption mechanism of organo-S-compounds on activated carbon impregnated into textiles" deur Cornelia Carolina Eloff, voorberei onder leiding van professor JF van Staden van die Departement Chemie, voorgelê ter gedeeltelike vervulling van die vereistes vir die graad Doctor Philosophiae in Chemie.

Die beskermingstyd van 'n koolstofbevattende tekstiel teen bis(2-chloro-etiel)sulfied (HD) word as enigste kriterium vir aanskaffing vir militêre aanwending gebruik. 'n Alternatiewe metode is ondersoek om tussen tekstiele wat gebruik word vir die vervaardiging van beskermingsklerasie te onderskei.

Die dinamiese toetsmetode is gebruik vir die deurbreekbepalings. Drie verskillende tekstiele is gebruik in die studie: poli-uretaanskuimrubber wat met geaktiveerde koolstofpoeier geïmpregneer is (PUCP), geaktiveerde koolstofpoeier (CC), en geaktiveerde koolstofsfere wat met binders aan 'n geweefde tekstiel geheg is (C-spheres).

Die aktiewe oppervlak en mikroporievolume van die CC was die kleinste (152 m^2/g en 0.0577 cm^3/g), gevolg deur PUCP (334 m^2/g en 0.1444 cm^3/g) en die C-spheres (383 m^2/g en 0.1716 cm^3 /g). Die CC het 'n verspreiding van porieë in die mikro- en mesoporiegebied getoon, terwyl die PUCP en C-spheres 'n klein verspreiding van porieë slegs in die mikroporiegebied getoon het.

Die adsorpsiesnelheidskonstante van HD, bereken met die Wheeler-, Yoon en Nelson- en Ackleyvergelykings vir die CC, was groter as dié bereken vir die PUCP en C-spheres. Dit kan aan die klein koolstofpartikel en gevolglik aan die kort afstand wat deur die HD-dampmolekule afgelê word om die mikroporie te bereik waar adsorpsie plaasvind asook die oop mesoporiestruktuur van die CC toegeskryf word. Die klein adsorpsiesnelheidskonstante van die PUCP en die C-spheres kan moontlik aan die groot partikeldiameter en klein mikroporieë toegeskryf word. Die

adsorpsiesnelheidskonstante het afgeneem met toenemende blootstellingskonsentrasie en -temperatuur.

Die adsorpsiekapasiteit van die CC vir HD-dampadsorpsie by 40°C en 0.5 cm/s het as funksie van HD-konsentrasie toegeneem. Die adsorpsiekapasiteit van die PUCP en C-spheres-tekstiele het nie verskil oor die blootstellingskonsentrasiegebied waaroor geëvalueer is nie.

Die resultate wat verkry is met die berekening van die persentasie van die residensietyd (τ) wat gebruik word vir adsorpsie van HD, het die waardes van die snelheidskonstantes bevestig.

Die karakteristieke vorm van die grafieke van die deurbreekresultate, na verwerking met Fick se diffusiewet, het daarop gedui dat hitteoordrag die transport van HD-damp na die koolstof beheer. Die diffusiekoëffisiënte, D_1 en D_2 is uit die twee hellings van die grafiek bereken. D_1 was baie klein, ongeveer 10^{-13} cm^2/s, wat gedui het op isotermiese diffusie wat die adsorpsieproses beheer. D_2 was groter, ongeveer 10^{-8} cm^2/s, wat daarop dui dat hitteoordrag- en/of interpartikeldiffusie die adsorpsieproses beheer.

Isotermiese diffusie in die CC kan toegeskryf word aan die relatiewe groot porieë waarin adsorpsie stadig plaasvind. Die PUCP en die C-spheres het 'n groter koolstofmassa (relatief tot die CC) wat 'n groter hittekapasiteit het. Die hitte-oordragkoëffisiënt is dus groter wat op isotermiese diffusie dui. In kleiner partikels (soos CC en PUCP) speel hitte-effekte 'n toenemende rol en was daar aansienlike afwykings van die isotermiese diffusie.

Die D_1 en D_2 vir die C-spheres was 'n faktor 100 en 1000 groter as die waardes vir die CC en die PUCP, onderskeidelik. Beide D_1 en D_2 het vir die CC, PUCP en C-spheres, met 'n toenemende HD-konsentrasie, toegeneem, wat op 'n hoë oppervlakmigrasie en 'n lae adsorpsie-energie gedui het. D_1 en D_2 vir die PUCP het met toenemende temperatuur toegeneem, wat op 'n toename in die sprongfrekwensie van die HD-

iv

molekuul gedui het.

Uit die studie volg dat die "ideale" koolstof vir tekstielimpregnering 'n groot aktiewe oppervlak (400 - 500 m²/g) vir 'n hoë kapasiteit, 'n porieverspreiding wat mesoporieë (20 - 24 Å) insluit en 'n koolstofpartikel kleiner as 30 μm vir 'n hoë snelheidskontante moet toon.

'n Metode is ontwikkel waarmee tekstiele wat geaktiveerde koolstof bevat, en vir die vervaardiging van beskermende klerasie gebruik word, anders gekarakteriseer kan word as slegs deur die beskermingstyd te bepaal.

SYNOPSIS

"Adsorption mechanism of organo-S-compounds on activated carbon impregnated into textiles" by Cornelia Carolina Eloff, prepared under the guidance of Professor JF van Staden of the Department of Chemistry, as partial fulfilment of the requirement for the degree Doctor Philosophiae in Chemistry.

Protection time against bis(2-chloroethyl)sulfide (HD) vapour penetration is used as the only criterion for procurement of protective clothing against chemical agents for military use. An alternative method was investigated to differentiate between textiles used for the manufacture of protective clothing.

The dynamic test method was used for the breakthrough measurements. Three different textile technologies were used for this study: polyurethane foam rubber impregnated with charcoal powder (PUCP), activated carbon powder (CC), and activated carbon spheres bonded to a woven textile by binder (C-spheres).

The active surface area and micropore volume of the CC were the smallest (152 m^2/g and 0.0577 cm^3/g), followed by the PUCP (330 m^2/g and 0.1444 cm^3/g) and the C-spheres (383 m^2/g and 0.1716 cm^3/g). The CC displayed a distribution of pores in the micro- and mesopore range, while the PUCP and the C-spheres showed a narrow distribution containing mainly micropores.

The rate constant calculated with the Wheeler; Yoon and Nelson; and Ackley equations for HD adsorption on the CC was larger than the values calculated for the PUCP and the C-spheres. This could be due to the smaller particle diameter of the carbon and consequently, a shorter distance to cover by the vapour molecule to the micropore where adsorption takes place, as well as the open mesopore structure of the CC. The smaller rate constant for the PUCP and C-spheres could be due to the large particle diameter and narrow micropore distribution. The rate constant decreased with increased exposure concentration and temperature.

The adsorption capacity for the HD adsorption on the CC at 40°C and 0.5 cm/s increased as a function of HD concentration. The adsorption capacity of the PUCP and C-spheres did not differ over the concentration range investigated.

Results obtained by calculating the percentage of the residence time (τ) used for HD adsorption, confirmed the rate constants.

Applying Fick's diffusion law to the breakthrough results gave a graph with a straight line with a distinct break indicating that heat transfer might be controlling the adsorption process. The diffusion coefficients, D_1 and D_2 were calculated from the two gradients in each graph. D_1 was very small $\approx 10^{-13}$ cm^2/s, which indicated that the adsorption process was controlled by isothermal diffusion. D_2 was larger $\approx 10^{-8}$ cm^2/s, which could be indicative of heat transfer and/or interparticle diffusion controlling the adsorption process.

Isothermal diffusion in the CC could be due to the larger mesopores in which adsorption takes place slowly. However, the PUCP and the C-spheres have a high carbon mass (relative to the CC) which has a higher heat capacity. The heat transfer coefficient is large, indicating isothermal diffusion. In smaller particles heat effects become significant (PUCP and the CC) and with time there is a significant deviation from the expected curve for isothermal diffusion.

The D_1 and D_2 for C-spheres were a factor 100 and 1000 larger than for the CC and the PUCP respectively. D_1 and D_2 increased with increasing HD concentration for the CC, PUCP and the C-spheres, which indicated a high surface migration and a low adsorption energy. D_1 and D_2 increased with increasing temperature for the PUCP as a result of the increase in the jump frequency of the HD molecules.

From the study it follows that the ideal carbon for textile impregnation must have a high active surface area (400 - 500 m^2/g) to ensure a high adsorption capacity, a pore distribution which includes mesopores (20 - 24 Å) and a particle with a diameter smaller than 30 μm to ensure a high sorption rate constant.

A method was developed for differentiating between textiles containing activated charcoal used for the manufacturing of protective clothing, based on other characteristics than the protection time alone.

CONTENTS

LIST OF FIGURES

predicted by the Ackley equation **(2.43)**.

LIST OF TABLES

LIST OF SYMBOLS AND ABBREVIATIONS

Chapter 1

BET	Brunauer, Emmett and Teller
CC	carbon powder sprayed onto a woven cloth
C-spheres	carbon spheres point bonded with binders to a woven cloth
$°\,C$	degrees Celsius
DFT	density functional theory
HD	mustard gas
K	Kelvin
k_v	rate constant (min^{-1})
OSHA	Occupational safety and health association
PUCP	polyurethane foam rubber impregnated with carbon powder
t_b	protection time (min)
W_c	critical weight (g carbon)
W_e	adsorption capacity (g adsorbate / g adsorbent)

Chapter 2

$\mathring{A}$	Angstrom
a	constant in equation *(2.5)*
a_1	condensation coefficient (p20)
A_m	apparent cross sectional area occupied by a molecule of the adsorbate in the completed monolayer *(2.23, 2.26)*
A_s	BET activated surface area $(m^2\,/\,g)$ *(2.33)*
B	constant in equation *(2.5)*
$B_{Dubinin}$	structural constant of the adsorbent related to the adsorption potential of the micropores *(2.32)*

b	constant, dependent on temperature but independent of surface coverage, and describing in some way the energetics of the surface in equation *(2.15)*
b_d	bed depth (mm) (p36)
c_1	speed of light (m/s) *(2.8)*
C_0	challenge (inlet) concentration (g / cm^3) *(2.37)*
C_1 or C	a dispersion constant associated with instantaneous dipole-dipole interaction in equation *(2.4, 2.7)*
C_x / C_0	ratio of outlet and inlet concentration (p33)
C_x	concentration in the outlet (g / cm^3) *(2.37)*
D	diffusivity in a straight cylindrical pore (cm^2 / min) *(2.45)*
D_c	intra crystalline diffusivity (cm^2 / min) *(2.51, 2.52)*
D_k	Knudsen diffusion (cm^2 / min) *(2.48)*
D_m	molecular diffusivity (cm^2 / min) *(2.46)*
D_p	pore diffusivity (cm^2 / min) *(2.44)*
DR	Dubinin-Radushkevich (p24, 26)
D_s	surface diffusion (cm^2 / min) *(2.49)*
E	energy of adsorption (cal / mol) *(2.31)*
F	field strength at the centre of the molecule, equation *(2.11)*
$f(H)$	total area of pores of size H in the sample *(2.35)*
f	packing factor *(2.26)*
h	Planck quantum constant *(2.9)*
ΔH_A	heat of adsorption *(2.22)*
ΔH_L	heat of liquefaction *(2.22)*
J	mass transfer *(2.44)*
k	Boltzman constant *(2.47)*
k_v	pseudo first order adsorption rate constant (min^{-1}) *(2.37)*
L	Avogadro's number (molecules / mole) *(2.16)*
M	molecular mass (g / mole) *(2.23, 2.26, 2.48)*
m	mass of the sample (g)
M_t / M_∞	fractional approach to equilibrium *(2.54)*

M_1, M_2	molecular masses (g / mole) *(2.47)*
N	Avogadro's constant *(2.23, 2.26)*
n	quantity of gas adsorbed (moles / gram of solid) *(2.1)*
nm	nanometer
n_m	monolayer capacity *(2.20)*
N_2	nitrogen
p	pressure of the vapour (Pa) *(2.1)*
p^0	saturation pressure (Pa) *(2.3)*
p/p^0	relative pressure
$pa_1\kappa\theta_0$	rate of condensation on unit area of surface (p19)
P_a	adsorbate pressure (Pa) *(2.50)*
P	total pressure (Pa) *(2.47)*
Q	volumetric flow rate of air (cm^3 / min) *(2.37, 2.41, 2.42)*
Qmom	quadrupolar moment of a gas molecule *(2.13)*
Qads	heat of adsorption (that is the amount of heat liberated when the molecules move from vapour to the adsorbed state). This is also the energy involved in evaporation of the adsorbed molecule from the surface *(2.14)*
q_L	molar heat of condensation (p21)
q(r,t)	adsorbed phase concentration (g/cm^3) *(2.51, 2.52, 2.53)*
$\bar{q}(t)$	average concentration through the particle (g/cm^3) *(2.54, 2.55)*
q_1	isosteric heat of adsorption (p19)
R	molar gas constant *(2.14)*
r_a	distance separating two atoms *(2.4-7)*
r	mean pore radius (cm) *(2.50)*
r_{ij}	distance between the molecule *i* in the gas phase and the centre of an atom *j* in the solid *(2.10)*
S	surface area (m^2/g) *(2.16, 2.23, 2.27-29)*
T	absolute temperature (Kelvin) *(2.1, 2.14)*
t	statistical thickness of the adsorbed layer *(2.30)*

TVFM	volume filling of micropores (p25)
t_b	gas breakthrough time (min) *(2.37)*
V_{eq}	equilibrium amount (mmol / g) of gas adsorbed per unit mass of adsorbent at relative pressures p/p^0 *(2.15)*
V	molar volume of the adsorbate in the liquid form (cm^3) equation *(2.29)*
V_A	volume of nitrogen adsorbed (cm^3) (p24)
V_f	superficial velocity (cm/min) (p36)
V_I	volume of the sorbent (cm^3) *(2.41)*
V_m	amount of gas required for monolayer coverage of adsorbent (mmol / g) *(2.15)*
V_N	micropore volume measured with N_2 (cm^3 / g) at 77K *(2.34)*
v_1	frequency of oscillation of the molecule in a direction normal to the surface *(2.17)*
W	mass of carbon (g) *(2.37, 2.42)*
W_0	micropore volume for DR adsorption isotherm on carbonaceous materials and organic vapours (cm^3 / g) *(2.31)*
W_e	kinetic adsorption carbon capacity (g adsorbate / g carbon) *(2.37)*
W_v	volume of adsorption filling micropore (cm^3 / g) *(2.31)*
x_m	monolayer capacity (g adsorbate / g adsorbent) *(2.23-25)*
$X(p)$	experimental quantity adsorbed at pressure p *(2.35)*
$x(p,H)$	quantity adsorbed per unit area at the same pressure (p), in a pore of size H *(2.35)*
x_s	saturation uptake *(2.23-25)*
z	distance of a molecule from the surface *(2.10)*
z_m	number of sites per unit area (so that $z_m\theta_1$ is the corresponding number of sites adsorbed molecules) *(2.17)*
α_A, α_B	polarizabilities of the atoms A and B *(2.8)*
β	adsorbate affinity coefficient *(2.32)*
ε_{ij}	total potential energy between two atoms *(2.10)*
$\varepsilon(r_a)$	total potential energy between two atoms termed the Lennard-

	Jones potential *(2.7)*
ε_{DR}	adsorption potential of the surface (cal / mol) *(2.31)*
$\varepsilon_D(\,r_a\,)$ or ϕ_D	potential energy of two isolated atoms separated by a distance r_a in equation *(2.4, 2.13)*
$\varepsilon = \sqrt{\varepsilon_1\,\varepsilon_2}$	Lennard-Jones force constant *(2.47)*
$\varepsilon_R(r_a)$ or ϕ_R	short range repulsive forces for two atoms *(2.5, 2.6, 2.13)*
ε_p	porosity of the adsorbent particle *(2.44, 2.49)*
θ	angle between the field and the axis of the dipole *(2.12)*
θ_0	fraction of bare sites on an adsorbent (p19)
θ_1	occupied fraction on an adsorbent (p19)
κ	constant given by the kinetic theory of gases ($\kappa = 0.5L/(MRT)^{1/2}$) (p19)
μ	mean pore radius (cm) *(2.48)*
U	viscosity (poise) *(2.50)*
μ	dipole moment of the molecule *(2.12)*
v^o_A, v^o_B	characteristic frequencies related to optical dispersion *(2.9)*
ρ	density of the adsorbate in liquid form *(2.26)*
ρ_β	bulk density of the packed carbon bed (g / cm^3) *(2.37, 2.42)*
σ	projected area of an adsorbate molecule (m^2 / molecule) *(2.16)*
σ_{12}	collision diameter from the Lennard-Jones potential (Å) *(2.47)*
τ_0	time of oscillation of the molecules in the adsorbed state(referring especially to the vibrations perpendicular to the surface) *(2.14)*
τ	residence time *(2.41)*, *(2.42)* and *(2.43)*
τ_F	time the gas molecule remains at the surface of the adsorbent *(2.14)*
β	tortuosity factor equation *(2.45)*
ϕ_P	interaction energy of a gas molecule *(2.11)*
$\phi_{F\mu}$	interaction energy of a gas molecule with a permanent dipole *(2.12)*

ϕ_{FQmom}	interaction energy of a gas molecule with a quadrupole moment *(2.13)*
$\phi(z)$	potential of a single molecule of the gas with reference to the solid *(2.10)*
$\phi(z)_{tot}$	overall interaction energy of a molecule at a distance z from the surface *(2.13)*
X_A, X_B	magnetic susceptibilities of the atoms A and B *(2.8)*
Ω	a function of ε/kT *(2.47)*

Chapter 3

ASAP 2010	active surface determination apparatus (p57)
CCl_4	carbon tetrachloride (p73)
CT	time-integral of the vapour concentration of exposure *(3.2)*
d_f	film thickness(μm) (p74)
DMMP	dimethyl methylphosphonate (p73)
FFAP	free fatty acid (p73)
FHG (CGFT)	Frauenhofer Gesellschaft (p58)
GC	gas chromatograph
GC-FID	gas chromatograph flame ionisation detector
H_2	hydrogen
l air/h	litre air per hour
l N_2/min	litre nitrogen per minute
M_d	mass deposited per unit area (g/m^2) *(3.2)*
mg.min/m^3	milligram minute per cubic meter
NATO (MUNSTER)	North Atlantic Treaty Organisation (German test facility) (p58)
NATO (TNO)	North Atlantic Treaty Organisation (Netherlands test facility) (p58)
N_2	nitrogen
$P_i(\ominus)$	pressure in the gap *(3.1)*
$P_o(\ominus)$	pressure outside the fabric *(3.1)*
TCT-GC-FID	thermal cryogenic trap-gas chromatograph-flame ionisation

	detector (p58, 75)
ΔR	gap between the solid surface and textile
RSA (PTN)	Republic of South Africa test facility (p58)
USA (CSL)	United States of America (testing laboratory) (p58)
V_d	deposition velocities (cm/s) *(3.2)*
V_n	face velocity entering a permeable layer (cm/s) *(3.1)*
W	mass of one to five textile layers
Γ	permeability (m/Pa.s) *(3.1)*

Chapter 4

| STP | standard temperature and pressure (p85) |

Chapter 5

CBW	chemical, biological warfare
$cm^3\ N_2\ /g\ C$	cubic centimeter nitrogen per gram carbon
d_b/V_f	bed depth over superficial velocity for the calculation of residence time (p118, 122)
g HD/ g C	gram mustard gas per gram carbon
V/Q	bed volume over volumetric flow for the calculation of residence time (p118)
W	mass of carbon impregnated into one to five textile layers
W_c	critical mass (p107)
W_e/C_0Q	gradient in the Wheeler equation used for the calculation of W_e (p107)
$W/Q\rho_B$	mass of the carbon bed over the product of volumetric flow times the bed density for the calculation of residence time (p118, 122)
$-W_e\rho_B ln(C_0/C_x)/C_0 k_v$	y-axis intercept in the Wheeler equation used for the calculation of k_v (p107)
$\mu g\ HD/l$	microgram mustard gas per liter

ρ density

Chapter 6

C_s	surface concentration *(6.1)*
D_1 and D_2	diffusion coefficients
dC_s/dx	surface concentration gradient *(6.1)*
E	size of the energy barrier which separates adjacent surface sites *(6.3, 6.4)*
N_s	flux in the x-direction across a line of width **b** *(6.1)*
q	differential heat of adsorption *(6.4, 6.5)*
v_0	frequency of vibration of the adsorbed molecule normal to the surface *(6.5)*

CHAPTER 1

MOTIVATION

1.0 INTRODUCTION

Impermeable suits are mostly used for personal protection when spraying agricultural fields with pesticides and herbicides. These suits are however very warm, due to the low or no water vapour transport. Furthermore, the perspiration pores of the wearer tend to widen in order to dissipate body heat faster. This action tends to aid adsorption of the pesticide through the skin. The pesticides leak into the suit at interfaces with the gloves, boots and mask, due to the "bellows effect" **[1]**. Owing to the low water vapour transport and high heat insulation, these suits cannot be worn for prolonged periods without causing heat stress and other heat stress related diseases.

The permeable textile has the great advantage in that the fabric can "breathe" and air and water vapour can pass freely from the interstices of clothing layers to the outer atmosphere. Permeable suits therefore, can be worn for longer periods and the wearer can indulge in low and medium rate work schedules with little discomfort and no risk of heat exhaustion. It must be stressed that high work rate activity in a permeable suit can lead to heat stress if the generation of water vapour is in excess of the maximum loss possible under the prevailing working environment.

In the permeable concept, unlike an impermeable garment, a means of removing harmful organic chemicals from the moving air must be included. This is achieved almost universally by including as a layer of activated carbon impregnated into various carriers. Various types of carbon impregnated carrier systems have been developed over the past thirty years **[2,3]**.

The development of activated carbon textiles for use in garments that protect the wearer against percutaneous chemical vapours is of potential interest to everyone in the chemical process industry, particularly in view of the OSHA regulations on

1

hazardous chemicals. Present methods of incorporating activated carbon in protective clothing involves impregnation of the material in some way with charcoal powder [4]. Powdered forms of an activated carbon readily adsorb hazardous chemical vapours, but they are not entirely satisfactory from other view points. Carbon particles must be physically entrapped in polymeric binders to remain in the material. This is detrimental to sorption and must be compensated for by incorporating an excess of carbon into the system in order to obtain a desired sorption level. Furthermore, impregnation ultimately produces fabric having reduced air permeability and increased weight. These factors, in addition to thickness, which is the major thermal insulation factor, contribute to excessive physiological stress experienced by the wearer when protective garments are worn in a hot environment.

Permeable suits with impregnated carbon are being developed to make the materials lighter and more comfortable for hot and humid climates. Most of the materials can be laundered at least ten times with warm water and a special detergent. This form of protection against hazardous vapour and aerosols (not solid particles) will become essential as legislation becomes more strict and exposure levels are more strictly monitored.

Carbon fibre fabrics and fabrics containing carbon are continually being developed for a variety of applications, including protective clothing and environmental control materials [5]. Textiles containing carbon were primarily investigated for military applications. These textiles can also be implemented as automotive in-cabin air filters used for particulate filtration as well as odour removal. Most of the chemicals to which these systems can be exposed in chemical warfare, are similar in structure to the organo phosphorous pesticides. However the chemical which was used for the evaluations was the blistering agent; bis(2-chloroethyl)sulfide, or mustard gas as it is commonly known. The chemical is referred to in this study as HD.

New developments in the field of materials require sophisticated and reliable evaluation of the materials.

2

1.1 SCOPE OF THE PROJECT

The scope of the project can be illustrated schematically as follows:

ENVIRONMENT

A range of harmful
chemicals:
Pesticides ➔
Herbicides (differing ➔
from each other in ➔
terms of chemical ➔
and physical charac- ➔
teristics, as well as ➔
purity) ➔

A protective layer
between the environment
and the individual

INDIVIDUAL

A range of
chemicals and
breakdown
products which
can be detected
depending on the
protection (or
breakthrough
concentrations) of
the protective
textiles

The ability of a textile containing activated charcoal to offer protection against a harmful or hazardous chemical is measured as the protection time, t_b. The protection time is the time that the textile can protect the individual wearing a suit, manufactured from these textiles, from exposure to harmful concentrations of the chemical vapour. The protection time can be increased by increasing the mass of carbon impregnated into the textile. Increasing the carbon load per unit area of the textile adds to the cost, but more importantly it adds to the physiological heat stress experienced by wearers of these suits. Therefore, the protection time can be increased by increasing the carbon load, but with more negative than positive consequences.

Another way of improving the protection time is to improve the quality of the activated carbon impregnated into the textiles. The activated charcoals impregnated into these

3

textiles are characterised by the active surface area and pore volume distribution. However, the active surface area of the carbon is only determined before impregnation. The amount of binders and adhesives used to impregnate the charcoal into the textiles in order to prevent carbon loss from the textiles due to friction, perspiration and general movement, causes a decrease in the active surface area, which causes a decrease in the protection time. This decrease in protection time due to the impregnation method and poisoning by the binders is not usually documented.

The active surface area of the activated charcoal, used for impregnation, is determined with N_2 at 77K and it is suspected that outgassing of the carbon (being the standard method) takes place at elevated temperatures, e.g. 200°C to 300°C. This method is acceptable for determining the quality of the carbon before impregnation into the textiles. However, after impregnation the porous structure of the carbon can be occupied by the binders and, what is more important, these textiles are used at normal atmospheric temperature and pressure. Thus the active surface available for physical adsorption of the hazardous chemical vapours is much smaller than the active surface available when outgassed at elevated temperatures.

1.2 OBJECTIVE AND OUTLINE OF THE STUDY

The goals of characterising textiles may be described as follows:
- to determine the active surface area, pore volume distribution and micropore volume;
- to determine the effect of the carbon micropore structure on the adsorption rate constant, capacity and critical mass;
- to determine the effect of the challenge concentration and temperature on the adsorption rate and capacity, and
- to determine the effect of the micropore structure on the diffusion coefficient of the organic compound.

In this study another method had to be found to differentiate between textiles containing activated charcoal based on characteristics other than the protection time which could

4

be altered by increasing the loading of the carbon per unit area. The active surface area was determined by degassing at room temperature and then determining the isotherm for nitrogen adsorption at 77 K [6]. The micropore volume was determined with the t-plot, and pore volume distribution of the charcoal after impregnation into the textile was determined by the density functional theory (DFT).

The breakthrough time of the organo-S-compound (HD) through the three different textiles containing charcoal was determined with the dynamic breakthrough test method, which was developed for the evaluation of these textiles. The textiles were exposed or challenged with a certain concentration of HD vapour in nitrogen, referred to as the challenge concentration. With the breakthrough times available, the rate constant (k_v), capacity (W_e) and critical mass (W_c) for adsorption of the organo-S-compound (HD) were determined for the three different textile technologies (polyurethane foam rubber impregnated with carbon powder (PUCP), carbon powder sprayed onto a woven cloth (CC), and carbon spheres point bonded with binders to a woven cloth (C-spheres)). Three equations, namely the Wheeler, Yoon and Nelson and Ackley equations, were used to calculate the aforesaid parameters [7,8,9].

Fick's second diffusion law was used to determine the diffusion coefficient of the organic chemical through the different charcoal layers [10]. The adsorption process of the organo-S-containing compound on the different charcoal systems was described in order to predict the behaviour of the textiles when exposed to HD vapour.

5

REFERENCES

1.   D.L. Griffiths, *"UK NBC Protective Clothing"*, Nucl., Biol. and Chem. Def. Int (NBCDI), 2, 1987. p37.

2.   J. Medema, *"Protective Clothing, Comparison of 17 Materials,"* Proc. 4th Int. Symp. Protection Against Chemical Warfare Agents, Stockholm, Sweden, 1992. p11.

3.   E.E. Alexandroff, *"Saratoga: Carbon Pellet Technology in Chemical Warfare Protective Fabrics"*, Proc. 2nd Int. Symp. Protection Against Chemical Warfare Agents, Stockholm, Sweden, 1986. p67.

4.   D.L. Griffiths, *"The Performance of Anti-Gas Fabric Type 9300G on Ageing and in the Presence of Water"* Unpublished Work.

5.   J. Skvoretz, S.F Ortaldo, J.A. Ritter and J.H. Wong, *"Adsorption Characteristics of Carbon Filter Materials"*, Fund. of Ads., Kluwer Academic Publishers, Boston, Massachusetts, 1996. p.847.

6.   P.N. Cheremisinoff and F.Ellerbusch (ed), *"Carbon Adsorption Handbook"*, 2nd Ed., Ann Arbor Science Publishers, Michigan, 1980. p891.

7.   L.A. Jonas and J.A. Rehrmann, *"The Rate of Gas Adsorption by Activated Carbon"*, Carbon, 1974, 12. p23.

8.   B. Kaluderović, B. Stojanović, M. Polovina, B. Babić and M. Jovašević, *"The Kinetics of Adsorption of Carbon Tetrachloride from Air Mixtures by Activated Carbon Cloth - the Application of Theoretical Models"*, J. Serb., Chem., Soc., 61, 6, 1996. p461.

9.   M. W. Ackley, *"Residence Time Model for Respirator Sorbent Beds"*, Am. Ind.Hyg. Assoc. J., 46, 11, 1985. p679. Wheeler

10.   D. M. Ruthven, *"Principles of Adsorption and Adsorption Processes"*, John Wiley and Sons, NY, 1984. p191.

6

CHAPTER 2

THEORETICAL BACKGROUND

2.0 INTRODUCTION

When the clean surface of a solid is exposed to a gas or vapour, adsorption of the gas takes place on the surface. The extent of adsorption is controlled by the gas concentration. In general the adsorption of a gas or vapour on the surface is always larger than the concentration in the gas phase [1]. The phenomenon of adsorption can be divided into two general classifications: physical adsorption and chemical adsorption.

Physical adsorption is a relatively weak adsorption process and is mainly caused by an attractive force between the surface atoms of the solid and the gas molecules [2]. This force is due to the dispersion forces which are caused by van der Waal's and electrostatic forces [3]. These forces are relatively weak compared to the covalent bonding which can occur in the chemisorption process. Physical adsorption is an exothermic process and usually occurs at low temperature. This can lead to multi-layer adsorption. Desorption, which is the reverse of adsorption, can lead to almost 100% recovery of gas from the surface of the solid by evacuation and heat treatment. Adsorption equilibrium can be influenced by adsorbate pressure, adsorption temperature and the interactive potential between the surface of the adsorbent and the adsorbate. Surface coverage increases with an increase in the adsorbate pressure and multi-layers eventually formed.

Physical adsorption can be described as a condensation mechanism on the surface of the solid without chemical bonding between the solid surface and adsorbate molecules, in contrast with chemisorption. In general, the amount of gas adsorbed on a microporous adsorbent at constant temperature after exposure to a gas as a function of increasing gas pressure is referred to as the adsorption isotherm. The adsorption isotherm depends on the nature of the adsorbent and the adsorbate.

7

The following section will describe the development of adsorption theories from simple monolayer adsorption to multi-layer adsorption for both non-porous and microporous adsorbents.

A. ADSORPTION THEORIES

2.1 CHARACTERISATION

2.1.1 Classification of pores

A convenient classification of pores according to their average width has been proposed by Dubinin [4]. Pores of widths below ~20 Å (2 nm) are described as micropores, those with widths above ~200 Å (20 nm) as macropores, and those with widths between ~20 Å and ~200 Å (between 2 and 20 nm) as transitional or mesopores.

The different ranges are not sharply demarcated. Each range of pore size is associated with a characteristic adsorptive behaviour and introduces a particular type of problem associated with the study of its adsorption techniques.

To understand the way in which measurements of the adsorption of gases and vapours can be used to obtain information about surface area and porosity, it is necessary to deal with the concept of the adsorption isotherm.

2.1.2 Adsorption isotherms

Measurement of adsorption of gases can yield information about the surface area and the pore structure of a solid. Adsorption (strictly physical adsorption) has internationally been defined as the enrichment (i.e. positive adsorption or simply adsorption) or depletion (i.e. negative adsorption) of one or more components in an interfacial layer [5]. A solid, such as charcoal, exposed in a closed space to a gas begins to adsorb the gas, and the process is accompanied by an increase in the mass of the solid and a decrease in the

8

pressure of the gas. After a time the pressure becomes constant at value p, and correspondingly the mass ceases to increase any further. The amount of gas thus adsorbed can be calculated from the fall in pressure by applying the gas laws if the volume of the vessel and volume of the solid are known; or it can be determined directly as the increase in mass of the solid, if the solid is suspended on a spring balance [6].

The solid is thus termed the adsorbent and the gas being adsorbed the adsorbate. Adsorption is brought about by physical and /or chemical forces acting between the solid and the molecules of the gas, giving rise to physical (or "van der Waals") adsorption and chemisorption respectively. The van der Waals' forces are the same as the forces that bring about condensation of a vapour to the liquid state [7].

The quantity of gas taken up by the sample of solid is proportional to the mass m of the sample, and also depends on the temperature T, the pressure p of the vapour, and the nature of both the solid and the gas [8]. If n is the quantity of gas adsorbed expressed in moles per gram of solid, then

$$n = f(p,T,gas,solid) \qquad\qquad (2.1)$$

For a given gas adsorbed on a particular solid maintained at a fixed temperature, equation *(2.1)* simplifies to

$$n = f(p)_{T,gas,solid} \qquad\qquad (2.2)$$

If the temperature is below the critical temperature of the gas, the alternative form can be used:

9

$$n = f\left(\frac{p}{p^0}\right)_{T,gas,solid}$$

(2.3)

where p^0 is the saturation pressure.

Equations *(2.2)* and *(2.3)* are expressions of the adsorption isotherm, i.e. the relationship, at constant temperature, between the amount of gas adsorbed and the pressure, or relative pressure respectively [9].

The adsorption processes occurring within the macropores behave in the same way as an open surface to adsorption and account for less than 1% of the adsorption process in the micropores [10].

The majority of isotherms which result from physical adsorption may conveniently be grouped into six classes. Types I to V were originally proposed by Brunauer, Deming, Deming and Teller and are also referred to as the Brunauer, Emmet and Teller classification [11]. Figure 2.1 illustrates the six major classes of isotherm shapes that are obtained from adsorption experiments. The isotherm shapes give information on the different sizes of porosity.

Amount adsorbed
(mmol / g)

Type I

Type II

Type III

Type IV

Hysteresis

Type V

Type VI

2 nd
layer

Monolayer
coverage

Relative pressure (p/p^0)
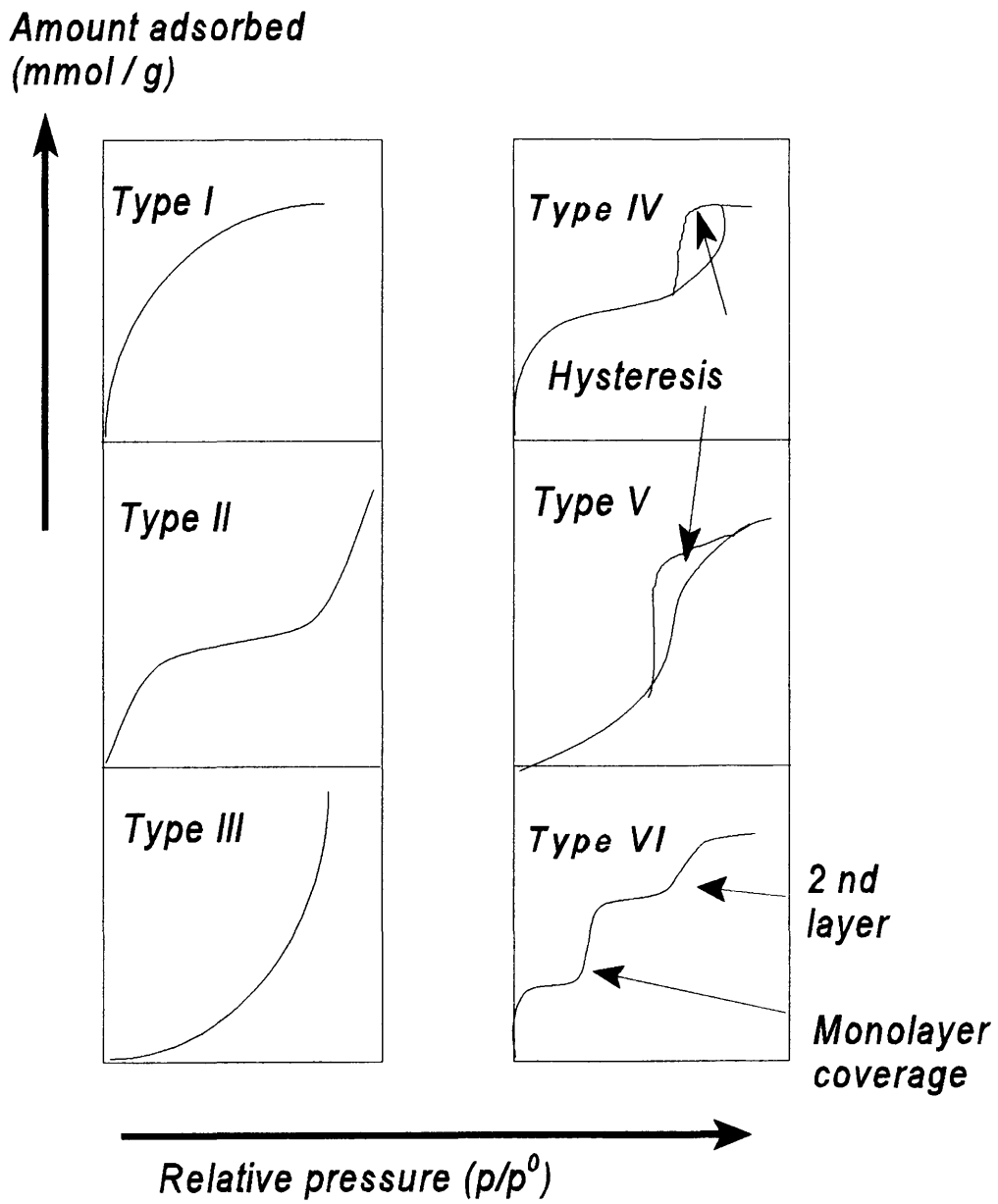
Figure 2.1:

Six different classes of isotherm shapes [12].

11

Type I isotherms are typically of microporous solids in that micropore filling occurs significantly at relatively low pressures < 0.1 p/p^0, the adsorption process being complete at ~ 0.5 p/p^0. A typical example of this isotherm would be obtained by adsorption of N_2 on microporous carbon at 77K.

Type II isotherms are obtained by physical adsorption of gases on non-porous solids. Monolayer coverage is succeeded by multi-layer adsorption at higher p/p^0 values. Type II isotherms can be obtained from carbons with mixed micro- and mesoporosity.

Type III and type V isotherms are convex to the relative pressure axis. These isotherms are characteristic of weak gas-solid interaction. Type III isotherms are obtained from non-porous and microporous solids and Type V isotherms are obtained from mesoporous or microporous solids.

Type IV isotherms possess a hysteresis loop, which is associated with mesoporous solids, where capillary condensation occurs.

Type VI isotherms are stepwise isotherms and represent complete formation of successive monomolecular layers.

2.1.3 Adsorption forces

The adsorption forces provide valuable insight into the nature of the adsorption process. Although elementary, the following discussion should show how the adsorption will be affected by an increase in the polarizability of the gas molecule or by a change in the polarity of the solid.

The forces involved in adsorption always include dispersion forces, which are attractive, together with short-range repulsive forces. In addition there will be electrostatic forces if either the solid or the gas is polar in nature. Dispersion forces were first characterised by London [13]. These forces arise from rapid

fluctuation in electron density within each atom, which induces an electric moment in a near neighbour and thus leads to attraction between two atoms. Making use of the quantum-mechanical perturbation theory, London arrived at an expression for the potential energy of two isolated atoms separated by a distance r_a [13]. By omitting certain small values the equation can be simplified to:

$$\varepsilon_D \left(r_a \right) = -C_1 r_a^{-6} = \phi_D \qquad (2.4)$$

where $\varepsilon_D(r_a)$ is the potential energy of two isolated atoms separated by a distance r_a, and C_1 is the dispersion constant associated with instantaneous dipole-dipole interaction.

An expression for the short-range repulsive forces can also be derived from quantum-mechanical considerations, as follows:

$$\varepsilon_R \left(r_a \right) = B \, exp(-a r_a) \qquad (2.5)$$

where B and a are constants. For mathematical convenience equation *(2.5)* is simplified to

$$\varepsilon_R \left(r_a \right) = B \, r_a^{-m} = B \, r_a^{-12} = \phi_R \qquad (2.6)$$

where B is an empirical constant and the index m is usually assigned to the value $m = 12$. The total potential energy between two atoms thus becomes (with $C_1 = C$),

$$\varepsilon(r_a) = -C \, r_a^{-6} + B \, r_a^{-12} \qquad (2.7)$$

13

which is often termed as the Lennard-Jones potential.

Several relations have been devised for the calculation of the parameter C from the molecular properties of two atoms A and B, e.g. that of Kirkwood and Müller [14]:

$$C = \frac{6mc_1^2 \alpha_A \alpha_B}{(\alpha_A/\chi_A) + (\alpha_B/\chi_B)} \qquad (2.8)$$

where c_1 is the speed of light, α_A and α_B are the polarizabilities, and χ_A and χ_B are the magnetic susceptibilities of the atoms A and B. Another expression is that of London [15]:

$$C = 3/2 \alpha_A \alpha_B h v^o_A v^o_B / (v^o_A + v^o_B) \qquad (2.9)$$

where v^o_A and v^o_B are characteristic frequencies related to optical dispersion (h being the Planck quantum constant).

To apply these various equations to the adsorption of a gas on a solid, it is necessary to consider the interaction of the surface layers of a solid composed of atoms (or ions) of a substance Y, say, with isolated molecules of gas X. The individual interactions of each atom in gas molecule X with each atom of the solid Y must be added up to obtain the potential $\phi(z)$ of a single molecule of the gas with reference to the solid:

$$\phi(z) = \Sigma \varepsilon_{ij}(r_{ij}) \qquad (2.10)$$

Here r_{ij} is the distance between the molecule i in the gas phase and the centre of an atom j in the solid.

14

If the solid is polar, it will give rise to an electric field which will induce a dipole in the gas molecule X. The resulting interaction energy ϕ_p is as follows:

$$\phi_P = -\frac{1}{2}\alpha^2 F \qquad (2.11)$$

where F is the field strength at the centre of the molecule and α is the polarizibility of the molecule.

If in addition the molecule possesses a permanent dipole, its interaction with the field will make a further contribution $\phi_{F\mu}$ expressed as:

$$\phi_{F\mu} = -F\mu\cos\theta \qquad (2.12)$$

where μ is the dipole moment of the molecule and θ is the angle between the field and the axis of the dipole.

Finally, if the gas molecule possesses a quadru polar moment **Qmom**, this will interact strongly with the field gradient F to produce a further contribution ϕ_{FQmom} to the energy.

Thus, the overall interaction energy $\phi(z)_{tot}$ of a molecule at a distance z from the surface may be represented by the general expression:

$$\phi(z)_{tot} = \phi_D + \phi_P + \phi_{F\mu} + \phi_{FQmom} + \phi_R \qquad (2.13)$$

Here ϕ_D and ϕ_R correspond to the terms in r_a^{-6} and r_a^{-12} respectively in equation *(2.7)*. These contributions are always present, whereas the

15

electrostatic energies ϕ_P, $\phi_{F\mu}$ and ϕ_{FQmom} may or may not be present according to the nature of the adsorbent and the adsorbate. In principle, equation *(2.13)* could be used to calculate the numeric value of the interaction potential as a function of the distance *z* of any given molecule from the surface of a chosen solid. The inevitable uncertainties are such that the final result can be no more than a rough approximation of the actual situation. It is useful to note that the interaction potential becomes larger as the solid atoms become smaller in relation to the size of a gas atom. The reason for this is that the number of solid atoms at a given distance from the gas atom increases when the solid becomes more closely packed.

2.1.4 Mobility of the adsorbed atoms

If a gas molecule collides with the surface of an adsorbent it can either remain at the surface for a time *(τ)* or rebound and return to the gas phase. The time a molecule stays on the surface was already defined by Frenkel in 1924 **[15]**, namely:

$$\tau_F = \tau_0 e^{Qads/RT}$$

(2.14)

where τ_0 - is the frequency of oscillation of the molecules in the adsorbed state (referring especially to the vibrations perpendicular to the surface);

Qads - is the heat of adsorption (that is the amount of heat liberated when the molecules move from the vapour to the adsorbed state), which is also the energy involved in evaporation of the adsorbed molecule from the surface;

T - is the absolute temperature, and

R - is the molar gas constant.

τ_0 is in the order of magnitude 10^{-13} s. (At room temperature τ_0 is equal to *h/kT*

which is 1.6×10^{-13}s. **[16]**) The heat of adsorption (**Qads**) is the determining factor for the magnitude of τ. Thus, τ is the time of adsorption.

During the time τ, which is spent at the adsorbent's surface, the following "activities" can take place **[16]**:

- exchange of thermal energy between the adsorbed molecules at the surface,

- continuous exchange of energy by means of collisions with other adsorbed molecules and adsorbing molecules,

- due to the said collisions the adsorbed molecules accumulate momentum so that the component of this momentum, perpendicular to the surface, increases till it exceeds the adsorption energy and the molecule desorbs,

- if the accumulated momentum is not sufficient for evaporation, the molecule moves sideways, maintaining contact with the surface, two-dimensional movement. The higher the temperature the faster the surface migration.

When the number of molecules adsorbed on the surface is not too high, the molecules are single adsorbed molecules and behave as a two-dimensional gas **[16]**. Referring to the lower regions of pressure in the adsorption isotherm there is an equilibrium between the gas adsorbed, which is a two-dimensional gas, and the three-dimensional gas above the adsorbent.

The heat of spreading, or surface migration, is the difference between the heat of evaporation and the heat of adsorption.

2.1.5 Multi-layers

The molecules in an adsorbed layer interact not only with the solid, but also with their neighbours within the layer. The effect is negligible when the fractional coverage θ_1 of the surface is small and the adsorbed molecules are therefore

17

far apart, but it becomes increasingly significant as the monolayer becomes more occupied. A fully occupied monolayer in some ways acts as an extension of the solid and will attract more gas molecules from the gas phase. The result is that at higher relative pressures an adsorbed layer which is several molecules thick (a multi-layer) is built up.

2.1.6 Adsorption equations

A significant literature base exists describing mathematical models to interpret shapes of isotherms obtained from porous and non-porous solids [17]. Information concerning the effective surface areas, pore size distribution, micropore volumes, etc., are incorporated within the isotherm. Extracting the information is a difficult task as direct experimental evidence is limited. The equations are based on assumptions placed into models and are then matched against experimental isotherms [17].

a. Langmuir equation

Surface areas from Type I isotherms can be determined with the Langmuir equation [17]:

$$\frac{p}{V_{eq}} = \frac{p}{V_m} + \frac{1}{bV_m} \qquad (2.15)$$

where V_{eq} - equilibrium amount (mmol / g) of gas adsorbed per unit mass of adsorbent at relative pressures p/p^0;

V_m - amount of gas required for monolayer coverage of adsorbent (mmol / g);

b - constant, dependent on temperature but independent of surface coverage, and describing in some way the energetics of the surface.

Surface areas are obtained using the relationship:

18

$$S = V_m N\sigma \qquad\qquad (2.16)$$

where S - surface area (m²/g);

N - Avogadro's number (molecules / mol)

σ - projected area of an adsorbate molecule (m² / molecule).

The Langmuir equation is based on the following assumptions:
- only monolayer adsorption can occur;
- adsorption is localized, with no adsorbate-adsorbate interactions;
- the heat of adsorption is independent of surface coverage, i.e. the adsorbent has a homogeneous surface [17].

b. BET equation

The Brunauer, Emmett and Teller equation was devised to improve the Langmuir model to account for multi-layer adsorption [17]. According to Greg and Sing [18], a state of dynamic equilibrium was postulated in which the rate at which molecules arriving from the gas phase and condensing on the bare sites is equal to the rate at which molecules evaporate from occupied sites.

If the fraction occupied is θ_1 and the fraction of bare sites is θ_0 (with $\theta_1 + \theta_0 = 1$), then the rate of condensation on unit area of surface is $pa_1\kappa\theta_0$ where p is the pressure and κ is a constant given by the kinetic theory of gases ($\kappa = 0.5L/(MRT)^{\frac{1}{2}}$); a_1 is the condensation coefficient, i.e. the fraction of incident molecules which actually condense on a surface. The evaporation of a molecule from the surface is actually an activated process in which the energy of activation may be equated with the isosteric heat of adsorption q_1. The rate of evaporation from the unit area of an active surface is therefore equal to:

19

$$z_m \theta_1 v_1 e^{-q_1/RT} \qquad (2.17)$$

where z_m is the number of sites per unit area (so that z_m θ_1 is the corresponding number of sites adsorbed molecules) and v_1 is the frequency of oscillation of the molecule in a direction normal to the surface. Thus, at equilibrium:

$$a_1 \kappa p \theta_0 = z_m \theta_1 v_1 e^{-q_1/RT} \qquad (2.18)$$

Since $\theta_0 = 1 - \theta_1$

$$\theta_1 = \frac{a_1 \kappa p}{a_1 \kappa p + z_m v_1 e^{-q_1/RT}} \qquad (2.19)$$

If n (in moles) is the amount adsorbed on 1 g of adsorbent, then $\theta_1 = n/n_m$, where n_m is the monolayer capacity. Insertion into equation (2.19) gives:

$$\frac{n}{n_m} = \frac{B_L p}{1 + B_L p} \qquad (2.20)$$

where

$$B_L = \frac{a_1 \kappa}{z_m v_1} e^{q_1/RT} \qquad (2.21)$$

Equation (2.20) is the Langmuir equation for monolayer adsorption [18]. By adopting the Langmuir mechanism but introducing a number of simplifying

20

assumptions, Brunauer, Emmett and Teller in 1938 **[18]** arrived at their well-known equation *(2.22)* for multi-layer adsorption: (a) that in all layers, except the first, the heat of adsorption is equal to the molar heat of condensation q_L; (b) that in all layers, except the first, the evaporation-condensation conditions are identical, i.e. that

$$V_2 = V_3 = ... = V_i \text{ and } a_2 = a_3 = ... = a_i$$

(c) that when $p = p^0$, the adsorptive condenses to a bulk liquid on the surface of the solid, i.e. that the number of layers becomes infinite (p^0 = saturation vapour pressure). The summation of the layers leads to the equation:

$$\frac{p}{n(p^0 - p)} = \frac{1}{n_m c} + \frac{c-1}{n_m c} \cdot \frac{p}{p^0} \qquad (2.22)$$

where p^0 - saturation vapour pressure,

   c - $exp[(\Delta H - \Delta H_L)/RT]$,

   ΔH_A - heat of adsorption, and

   ΔH_L - heat of liquefaction.

The BET equation is widely used to interpret isotherms, obtained by using nitrogen at its boiling point 77K, as adsorbate. The BET equation is restricted in validity to relative pressures below approximately 0.30 (p/p^0), or often less, and cannot be used for calculating the adsorbed layer thickness or specific surface area in higher pressure ranges.

If plotted as n/n_m against p/p^0, equation *(2.22)* gives a curve having the shape of a Type II isotherm, as long as **c** exceeds 2. This point is close to, but not necessarily coincident with, the point where the amount adsorbed is equal to the BET monolayer capacity. When $0 \le c \ge 2$ the BET equation results in a curve having the general shape of a Type III isotherm.

Plotting $(p/p^0)/n(1-p/p^0)$ against p/p^0 should yield a straight line with the slope equal to $(c-1)/n_m c$ and an intercept $1/n_m c$. Solution of the two simultaneous equations gives n_m and c. From the monolayer capacity n_m, the specific surface S can be calculated with equation (2.23).

From the monolayer capacity the specific surface $(S$ in $m^2 / g)$ can then be calculated by using the following relationship:

$$S = \frac{X_m}{M} A_m N \times 10^{-20} \qquad (2.23)$$

where X_m - is the monolayer capacity (g adsorbate / g adsorbent);

A_m - is the apparent cross sectional area occupied by a molecule of the adsorbate in the completed monolayer ($Å^2$, for N_2 this is 16.2 $Å^2$);

N - is the Avogadro constant, and

M - is the molar mass of the adsorbate (g/mole).

According to the Gurvitsch Rule the uptake x_s is equal to the monolayer capacity x_m [19]. Referring to the previous equation, the classical model will lead to the relation:

$$x_m = SM/A_m N \qquad (2.24)$$

$$x_s = SM/A_m N \qquad (2.25)$$

where x_s is the saturation uptake.

22

Then $x_m = x_s$, but A_m can also be calculated as follows:

$$A_m = f(M/\rho N)^{2/3} \tag{2.26}$$

where ρ - is the density of the adsorbate in liquid form, and

f - is the packing factor (usually taken as 1.091).

Inserting the expression for A_m into the equation (2.25):

$$x_s = [SM^{1/3}/fN^{1/3}]\rho^{2/3} \tag{2.27}$$

or

$$x_s = \frac{S}{fN^{\frac{1}{3}}}\left(\frac{M}{\rho}\right)^{\frac{1}{3}}\rho \tag{2.28}$$

Thus

$$\frac{x_s}{\rho} = \frac{S}{fN^{\frac{1}{3}}} \cdot V^{\frac{1}{3}} \tag{2.29}$$

where V (cm^3) is the molar volume of the adsorbate in liquid form.

c. t-plots

t-plots were devised to detect deviations of experimental isotherms from a standard isotherm by testing whether the isotherm under examination is super

23

imposable on the standard isotherm by altering the scale of ordinates [20]. The concept of a standard isotherm implies that a solid surface, when free of complications of adsorption in porosity, adsorbs to equal extents of surface coverage at constant relative pressure.

De Boer, [16] proposed a method for determining pore surface and volume distributions for microporous materials based on the t-curve, a plot of t, the statistical thickness versus the relative pressure, p/p^0. The t-method uses a composite t-curve obtained from data on a number of nonporous adsorbents, with the BET C constants similar to those of the microporous samples. A plot of the volume of nitrogen adsorbed (V_A) as function of t, obtained from the t-curve, afforded both a technique for differentiating between narrow and wide pores and a means of determining the distribution of narrow pores.

The initial slope of V_A-t curve corresponds with small values of t which represents an adsorbed film within large pores and complete filling of smaller radii pores. Therefore, from the initial slope of the V_A-t curve the total surface area of the sample can be obtained by using the equation:

$$t = \frac{V_{liq}}{S} \times 10^4 \qquad\qquad (2.30)$$

The surface area of the wider pores is similarly obtained from the slope of the line from the slope of the second straight part of the curve. The difference between these two surface areas is the surface area of the micropores alone. An abrupt break in the two linear parts of the V_A-t curve indicates the presence of a group of micropores in a narrow radius range, whereas a curvature between the two parts of the curve is an indication of a distribution of micropores.

d. Dubinin-Radushkevich (DR) equation
This equation differs from the Langmuir and BET equations in that it is not based on a model process to describe the physical adsorption of gases [21]. It is

24

based on the energies of adsorption. Dubinin, [21] found empirically that characteristic curves for adsorption of many microporous carbons could be linearized using the DR equation:

$$W_v = W_0 exp(-\varepsilon_{DR}/E)^2 \qquad (2.31)$$

where W_v -   is the volume of adsorbate filling micropore (cm^3 / g) at relative pressures p/p^0 and temperature T (K),

W_0 -   is the total volume of micropores (cm^3 / g),

ε_{DR} -   is the adsorption potential of the surface (cal / mol), and

E -   is the energy of adsorption (cal / mol).

The value of the DR equation is the realization that the characteristic curve of adsorption is a measure of the pore-size (or pore-energy) distribution. Dubinin recognised that the adsorption energy for micropores is much higher than for super micropores, due to enhanced adsorption effects in microporosity. He proposed that micro- and super micropores be filled differently according to their respective adsorption force fields and the interaction between the adsorbed molecules. This mechanism is known as TVFM (the volume filling of micropores). Dubinin used a slit-shaped pore model as the basis for his theory. He also assumed that the distribution of pore sizes was heterogeneous and followed a Gaussian distribution.

Evidence to support Dubinin's theory was obtained from active carbons, which at low levels of burn-off have a homogeneous micropore distribution [22]. The derivative of the DR equation may be written as:

$$W_v = W_0 exp\left[-\frac{B_{Dubinin}T}{\beta} \cdot log^2\left(\frac{p^0}{p} \right) \right] \qquad (2.32)$$

where W_v and W_0 - are terms defined in equation *(2.31)*,

β - is the adsorbate affinity coefficient, and

$B_{Dubinin}$ - is a constant, related to the adsorption potential of the micropores.

A plot of *log* W_v against *log* ^{2} *(p^0/p)* should be rectilinear [22]. Figure 2.2 illustrates plots of adsorption data, as isotherms and in DR coordinates.

Figure 2.2:

Adsorption data presented as an isotherm (left) and in DR coordinates (right).

n

X

Y

Z

Adsorption

p/p^o

log n

X

Y

Z

DR plots

log^2 p/p^o
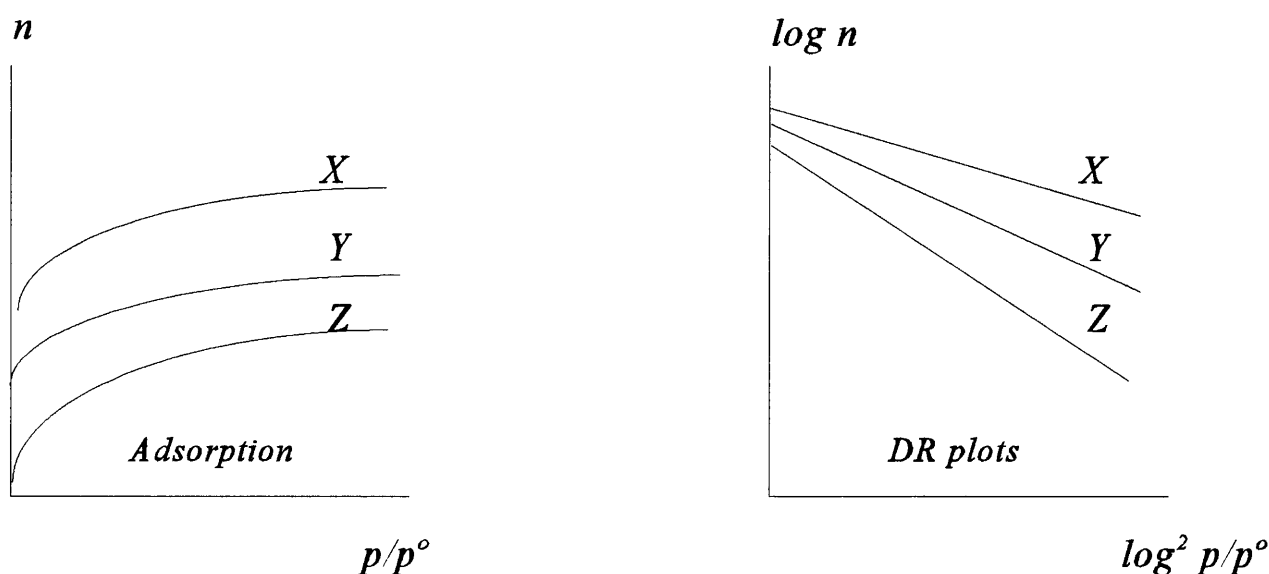
The micropore volume is equal to the *y*-axis intercept at $x = 0$ in the DR plot. The parameter $B_{Dubinin}$ (in equation **(2.32)**) can be calculated from the slope and is referred to as the structural constant of the adsorbent. The value of $B_{Dubinin}$ is a qualitative measurement of the relative average micropore sizes of the adsorbent. The steeper the gradient, the larger the average micropore size (i.e. a wider distribution). Hence the following information can be obtained by

26

interpretation of an adsorption isotherm using the DR equation

- extents of micropore volume capacity;
- relative pore-size distributions;
- deviations of adsorption energies from a Gaussian or related type distribution.

Langmuir and BET equations predict values of V_m, the number of mmol / g required to establish a monolayer. Conversion into a surface area value (m^2 / g) requires the projected area of an admolecule. For N_2 this is 14.2Å^2. The DR equation predicts values of micropore volume (W_0). This number is converted into surface area.

It was shown by Wood, Rehrmann and Karwacki [23] that the DR micropore volume for organic molecules can be estimated, as follows, if the BET surface area determined by N_2 at 77K is known:

$$W_0 = 0.00041A_s \qquad\qquad (2.33)$$

and

$$W_0 = 1.1V_N \qquad\qquad (2.34)$$

where W_0 - is the micropore volume for DR adsorption isotherm on carbonaceous materials and organic vapours (cm^3 / g),

A_s - is the BET activated surface area (m^2 / g), and

V_N - is the micropore volume measured with N_2 (cm^3 / g) at 77K.

27

2.1.7 Activated diffusion

Physical adsorption is a rapid process (hours); longer equilibration times are an indication of activated diffusion **[24]**. This can be confirmed by obtaining an adsorption isotherm at a higher temperature. A reduction in the equilibrium times is an indication of activated diffusion. Activated diffusion operates when the dimensions of the adsorbate molecules are only slightly smaller than the pore diameter. At lower temperatures the molecules have insufficient kinetic energy to enter the pore. With increasing temperature the amounts adsorbed increase. A stage is eventually reached where the amounts adsorbed decrease with increasing temperature.

2.1.8 Molecular sieve effects

Each adsorption site is unique in shape, size and potential energy **[25]**. A critical stage exists when the diameter of one of the sites and the effective diameter of the adsorbate molecule do not fit. When the site size is smaller than the adsorbate molecule it cannot occupy the particular site and adsorption is reduced. This is the basis for molecular sieving effects.

Molecular sieving can be used for separation processes. The critical dimension of a pore is the diameter at which the adsorbate has sufficient energy to be able to enter the pore. In addition to the energy barrier at the entrance to the pore, diffusion rates are also dependent on the energy barriers for diffusion within the porosity.

2.2 TYPE I ISOTHERM

If a solid contains micropores the potential fields from neighbouring walls will overlap and the interaction energy of the solid with a gas molecule will be correspondingly enhanced **[26]**. This will result in the distortion of the isotherm, especially at low relative pressures, in the direction of increased adsorption. There is evidence that this interaction may be strong enough to bring about complete filling of the pores at a low relative pressure, rather than just surface coverage.

Type I isotherms are characterised by a plateau which is nearly horizontal, and which may cut the $p/p^0 = 1$ axis sharply or may show a "tail" as saturation pressure is approached. The incidence of hysteresis varies: some isotherms do not display any, others display a definite loop.

The uptake does not increase continuously but comes to a limiting value in the plateau. The classic interpretation of this limit is that the pores are so narrow that they cannot accommodate more than a single molecular layer on their walls; the plateau thus corresponds to the completion of the monolayer.

The shape of the isotherm can be explained in terms of the Langmuir model. The Type I isotherm was therefore assumed to conform to the Langmuir equation *(2.20)*. In practice the conformity with the equation varies considerably. In some cases a straight line is obtained when plotting *$(p/p^0)/n$* against *p/p^0*, but for some adsorbents the line is distinctly curved. Conformity to the Langmuir equation is not automatic proof of the mechanism. x_m is considered to be equal to the monolayer capacity, and can be converted into the specific surface *S* with equation *(2.23)*. There are suggestions that would indicate that this interpretation is invalid, and that the value of *S* arrived at does not represent a true specific surface.

However, the Gurvitsch rule is often obeyed by systems displaying a Type I isotherm. According to Gurvitsch's rule the quantity x_s / ρ should be a constant for different adsorbates on the same adsorbent [27]. This constancy can only be assumed if the adsorbates are chosen to have the same value of *V* and therefore of *$V^{1/3}$* - since *S* is constant for a given adsorbent and the packing factor *f* is assumed to have the same value for all the adsorbates. The variation in *V* between typical adsorbates is greater than the variation in the x_s-values for a given adsorbate. (According to equation *(2.29)*, *$V^{1/3}$* for N_2 at 77 K is 3.3 cm with $\rho = 0.81$ g / cm^3 and *M* = 28 g, *M/ρ* = *V* = 35 cm^3.) [19]

The conformity to Gurvitsch's rule, shown by systems giving Type I isotherms, is sufficiently general to suggest that the adsorbate is condensed in the pores in a form

29

having a density close to that of the bulk liquid adsorptive. This in turn suggests that the pore has a width in excess of two molecular diameters, since the individual characteristics, namely size and shape, of the different molecules are bound to influence the way in which they pack into such a narrow capillary. A width of several molecular diameters would be required to ensure the smoothing out of such effects and enable the packing to simulate that in a bulk liquid. Thus, in very fine pores the mechanism of adsorption is pore filling rather than surface coverage. The plateau of the Type I isotherm thus represents the filling-up of pores with adsorbate by a process similar but not identical to capillary condensation, rather than a layer-by-layer building up of a film on the pore walls.

Microporosity is sometimes associated with an appreciable external surface, or with mesoporosity, or with both, which is displayed as a hysteresis curve in the isotherm. In general, there are three processes prior to capillary-condensation associated with the hysteresis loop of a Type IV isotherm, which may occur in a porous adsorbent containing micropores along with mesopores; a primary process taking place in very narrow micropores (for N_2 at 77K ~3 Å to ~7 Å); a secondary, cooperative process, taking place in wider micropores (~7 Å to ~18 Å), succeeded by a tertiary process governed by a modified Kelvin equation (> ~18 Å).

The limits of pore size corresponding to each process will depend on the geometry and the size of the adsorbate molecule.

2.3 PORE SIZE DISTRIBUTION: DFT MODEL

A sample of porous material may be characterised by its distribution of pore sizes [28]. Each pore size present will contribute to the total adsorption isotherm in proportion to the fraction of the total area or pore volume of the sample it represents. Mathematically, this relation is expressed by [28]:

$$X(p) = \int x(p,H)f(H)dH \qquad (2.35)$$

30

where $X(p)$ - is the experimental quantity adsorbed at pressure p,

$x(p,H)$- is the quantity adsorbed per unit area at the same pressure (p), in a pore of size H, and

$f(H)$ - is the total area of pores of size H in the sample.

The integration is over all pore sizes in the sample. The function $x(p,H)$ is called the *kernel function* and describes the model isotherms that have been evaluated numerically using the density functional theory. The function $f(H)$ describes how pore area is distributed by size in the sample and is easily converted to a pore volume distribution by size. Because there are no analytic equations for any of these functions, the problem must be solved in a discrete form; the integral equation becomes a summation:

$$X(p) = \sum_i x(p,H_i)\,f(H_i) \qquad (2.36)$$

Given a set of model isotherms, $x(p,H)$, and an experimental isotherm, $X(p)$, the DFT software determines the set of positive values $f(H)$ that most nearly, in a least square sense, solve the equation shown above. DFT also allows a selectable regularisation constraint to be applied to avoid over fitting in the case of noisy data. This process is referred to as smoothing in the DFT program.

The current models assume a slit-like pore geometry. The pore sizes range from 4.0 to 4000 Å and are covered in 91 classes in a geometric progression, and a model for the free or external surface is also included. Each of the 92 model isotherms has been calculated at 181 pressure points.

B. ADSORPTION KINETICS

2.4 THE WHEELER EQUATION

The sigmoid curve, resulting from a plot of vapour concentration exiting a packed bed of activated carbon granules against time, displays, according to Jonas and Rehrmann, [29] second-order kinetics only in the linear or mid-portion of the curve where the exit concentration rises rapidly with time. The first portion of the curve, showing trace gas penetration of the bed and characterised by the convexity with the time axis, represents the condition of an excess of active sites over free gas molecules and displays pseudo first-order kinetics with respect to the gas molecules. This study deals only with the adsorption characteristics of the textiles up to first traces of gas penetration, and therefore is characterised by pseudo first-order adsorption kinetics.

The modified Wheeler adsorption kinetics equation was initially derived from a continuity equation of mass balance between the gas entering an adsorbent bed and the sum of the gas adsorbed by, and that penetrating through the bed [30]. This equation, shown in the polynomial form, has been successfully used by Jonas and Rehrmann in studies of the kinetic adsorption of gases by activated carbons [29]:

$$t_b = W_e W / C_0 Q - W_e \, \rho_\beta \, ln(C_0 / C_x) / C_0 \, k_v \qquad (2.37)$$

where t_b - is the gas breakthrough time at which the concentration C_x appears in the exit stream (min),

W_e - is the kinetic adsorption carbon capacity at the arbitrarily chosen ratio of C_x / C_0 (g adsorbate / g carbon),

W - is the mass of carbon (g),

C_0 - is the challenge (inlet) concentration (g / cm^3),

Q - is the volumetric flow rate of air (cm^3 / min),

ρ_β - is the bulk density of the packed carbon bed (g / cm^3),

C_x - is the concentration in the outlet at time t_b (g / cm^3), and

k_v - is the pseudo first-order adsorption rate constant (min^{-1}).

In equation *(2.37)*, ρ_β is determined as a property of the granular size and shape of the adsorbent when filled by gravity settling in a container column. The density of the carbon bed in the case of the textiles was determined by density measurement of a sample of the textile.

The values for C_0, W and Q are established by the experimental conditions, while the temperature is maintained constant. Using different charcoal bed weights (W) and determining the breakthrough times (t_b) at a selected penetration fraction (C_x/C_0), values for W_e and k_v can be calculated from equation *(2.37)*. The theory predicts that a plot of the breakthrough time (t_b) as a function of the bed weight (W) gives a straight line, with the slope equal to $W_e / C_0 Q$ and the intercept equal to:

$$\left(-\frac{W_e\,\rho_\beta}{k_v C_0}\right)\,\ln\left(\frac{C_0}{C_x}\right) \tag{2.38}$$

The values obtained for the slope and the intercept allow for the calculation of the adsorption capacity (W_e) and rate constant (k_v) respectively.

The breakthrough time was taken as the time from the start of the experiment up to the time the concentration in the outlet reached 1% (0.01 times) of the inlet concentration. Typical breakthrough curves are displayed for the three different textiles in Figures 3.4, 3.5 and 3.6 in Chapter 3. An example of a graph obtained by applying the Wheeler equation to the experimental results is shown in Figure 2.3. The graph shows a linear relationship as is predicted by the Wheeler equation *(2.37)*. Linear regression of the first three points, representing one, two and three textile layers, showed a coefficient of correlation of $r^2 = 0.999$ and a coefficient of $r^2 = 0.988$ was obtained for regression of all five points. The deviation from linearity for the last two layers could be attributed to an increased resistance against air flow through four and five textile layers. (Air flow through the textile layers was measured with an electronic air flow meter with an

33

accuracy of 0.1 ml/min.) The sorption rate constant, vapour capacity and minimum mass to provide protection against the hazardous chemical could be determined with this experimental setup and the equation *(2.37)*. These parameters were calculated and depicted in Tables 5.1, 5.2, 5.3 and 5.4. The results are discussed in detail in Chapter 5.
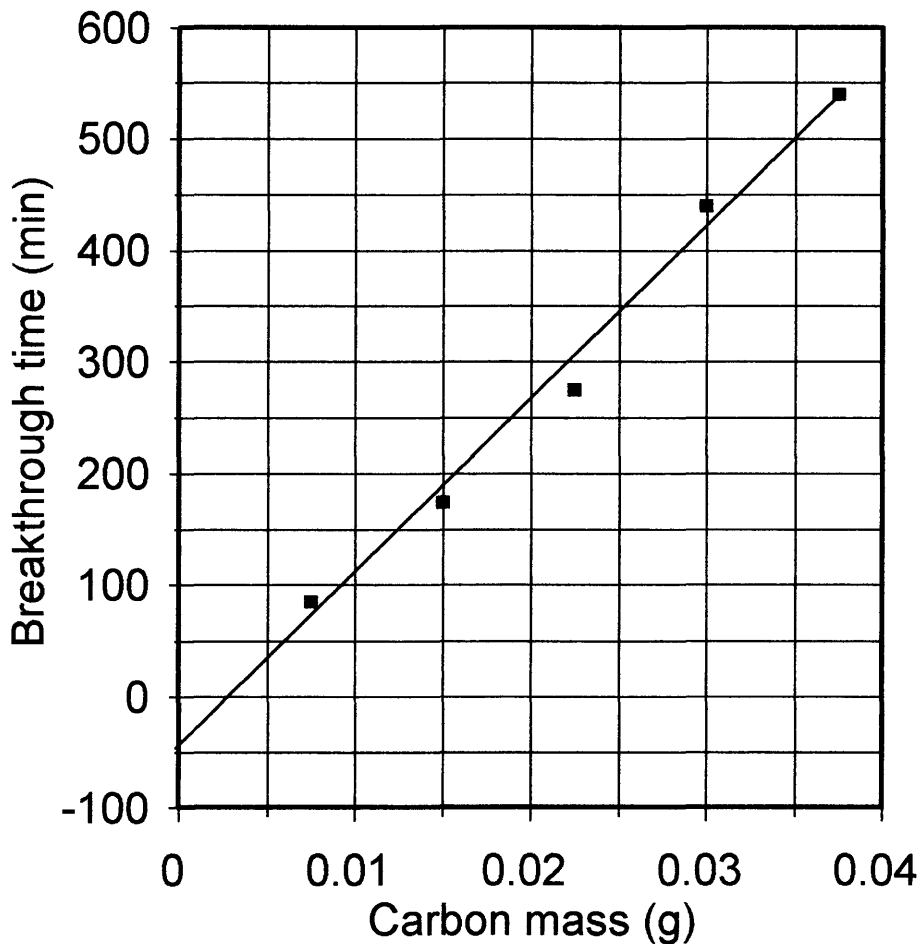
FIGURE 2.3:

Adsorption data for HD vapour on the CC. A plot of t_b vs carbon mass impregnated into the textile layers shows a linear relationship as predicted by the Wheeler equation (2.37).

2.5 THE YOON AND NELSON EQUATION

Yoon and Nelson have presented a gas adsorption kinetic model which is a further modification of the modified Wheeler equation **[31]**. When comparing the Yoon and Nelson equation with the Wheeler equation, the major difference observed is in the logarithmic concentration ratio form. Thus, the *ln (C $_0$ / C $_x$)* in the Wheeler equation becomes *ln (C $_0$-C $_x$)/C $_x$*. The Yoon and Nelson equation may be written as:

$$t_b = \left(\frac{W_e}{C_0 Q}\right) W - \left(\frac{\rho_\beta W_e}{k_v C_0}\right) \ln \left(\frac{C_0 - C_x}{C_x}\right) \qquad (2.39)$$

which may be rewritten as follows:

$$\ln \left(\frac{C_0 - C_x}{C_x}\right) = - \left(\frac{k_v C_0}{W_e \rho_\beta}\right) t_b + \left(\frac{k_v W}{Q \rho_\beta}\right) \qquad (2.40)$$

The equation *(2.40)* predicts that the graph of *ln (C $_0$-C $_x$) / C$_x$* as a function of t_b will be a straight line with the slope equal to *(-k $_v$C $_0$ / W $_e\rho_\beta$)* and the y - intercept equal to *k $_v$ W / Qρ_β*. The Yoon and Nelson equation differs from the modified Wheeler approach by:

-   using data over a range of breakthrough concentrations compared to the Wheeler equation which only uses data of the breakthrough values smaller than 1% of the inlet concentration (C_o),

-   assuming different values for W_e and k_v at varying sorbent masses compared to the Wheeler (and Ackley) approach which assumes that the parameters are independent of the sorbent bed mass.

The graph in Figure 2.4, deviates from linearity at the breakthrough concentration equal to 20% of C_o. This could be due to the partial saturation of the micropores of the carbon and different processes playing a role in the adsorption process. The results are discussed in detail in Chapter 5.
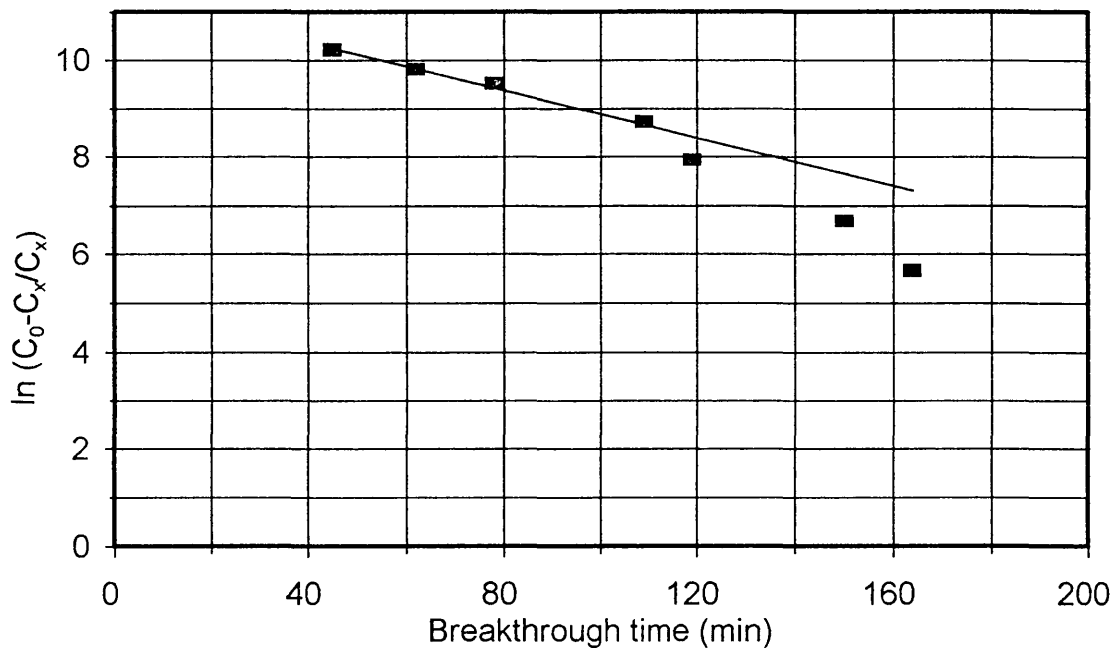
FIGURE 2.4:

Adsorption data for HD vapour on the CC. A plot of ln $(C_0 - C_x)/C_x$ versus t_b shows a linear relationship as predicted by the Yoon and Nelson equation (2.40).

2.6 THE ACKLEY EQUATION

Ackley has proposed a residence time model for describing respirator sorbent beds [32]. The relationship between the breakthrough time and the bed residence time allows correlations of data and predictions of bed performance. The residence time (τ) is equal to the bed depth (b_d) divided by the superficial velocity (V_f) and can thus be expressed in terms of the volume of the sorbent (V_l) and the air flow rate (Q) as follows:

$$\tau = \frac{V_l}{Q} \qquad (2.41)$$

36

The volume of the sorbent is equal to the sorbent weight divided by the bed density. Thus, τ may be expressed as follows:

$$\tau = \frac{W}{Q\rho_\beta}$$

(2.42)

The term can be substituted into equation (2.37) to give the Ackley equation:

$$t_b = \left(\frac{W_e\,\rho_\beta}{C_0}\right)\tau - \frac{W_e\,\rho_\beta}{k_v\,C_0}\ln\left(\frac{C_0 - C_x}{C_x}\right)$$

(2.43)

The graph of the breakthrough time (t_b) as a function of the residence time (τ) is illustrated in Figure 2.5. The equation (2.43) predicts a straight line with the slope equal to $W_e\,\rho_\beta / C_0$, and the intercept equal to $\{-(W_e\,\rho_\beta / C_0\,k_v\,)\}\{\ln(C_0 - C_x)/C_x\}$. The graph sowed a deviation from linearity for the fourth and fifth point representing four and five textile layers. This deviation could be due to a resistance to the air flow through the textile layers. The results are discussed in detail in Chapter 5.

Theoretically these three models should yield the same values for W_e and k_v from the slopes and intercepts of straight line plots of the experimental data. Calculation of these parameters with the Wheeler and Ackley equations showed a high degree of agreement. Values obtained with the Yoon and Nelson equation differed largely from the values. This could be due to the saturation of the carbon. The parameters calculated with the Wheeler and Ackley equation is only done on the initial stage of adsorption, whereas calculations with the Yoon and Nelson equation is done over a longer time period. The discussion of these experimental results is given in paragraph 5.2.

37
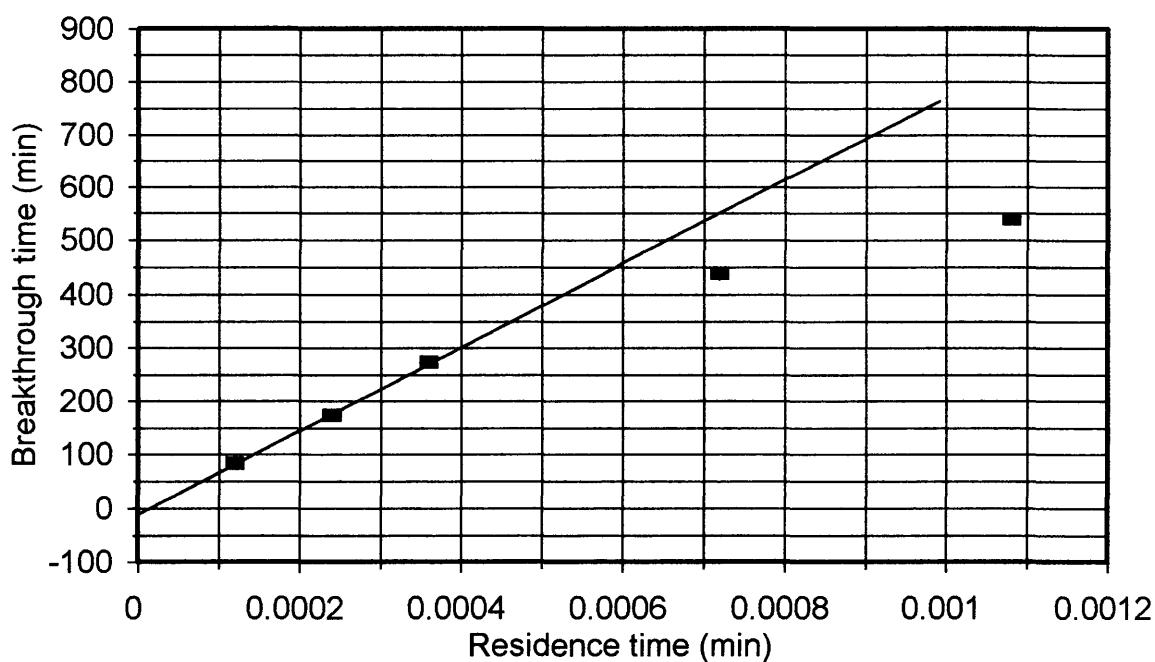
FIGURE 2.5:

Adsorption data for HD vapour on the CC. A plot of τ vs t_b shows a linear relationship as predicted by the Ackley equation (2.43).

C. TRANSPORT MECHANISMS

2.7 PRINCIPLES OF ADSORPTION

Physical adsorption of gases is a surface process but also involves transfer of a molecule from one phase to another. In porous adsorbents, adsorption takes place by different processes:

1.   Mass transfer through the external boundary surface area of the particle, thus external mass transfer.

2.   Internal transfer taking place in the interior of the solid particle or sorbent. The pores are thus characterized by an effective transfer coefficient that can describe the diffusion through the pores. The adsorbate diffuses

38

through the fluid filled pores or solid phase diffusion where transfer takes place via surface diffusion along the pore walls.

3. Adsorption or desorption on the surface at active sites of the adsorbent that transform the adsorbate to its adsorbed state, which can be reversible (physical adsorption), or to a surface complex, which is irreversibly adsorbed (chemisorption).

Adsorption on charcoal is stronger for components with higher molar mass and can be influenced by other characteristics such as unsaturation, or by strong electrostatic forces. The concentration distribution curves of less strongly adsorbed component move through the adsorbent bed more rapidly. Thus, the distribution curve is more elongated. A complicating factor is that exchange adsorption of the stronger bound component takes place, thus influencing the initial concentration distribution. Silov's rule of parallel adsorption-zone-displacement cannot therefore be applied to the description of mixed adsorption zones, and Langmuir's rule that the presence of a second adsorbed component in equilibrium decreases the adsorbed amount of the first component, does not apply either [33].

It was demonstrated that adsorption on the sorbent surface occurs in a relatively short time (10^{-5} s) compared with the time necessary for external mass transfer or diffusion in the pores, which can be in the range of up to a few minutes [34]. Therefore only the first two processes of the above-mentioned are covered in the literature [35].

2.7.1 Intra particle transport: Macropore diffusion

Five distinct mechanisms of transport through the pores were identified in the literature: molecular diffusion, Knudsen diffusion, Poiseuille flow, eddy diffusion and surface diffusion [36]. The effective pore diffusivity is thus a complex quantity which often includes contributions from more than one of the aforesaid mechanisms. The following parameters may play a role in the mass transfer operation, which will influence the above mechanism in controlling the mass transfer to a lesser or greater extent:

39

- the pore structure and thus the composition of the adsorbent;

- the character of the sorbate, whether an organic or inorganic mixture or only one component;

- the concentration of the sorbate;

- the linear velocity of the adsorbate around an adsorbent particle or through an adsorbent bed.

If pore diffusion controls the mass transfer process, the diffusivity *(D_p)* is based on the pore cross-sectional area:

$$J = -\varepsilon_p D_p \frac{\partial c}{\partial x} \qquad (2.44)$$

D_p is influenced by:

- the random orientation of the pores, thus giving a longer diffusion path,

- a reduction in the concentration gradient, which reduces in the direction of flow, and

- the variation in the pore diameter.

The above effects are accounted for by the tortuosity factor *(θ)*:

$$D_p = \frac{D}{\theta} \qquad (2.45)$$

where **D** is the diffusivity under the same conditions but in a straight cylindrical pore.

For straight, randomly orientated cylindrical pores it was shown that *θ* = 2. The tortuosity factors fall within the 2-6 range. However, the tortuosity is usually treated as an empirical constant. The determination of the *θ* factor calls for an

40

in-depth study of the pore shape and size.

a. Molecular diffusion

In molecular diffusion the resistance to flow arises from collisions between diffusing molecules. The effect of the pore is merely to reduce the flux as a result of geometric constraints which are accounted for by the tortuosity factor. Molecular diffusion is dominant whenever the mean free path of the gas (i.e. the average distance travelled between molecular collisions) is small relative to the pore diameter.

If transport within the macropores occurs only by molecular diffusion, the pore diffusivity is given as:

$$D_p = \frac{D_m}{T} \qquad (2.46)$$

where D_m is the molecular diffusivity and may be estimated by the Chapman-Enskog equation which describes the molecular diffusivity of binary gas mixtures:

$$D_m = \frac{0.00158T^{3/2}(1/M_1 + 1/M_2)^{1/2}}{P\sigma_{12}^2\Omega(\varepsilon/kT)} \qquad (2.47)$$

where

	M_1, M_2	-	are the molar mass,
	P	-	is the total pressure (Pa),
	σ_{12}	-	is $\sigma_{12} = \frac{1}{2}(\sigma_1 + \sigma_2)$ the collision diameter from the Lennard-Jones potential (Å),
	Ω	-	is a function of ε/kT where $\varepsilon = \sqrt{\varepsilon_1\varepsilon_2}$ is the Lennard-Jones force constant with k the Boltzman constant.

b. Knudsen diffusion

In small pores and at low pressure the mean free path is greater than the pore diameter, and collisions of molecules with the pore walls occur more frequently than collisions between diffusing molecules. The collision between molecule and pore wall provides the main diffusion resistance and these phenomena are described as Knudsen diffusion or Knudsen flow.

The feature characteristic of the diffusion process is illustrated by a randomness of the collisions and re-emission of the adsorbate molecule into the sorbate stream in a random direction.

Knudsen diffusivity may be estimated from the expression:

$$D_k = 9700\mu \ (T/M)^{1/2} \tag{2.48}$$

where μ -   is the mean pore radius (cm),

T -   is the temperature (K), and

M -   is the molecular mass of the diffusing species.

In the Knudsen regime each species diffuses independently so that the diffusivity does not depend on either composition or total gas concentration. The temperature dependence is slight and D_k is inversely dependent on the square root of the molecular mass.

From the above it follows that both Knudsen and molecular diffusion can control the mass transfer at the same time, i.e. molecular diffusion is dominant in the macropores while Knudsen flow is dominant in the smaller pores. Owing to the dependence of the mean free path on pressure, there will be a transition from molecular diffusion at high pressure to Knudsen flow at low pressures.

c. Surface diffusion

The contribution to the flux from transport through the physically adsorbed layer on the surface of the macropore is referred to as surface diffusion. A significant contribution of the flux is possible because of the high concentration present as adsorbed phase. Thus for surface diffusion to be noticeable significant physical adsorption is necessary. This requires temperatures not too far above the boiling point of the species considered. At high temperatures the thickness of the adsorbed layer decreases and the surface flux becomes relatively small to the flux through the gas phase. Thus direct measurement of diffusion is not feasible since the flux due to diffusion through the gas phase is always present in parallel.

The overall diffusivity is given as:

$$D = D_k + (\frac{1 - \varepsilon_p}{\varepsilon_p}) KD_s \qquad (2.49)$$

d. Poiseuille flow

If there is a difference in total pressure across a particle, then there will be a direct contribution to the adsorption flux from forced laminar flow through the macropores. This is generally negligible in a packed bed since the pressure drop over an individual particle is very small. The effect is usually of greater influence in the direct laboratory measurement of uptake rates in a vacuum system. Thus, the Poiseuille equation shows the equivalent diffusivity as:

$$D = P_a r^2/8 U \qquad (2.50)$$

where P_a -   is the adsorbate pressure (Pa),

    U -   is the viscosity (poise), and

    r -   is the mean pore radius (cm).

2.7.2 Micropore diffusion

Diffusivity is a function of temperature and concentration. In addition, the diameter of the sorbate molecule has a relatively large influence on the activation energy. The van der Waals' radius can be used to calculate the molecular diameter. The molecular shape also plays an important role in the diffusion process. This was illustrated by adsorption of cyclohexane or the linear paraffins for which the van der Waals' radius is much larger than that for the cyclohexane [37].

2.8 KINETICS OF SORPTION

Adsorbents exert three distinct diffusional resistances on mass transfer:

a.   the micropore resistance of a particle, and

b.   the macropore diffusion resistance of the adsorbent, and

c.   for adsorption from a (multi-component) fluid mixture there may be an additional resistance to mass transfer associated with transport through the laminar fluid boundary layer surrounding the particle.

The relative importance of micropore and macropore resistances depends on the ratio of the diffusion time constants, which varies widely depending on the system and conditions. As the time constant is a function of the square of the particle radius, variation of the particle size serves as confirmation of the controlling resistance.

Since adsorption is exothermic and the heat of sorption must be dissipated by heat transfer, there is, generally, a difference in temperature between the adsorbent particle and the adsorbate while sorption is taking place. The significance of this temperature difference depends on the relative rates of mass and heat transfer. Theoretical analysis may show that: in a batch adsorption experiment, it is the dissipation of heat from the external surface of the adsorbent sample, rather than the conduction of heat within the adsorbent, which is generally the rate limiting heat transfer process.

The simplest case to consider is a single microporous adsorbent particle exposed to

a step change in sorbate concentration on the external surface of the particle at time zero. Heat transfer is assumed to be sufficiently rapid, relative to the sorption rate, so that temperature gradients through the particle and between the particle and surrounding fluid are negligible. Representation of a particle equivalent to a sphere is an acceptable approximation, then the transport described by Fick's diffusion equation is:

$$\frac{\partial q}{\partial t} = \frac{1}{r^2}\frac{\partial}{\partial r}\left(r^2 D_c \frac{\partial q}{\partial r}\right)$$

(2.51)

If the diffusivity is constant, then:

$$\frac{\partial q}{\partial t} = D_c\left(\frac{\partial^2 q}{\partial r^2} + \frac{2}{r}\frac{\partial q}{\partial r}\right)$$

(2.52)

where D_c - is the intra crystalline diffusivity,

$q(r,t)$ - is the adsorbed phase concentration.

If diffusivity depends on concentration, the approximation is still acceptable, provided that the uptake curve is measured over a small differential change in adsorbent phase concentration.

If the uptake of sorbate by the adsorbent is small relative to the total sorbate introduced, the ambient sorbate concentration will remain constant (essentially) and the initial and boundary conditions are given by:

$$q(r,0) = q_0^1, \ q(r_c,t) = q_0, \ \left.\frac{\partial q}{\partial r}\right|_{r=0} = 0$$

(2.53)

The solution for the uptake curve is given by:

45

$$\frac{\bar{q} - q_0^1}{q_0 - q_0^1} = \frac{M_t}{M_\infty} = 1 - \frac{6}{\pi^2} \sum_{n=1}^{\infty} \frac{1}{\pi^2} exp\left(-\frac{n^2 \pi^2 D_c t}{r_c^2}\right) \qquad (2.54)$$

where $\bar{q}$ (t) is the average concentration through the particle, defined by:

$$\bar{q} = \frac{3}{r_c^3} \int_0^{r_c} q r^2 dr \qquad (2.55)$$

where M_t / M_∞ -   is the fractional approach to equilibrium.

Equation (2.54) converges rapidly as $t \to \infty$ since the higher terms of the summation become very small. For fractional uptakes greater than 70% only the first term is retained to give:

$$1 - \frac{M_t}{M_\infty} \approx \frac{6}{\pi^2} exp\left(-\frac{\pi^2 D_c t}{r_c^2}\right) \qquad (2.56)$$

As $t \to \infty$ a plot of $ln(1 - M_t / M_\infty)$ versus t should be linear with the gradient equal to $\pi^2 D_c / r_c^2$ and the y-axis intercept equal to $ln(6 / \pi^2)$. Such a plot provides a simple method for checking conformity to the diffusion equation and determining the diffusion time constant.

When heat transfer is controlling, the uptake curves commonly show a rapid initial uptake followed by a slow approach to equilibrium. The observation of a distinct break

46

in an experimental uptake curve provides a useful clue that heat transfer resistance may be important. If the process is substantially isothermal, the intercept of such a plot ($ln [1 - M_t / M_\infty]$ versus t) should be $ln (6 / \pi^2)$, and a significant deviation from this value can provide useful evidence of the intrusion of heat transfer effects. Isothermal behaviour is obtained when the heat transfer coefficient is infinitely high (low adsorbate concentration) or when there is an infinitely large adsorbent capacity. When diffusion is rapid, the kinetics of adsorption are controlled entirely by heat transfer. Therefore, a variation of concentration of the adsorbate will show the influence on the heat transfer coefficient. Variation in the configuration of the adsorbent provides a convenient experimental test for heat transfer and bed diffusion resistances.

Adsorption in large pores is relatively slow and the uptake is controlled by isothermal diffusion and is independent of the quantity adsorbent used. In the smaller pores heat effects become significant and deviate from the isothermal curve [38].

For fast diffusion processes the transport is controlled by heat transfer. Uptake curves are independent of pore size but vary with sample size due to changes in the effective heat capacity and external area to volume ratio (A/V).

Figure 2.6 shows the theoretical uptake curve calculated according to equation *(2.56)* with the gradient equal to $-\pi^2 D_c / r_c^2$ and the intercept equal to $ln (6/\pi^2)$. Significant deviation from this value can provide evidence of intrusion of heat effects. Increased thermal effects become increasingly important, especially at high sorbate concentrations.

47
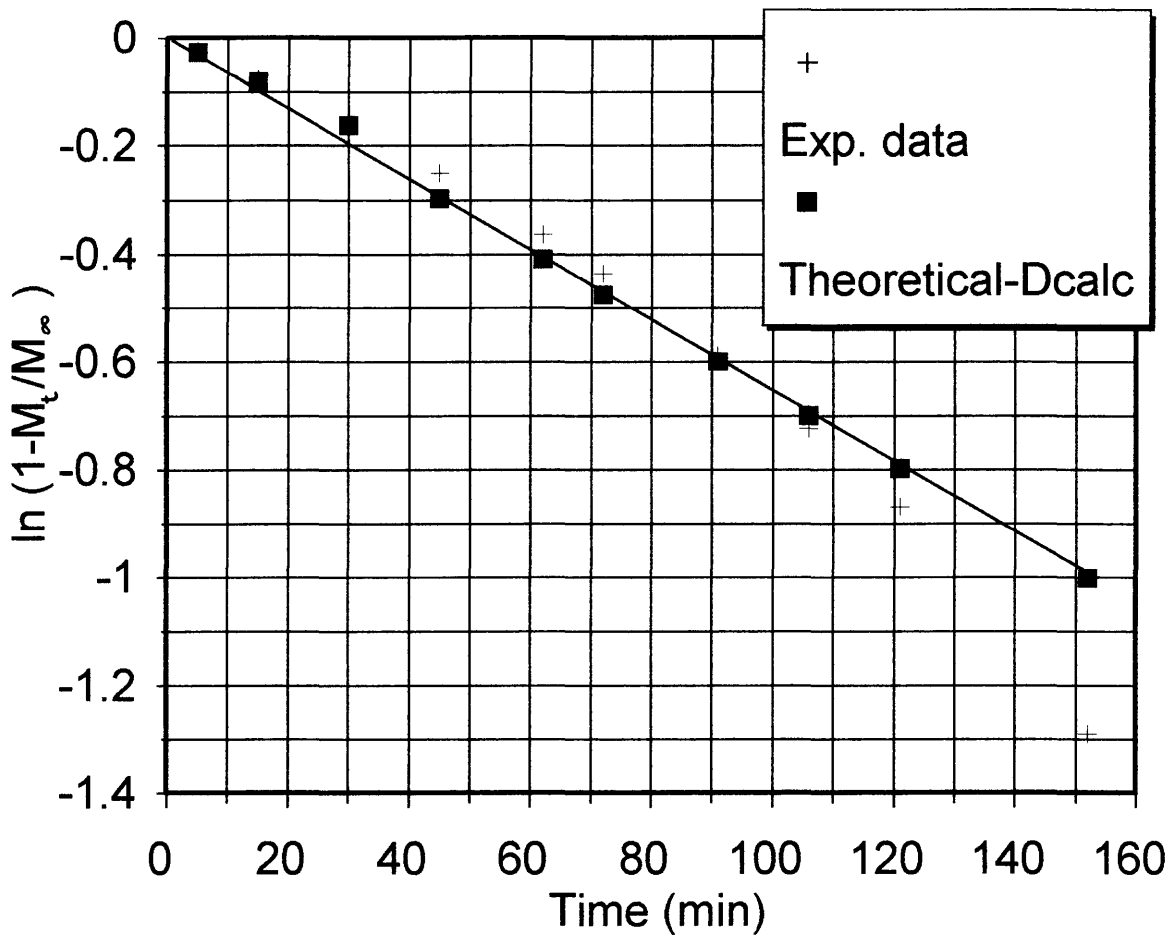
FIGURE 2.6:

Experimental and theoretical uptake curve calculated according to equation

(2.56). The data used, were obtained with the CC textile at the test conditions:

40 °C, 124 μg HD/l, and an air velocity of 0.50 cm/s.

48

REFERENCES

1. J. W. Patrick, Ed., *"Porosity in Carbons"*, Edward Arnold, London, UK, 1995. p19.

2. C. Pierce, J. Willey and R. Smith, *J. Phys. Chem.*, 53, 669, 1949.

3. F. London, *Z. Physics*, 63, 245, 1930.

4. J. W. Patrick, Ed., *"Porosity in Carbons"*, Edward Arnold, London, UK, 1995. p49.

5. S. Tanada, T. Nakamura, M Xiaohong and S Shinoda, *"Adsorption Characteristics of Trichloroethylene and 1,1,1-Trichloroethane onto Activated Carbon Fiber in Gaseous Phase"*, Bull. Environ. Contam.Toxicol., 49,1992.p112

6. S. Gregg and K.S.W. Sing, *"Adsorption, Surface Area and Porosity"*, Academic Press, London. 1982. p2.

7. H. Marsh, *"Adsorption Methods to study Microporosity in Coals and Carbons-A Critique"*, Carbon, 25.1,1987. p49.

8. S. Gregg and K.S.W. Sing, *"Adsorption, Surface Area and Porosity"*, Academic Press, London. 1982. p2.

9. S.J. Greg and K.S.W. Sing, *"Adsorption, Surface Area and Porosity"*, 2nd Ed, Academic Press, London, UK, 1995. p3.

10. T. Vermeulen, *"Separation by Adsorption Methods"*, Advances in Chemical Engineering, Vol.2, 1958.p147.

11. S.J. Greg and K.S.W. Sing, *"Adsorption, Surface Area and Porosity"*, 2nd Ed, Academic Press, London, UK, 1995. p3.

12. J.W Patrick, Ed., *"Porosity in Carbons"*, Edward Arnold, London, UK, 1995. p54.

13. S.J. Greg and K.S.W. Sing, *"Adsorption, Surface Area and Porosity"*, 2nd Ed, Academic Press, London, UK, 1995. p5.

14. C. Kemball, *"Entropy of Adsorption"*, Advances in Catalysis, Academic Press, NY,1956. p233.

15. J. Crank, *"The Mathematics of Diffusion"*, Clarenden Press, Oxford, 1975.

p354.

16. J.H. de Boer, "*The Dynamic Character of Adsorption*",2nd Ed., Clarendon Press, Oxford, UK, 1968.p35.

17. J.W Patrick, Ed., *"Porosity in Carbons"*, Edward Arnold, London, UK, 1995. p54.

18. S. Gregg and K.S.W. Sing, "*Adsorption, Surface Area and Porosity*", 2nd Ed., Academic Press, London. 1982. p42.

19. S. Gregg and K.S.W. Sing, "*Adsorption, Surface Area and Porosity*", Academic Press, London. 1967. p204.

20. S. Gregg and K.S.W. Sing, "*Adsorption, Surface Area and Porosity*", 2nd Ed., Academic Press, London. 1982. p94.

21. J. W. Patrick, Ed., *"Porosity in Carbons"*, Edward Arnold, London, UK, 1995. p33.

22. Ibid. p34.

23. G.Wood, J.A.Rehrmann and C.J. Karwacki, *"Estimating Micropore Volumes of Activated Carbonaceous Adsorbents for Organic Chemical Vapours"*, "CARBON 96" New Castle, UK, 1996.

24. J. W. Patrick, Ed., *"Porosity in Carbons"*, Edward Arnold, London, UK, 1995. p37.

25. Ibid. p38.

26. S.J. Gregg and K.S.W. Sing, *"Adsorption, Surface Area and Porosity"*, 2nd Ed.,Academic Press Ltd., London, UK.1995.p195.

27. S. Lowell and J.E.Shields, "*Powder Surface Area and Porosity*", 2nd Ed.,Chapman and Hall, London, UK, 1984. p61.

28. "*Calculating the Pore Size Distribution from the Experimental Isotherm*",User's Guide, Micromeritics, 1993. p9.

29. L.A. Jonas and J.A. Rehrmann, "*The Rate of Gas Adsorption by Activated Carbon*", Carbon, 1974, <u>12</u>. p23.

30. G.O. Wood and E.S. Mayer, "*A Review of the Wheeler Equation and Comparison of its Applications to Organic Vapour Respirator Cartridge Breakthrough Data*", Am. Ind. Hyg. Assoc. J., 1989, <u>50</u>. p400.

31. B. Kaluderović, B. Stojanović, M. Polovina, B. Babić and M. Jovašević, *"The Kinetics of Adsorption of Carbon Tetrachloride from Air Mixtures by Activated Carbon Cloth - the Application of Theoretical Models"*, J. Serb., Chem., Soc., 61, 6, 1996. p461.

32. M. W. Ackley, *"Residence Time Model for Respirator Sorbent Beds"*, Am. Ind.Hyg. Assoc. J., 46, 11, 1985. p679.

33. M. M. Dubinin, *"Adsorption of Gases and Vapors in Micropores"*, Oxford Press, UK. 1967. p5.

34. D.M. Ruthven, *Principles of Adsorption and Adsorption Processes"*, John Wiley & Sons, NY, 1984. p.128.

35. Ibid. p133.

36. Ibid. p134.

37. Ibid. p140.

38. D. M. Ruthven, *"Principles of Adsorption and Adsorption Processes"*, John Wiley and Sons, NY, 1984. P191.

CHAPTER 3

EXPERIMENTAL DESIGN AND DETECTION PROCEDURES

3.0 INTRODUCTION

Breakthrough test methods, used for evaluation of the protection time against hazardous chemicals, were studied. Various nonquantitative and quantitative methods are used internationally [1]. A method, *"The Mustard Gas Droplet Test, FINABEL Test"*, was studied and implemented to do quality assurance testing on the chemical textiles used for the manufacture of protective suits [2]. This method is a static test, which implies that no air movement is involved. The dynamic tests consist of air movement through or over the textile, while it is also possible to control various parameters, e.g. air velocity, challenge concentration of the chemical vapour and relative humidity. It is also very important that the test method used simulates as closely as possible the actual conditions under which it will be used. For this reason two methods were developed by the author: a dynamic breakthrough method, which is used to study the characteristics of the activated charcoal impregnated into the textile, and an aerodynamic test method to study the characteristics of the textile system, which usually consists of at least two layers, the outer (woven) and inner (charcoal containing) layers.

3.1 CHEMICALS

Analytical grade reagents were used in this study.

3.1.1 Solvents

Ethyl alcohol, CH_3-CH_2-OH (preparation of GC-calibration standards)

3.1.2 Gases

Gas chromatograph operating gases:

High purity nitrogen, N_2 99,9999% pure (carrier gas).

High purity hydrogen, H_2 99,99% pure (detector gas).

High purity synthetic air, 21% O_2 + 79% N_2(detector gas).

Standard grade nitrogen, N_2 99,99% pure (test setup).

Liquid nitrogen, N_2 (cryogenic cooling).

3.1.3 Challenge chemicals

bis(2-chloroethyl)sulfide, $(Cl-CH_2-CH_2)_2S$, (HD), 98% pure.

Physical properties of HD:

d_{20}^4 = 1.274 kg/l

Molecular mass = 159 g/mole

Freezing point = 14 °C

Boiling point = 227.8 °C

Vapour pressure = 10.3 mm Hg at 20 °C

Volatility = 610 mg / m^3 at 20 °C and 2851 mg / m^3 at 40 °C

3.2 TEXTILES

The textiles used in this study can be grouped into three different technologies, namely CC, PUCP, and C-spheres.

3.2.1 Charcoal cloth (CC)

This textile consists of a nonwoven carbon carrier. The current method used for the manufacture of these textiles favours high production rates and disposable systems. Polyamide or polyester fibres constitute the major part of the nonwoven matrix. Therefore, organic vapours will not be adsorbed into the body of the fibre and will either evaporate quickly or be attracted to and held by the activated carbon. The carbon (50 ± 10 g / m^2) is used as an extremely fine powder (96% having a dimension of less than 25 microns) which requires a minimum of binder to bind the carbon to the fibres. The minute dimensions of the particle also ensure rapid adsorption of vapour from the gaseous phase.

This can be further optimised by choosing an activated carbon with the correct ratio of macro-, meso- and micropores. It was assumed that a predominantly

53

microporous structure will ensure enhanced adsorption **[3]**. However, it is vital that the organic vapour molecules can penetrate the interstices of the activated carbon structure with ease, otherwise the vapour will pass the carbon en route for the skin surface. The optimum ratio of pore distribution will ensure the most effective rapid distribution and adsorption. Another aspect in efficient adsorption of vapour is the use of carbon particles of minimum size so that the path length for adsorption on the carbon surface is kept to a minimum.

Careful choice of the binder chemistry helps to minimise the effect of pore blocking and enhances the shelf life of the final product. In the textile studied, the carbon is impregnated from the one side of the nonwoven material only, the other surface being treated with an oil and water repellent finish.

The outer layer is a two-by-two twill fabric, using a polyamide warp thread and a modified acrylic, Teklan, in the weft. The weave structure of a twill fabric is such that the warp thread predominates on one side of the fabric and the weft thread on the other. A shower proofing silicone treatment is applied to the outer layer.

An average service wear life of 28 days is obtainable, although the wear life could vary to as long as 150 days, depending on the duties of the wearer. These levels are considered adequate for a disposable clothing item.

The biggest disadvantage of this material is that it has low physical strength and is easily damaged through friction and tearing. Thus the textiles are usually laminated to a textile with high physical strength, e.g. polyamide or polyester, which unfortunately adds to the heat load of these textiles.

3.2.2 Polyurethane foam rubber impregnated with charcoal powder (PUCP)

The foam rubber system consists of a two-layered textile:

- an inner layer of light nylon tricot cloth bonded to a 2 mm fully reticulated

polyurethane foam sheet. The foam is impregnated with active carbon approximately 180 ± 20 g/m^2;

- an outer layer of heavy-duty corespun polyester cotton, in which polyester is the core and cotton the wrapping. The outer layer has a mass of approximately 180 g/m^2, and is water and oil repellent treated with "Quarpel".

a. Inner layer

The foam is manufactured from an open cell polyurethane. The backing on the polyurethane and laminated to the polyurethane is a knitted 100% polyamide material. The mass of the backing material is 40 ± 4 g/m^2. The polyamide is laminated to the foam layer by thermal fixing with a hot-air process. The mass of the inner layer laminate is 200 ± 30 g/m^2. The inner layer is 1.9 mm $\pm$ 0.3 mm thick.

At first sight polyurethane appears to be an ideal substrate to impregnate with carbon. Very high loading levels of up to 200 g/m^2 can easily be achieved and the added binder gets ample opportunity to attach the carbon to the foam structure, thus reducing the loss of carbon from the foam matrix. In operational use the impregnated foam system has however major disadvantages.

Polyurethane foam has high insulation properties and a suit made from this carrier results in a product with high physiological load. A person wearing this suit can only survive for approximately 60 minutes while conducting work at a medium work rate (180 W) before displaying signs of heat stress [4].

b. Outer layer

The material is woven from corespun polyester:cotton (50:50) yarn. The weave structure is a 2/1 twill. The mass of the outer layer is 169 ± 8 g/m^2. The breaking strength of the outer layer is high in order to protect the inner layer from physical damage. The outer layer is also impregnated to display infrared

55

remission and is further impregnated to display water and oil repellency. The outer layer is also impregnated to have flame retardancy characteristics.

The biggest disadvantages of this textile are:
- high insulation, which causes a high physiological load,
- adsorbs water to a high degree, and
- the foam depolymerises after a few years, therefore decreasing the shelf life.

3.2.3. Spherical carbon (C-spheres)

In these system, activated carbon spheres, 0.5 to 1 mm in diameter, are point bonded in a predetermined pattern onto one surface of a polyamide, polyester or mineral fibre fabric. This method of impregnation gives rise to almost a millimetre of adsorbing carbon to remove vapour from the air [5,6].

This is a most effective protection system but it takes time for the vapour to penetrate the spheres and adsorb onto the carbon. Thus approximately 200 ± 30 g/m^2 of activated carbon are required, compared with the 50 g/m^2 of carbon in an impregnated nonwoven system, in order to obtain the same rate of adsorption from the diffusing contaminated air. The total capacity of the bonded sphere type system for organic chemicals is about three times the level of the impregnated nonwoven textile. However, the total micropores structure restricts penetration of carbon particles by organic vapour molecules and the adsorption phenomenon is delayed and minimised. This is not usually the major consideration. Additional carbon adds to the weight, heat stress and cost.

A common weakness of this type of textile is that it must be stored under a vacuum as the active surface area is easily contaminated by adsorption of organic vapours.

56

3.3 ELECTRON MICROSCOPE STUDIES

A scanning electron microscope from the Botany Department, University of Pretoria, was used to conduct the studies of porosity of the carbon impregnated in the textiles.

3.4 ACTIVE SURFACE DETERMINATION

A textile sample (approximately 4 cm^2) was dried in an oven at 70°C ± 5°C until constant mass was reached. The textile was cut into small pieces to fit into the sample holder of the BET (Model ASAP 2010). 0.4 g was weighed out accurately to four decimal places by cutting small pieces of the textile and placing the pieces into the sample holder through a funnel The funnel was used to ensure that no carbon powder from the textile was lost. The holder was closed with the air tight fitting which allows for a vacuum to be drawn on the sample holder through a stainless steal ball valve. The sample was then connected to the degassing port of the ASAP 2010.

Degassing was done by placing a heating mantle around the sample holder and drawing vacuum on the sample overnight at 25°C. After 16 hours of degassing the active surface was determined by adsorption of N$_2$ at 77 K.

The degassing was done at ambient temperature as the textiles are used at these temperatures and degassing at a higher temperature could give a too high surface area and micropore volume, which is not available for adsorption at normal ambient temperatures. The degassing could not be done at temperatures higher than 70°C as the polyurethane and binders used for impregnation of the carbon would degrade and possibly poison the carbon.

3.5 BREAKTHROUGH TEST APPARATUS

3.5.1 The dynamic breakthrough test setup

Experimental setups used by different international institutes were studied [7]. These test setups and parameters are illustrated in Table 3.1.

57

TABLE 3.1:

Different dynamic test setups

VAPOUR BREAKTHROUGH TEST: DIFFERENT EXPOSURE METHODS AND CONDITIONS					
TEST PARAMETERS	USA (CSL)	NATO (MUNSTER)	NATO (TNO)	FHG (CGFT)	RSA (PTN)
CHALLENGE METHOD	Air drawn through textile	Air blown over textile	Air blown over textile	Air blown through textile	Air blown through textile
FLOW	1 l N_2/min	10 000 l air/h	5600 l air/h	24 ml air/min	45 ml N_2/min
VELOCITY (cm/s)	0.17	0.075	0.3875	0.509	0.50
TEMPERATURE (°C)	32.5	30	20	30	20-40
RELATIVE HUMIDITY (%)	80	80	ambient	dry	dry
SAMPLE SIZE (cm²)	100	4	1.5	0.785	1.5
DETECTOR	specific	DB-3	GC	photo-ionisation	TCT-GC-FID
DETECTION LIMIT (μg / cm³)	<0.5	<0.1	<0.1	0.001	0.009
TEST DURATION (h)	6-24	6	6	24	till breakthrough
SOLVENT RESERVOIR	20ml/60min	2.5ml/45min	2.5ml/45min	none	none
CONCENTRATION (μg/l)	20	20	20	80.5	20-124
CHEMICAL COMPOUND	organo-S-compound	organo-S-compound	organo-S-compound	organo-S-compound	organo-S-compound
DOSES INFLUENT AFTER 6h (μg)	7200 (~72 μg/cm²)	1200 mg (86 - 120 μg/cm²)	672mg (86 - 179 μg/cm²)	695.5 (886 μg/cm²)	324 (216 μg/cm²)
PENETRATION LIMIT	<4 μg/cm²	CT<500 mg.min/m³	CT<500 mg.min/m³	time elapsed for C = 0.01.C_0	time elapsed for C = 0.01.C_0

a. Procedure

Little information was available on the test setups. A setup was therefore designed and built to suit local climatic test conditions. This test setup is illustrated in Figure 3.1.
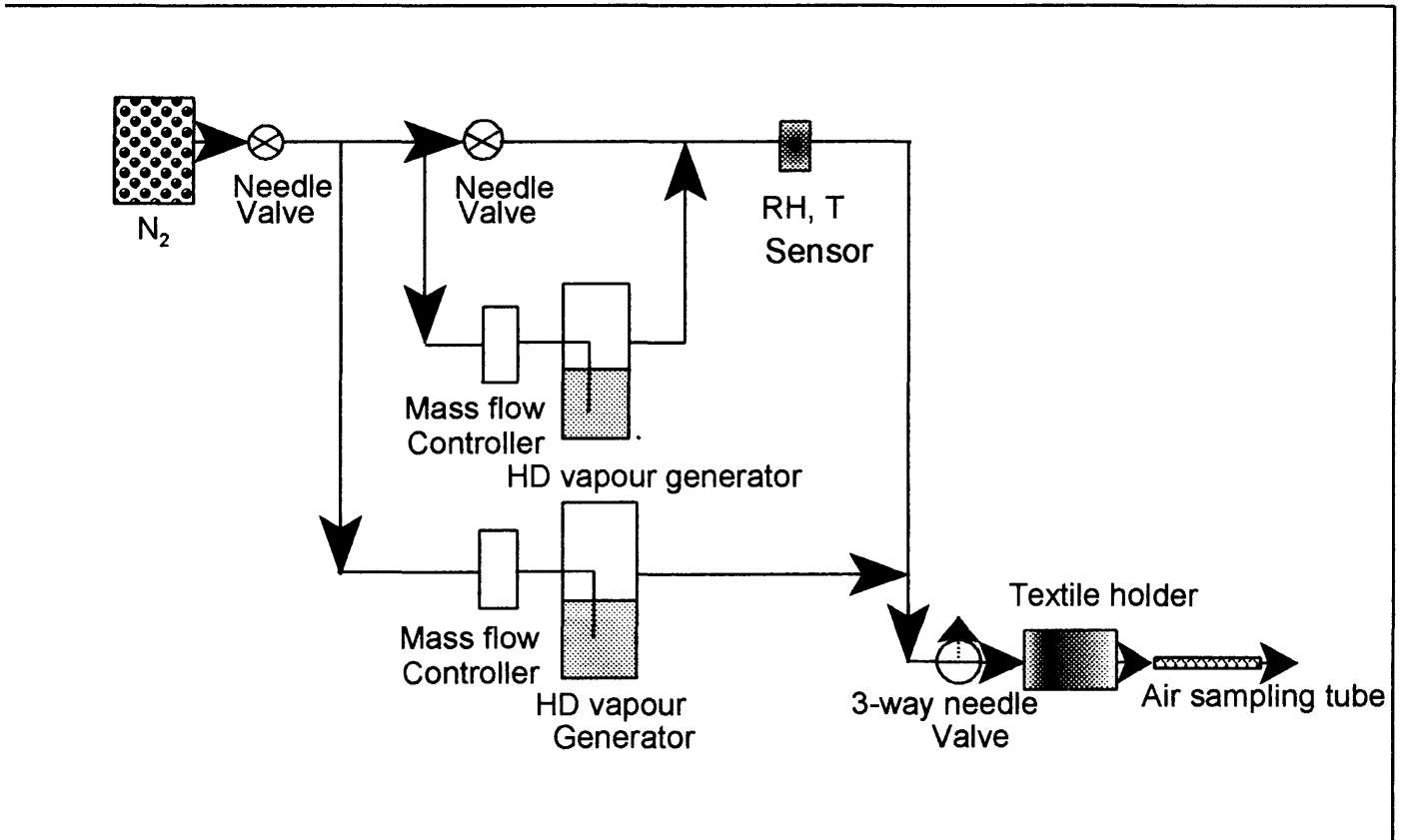
FIGURE 3.1:

Dynamic breakthrough test setup.

The exposed area of the textile was 1.5 cm ^{2}. The flow through the system was varied between 13 cm^3 / min and 45 cm^3 / min which is equal to a velocity of 0.15 cm / s and 0.50 cm / s respectively.

b. Standard atmosphere

A standard atmosphere of organic vapour was prepared by means of a dynamic flowthrough vapour generator. Standard grade nitrogen (N_2 99,99% pure) was blown through a 1/8th inch (outer diameter) stainless steal tube at a pressure of 100 kPa. The tube was turned into a spiral of approximately 10 circumferences with an inner diameter of approximately 5 cm. This spiral was immersed into a waterbath at the set temperature, to ensure that the nitrogen was at the same temperature as the rest of the test setup, e.g. the organic liquid in the vapour generator. The nitrogen was spilt into 2 or 3 "air" streams, depending on the agent concentration needed. The main nitrogen stream bypassed the vapour generator(s) and was mixed with the one or two nitrogen streams after passing through the vapour generator(s).

The second (and third) nitrogen stream was blown through a vapour generator(s). The flow through the vapour generator, and thus the vapour concentration, was controlled by a mass flow controller(s). A vapour generator consisted of a 40 ml glass tube sealed off at the top. The inlet and outlet tubes at the top were 15 mm long each, with an inner diameter of 4 mm and an outer diameter of 6 mm. Nitrogen was blown in at the inlet tube, which extended to the bottom of the generator where it opened into the generator through a sintered glass tube (No. 1 porosity) to ensure efficient gas dispersion through the organic liquid in the generator. The nitrogen was dispersed through the liquid. The nitrogen carrying vapour exited the vapour generator through the outlet tube and was mixed with the bypass nitrogen before the vapour entered the in-line filter holder containing the textile sample.

Before the vapour stream was blown through the in-line filter holder it could be

60

channelled either through an air sampling tube for calibration purposes or through the in-line filter holder containing the textile sample by using a three-way valve. This valve was introduced to aid switching between the calibration point and the in-line textile sample holder.

c. Vapour calibration in the test setup

A three-way valve was introduced into the nitrogen line for calibration and safety purposes. During the calibration the valve was turned in the direction of the air sampling tube. The sampling tube was connected to the valve with a specially manufactured tube holder. The holder was machined from stainless steal and an O-ring was fitted inside the holder to ensure a gas-tight seal onto the glass sampling tube. The vapour concentration in the setup is calibrated by sampling the nitrogen containing the vapour from the setup with an air sampling tube.

The air sampling tube (15 cm in length) is made of glass, with an inner diameter of 3.5 mm and an outer diameter of 6 mm. The tube is filled with 100.0 mg Tenax TA (20 - 35 mesh) with a plug of glass wool at both ends of the Tenax bed.

The water in the waterbath was heated with a heating element and the temperature was controlled with a thermostat. The temperature of the waterbath was also measured with a mercury thermometer. The regulator on the nitrogen cylinder was opened to a pressure of 100 kPa and the three-way valve on the outlet of the test setup turned towards the sampling tube. The nitrogen flow through the total test setup was set to the desired flow with a calibrated needle valve. The flow through the vapour generator was set on the mass flow control box and the flow through the controller, and thus the vapour generator, was read as a percentage of the total flow from the digital controlled readout. The total flow through the test setup was measured with an electronic flowmeter. Proper functioning of the electronic flowmeter was ensured by regularly checking the flow with a soap bubble flowmeter. After the temperature of the waterbath had stabilized, the flow was checked again.

61

After the concentration generated is calibrated, the three-way valve is turned and the N_2 is blown through a textile sample which is placed in an in-line filter holder and connected in the N_2 stream. The challenge area is 1.5 cm^2. The superficial velocity of the N_2 through the textile was varied between 0.50 cm/s and 0.15 cm/s.

3.5.2 The aerodynamic breakthrough test setup

A study of the effect of different challenge methods on the protection (or breakthrough) measurements obtained with the different textiles, showed that different challenge methods influenced the protection times of the different textiles.

The three different textiles were used for the evaluation of a different chemical challenge method: the aerodynamic method on the adsorption rate constant and thus the protection offered by the textiles. This method was developed specifically to simulate the application of the textile more realistically than for example with the dynamic test, which can only be used in comparative studies to evaluate the quality of the carbon and impregnation method.

The aerodynamic test method was a variation of the method described by Klotz [8]. This method was developed to simulating the real method of exposure more accurately. The method characterizes the individual's body and the clothing system by geometry, air permeability, vapour penetration efficiency and vapour deposition.

HD in vapour form was used to evaluate the textiles. Breakthrough was detected with the same method as that used with the dynamic method.

Results obtained with the aerodynamic test method were compared with the dynamic breakthrough results.

62

Concerns regarding hazardous chemicals in the workplace and on the battlefield motivated efforts to model the protective capacity of permeable clothing against aerosols and to identify the physical mechanisms involved in aerosol protection by permeable clothing systems. The modelling effort has produced a physical predictive model for the processes of aerosol penetration and deposition associated with permeable garment systems. The model calculates air flow, aerosol penetration and deposition both within the fabric and on a cylindrical surface beneath the fabric. Although the model was developed for an aerosol, with a few alterations it can also be applied to vapour penetration through a permeable textile.

Vapour penetration of the fabric is used to calculate the vapour concentration between the fabric and the cylinder and the vapour adsorbed in the charcoal. Using the airflow between the fabric and the cylinder, the model calculates the vapour on the cylinder surface, which provides an estimate of the skin contamination, while the vapour adsorbed in the textile/garment provides an estimate of garment contamination.

The model is illustrated in Figure 3.2 **[9]**. The distance between the fabric and the surface of the solid cylinder surface, ΔR, is called the gap. This geometry allows flow into and out of the fabric.

63
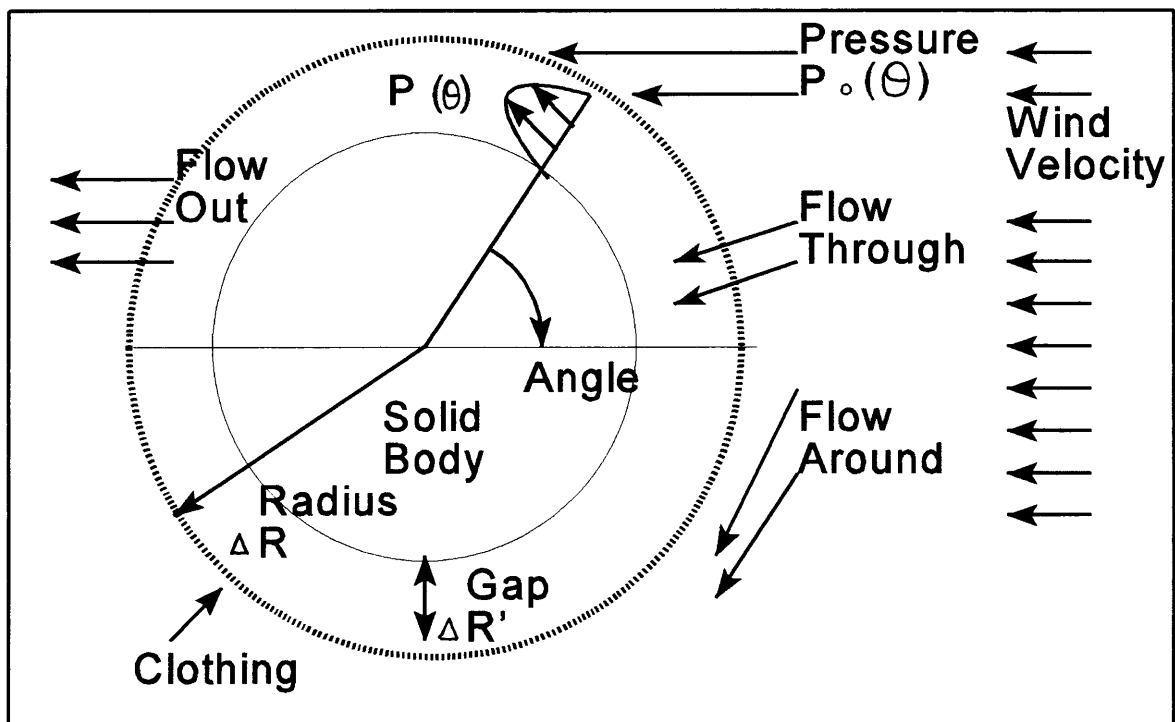
FIGURE 3.2:

Model of air flow through the textile in the aerodynamic test setup.

With the geometry, external pressure distribution, and permeability of the fabric, Γ, the air flow through a fabric is calculated. Permeability is the ratio of the velocity of air flow into the fabric surface to the pressure drop across the fabric. The velocity of flow through the fabric is determined by the difference between the pressure outside the fabric, $P_o(\theta)$, and the pressure in the gap, $P_i(\theta)$. The normal velocity entering the permeable layer (face velocity) is:

$$V_n\theta = \Gamma(P_o(\theta) - P_i(\theta))$$

(3.1)

For clothing geometries the thickness of the fabric layer and the gap are generally much smaller than the overall radius, thus radial dependence of the pressure inside the gap is neglected.

Once in the gap, air flows around the cylinder, until the internal pressure is greater than the external pressure. Then the air flows out, through the textile.

a. *Vapour deposition*

Vapour deposition processes are quantitatively expressed by the deposition velocities, V_d, which is the speed with which a vapour moves into the surface. The deposition velocity can be measured by dividing the mass deposited per unit area, M_d, by the time-integral of the vapour concentration of exposure, CT, as

$$V_d = \frac{M_d}{CT}$$

(3.2)

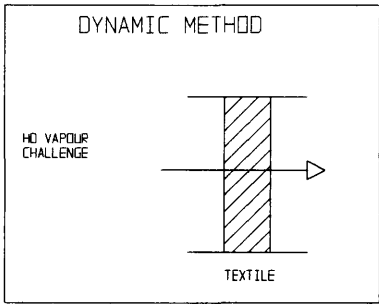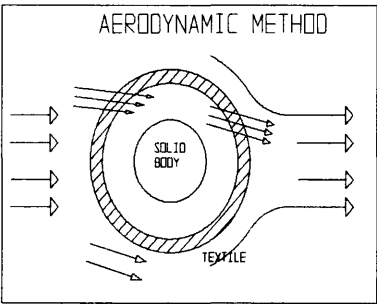Thus the mass that will deposit on a surface, per unit area may be expressed as follows:

$$M_d = V_d \cdot CT$$

(3.3)

65
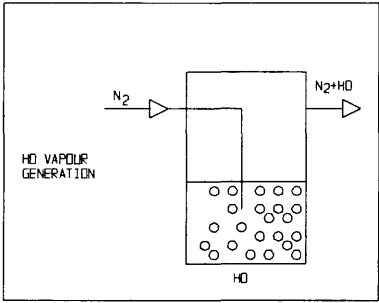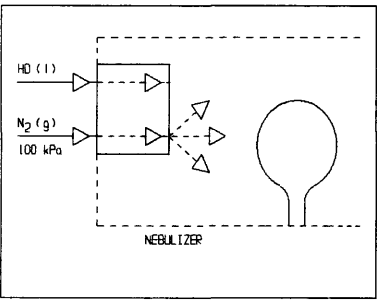
b. Experimental procedures

The differences in vapour generation and challenge methods of the dynamic and aerodynamic test methods are illustrated in Table 3.2:

TABLE 3.2:

Differences between the dynamic and aerodynamic test methods

	Dynamic Method	Aerodynamic Method
HD Vapour Challenge		
HD Vapour Generation		
HD/air velocity through textile	Set at predetermined velocity	A function of challenge air velocity (V_n) and air permeability of textile
Control of HD conc.	Mass flow controller in N_2 line	Peristaltic pump controlling HD flow rate
Monitoring/Sampling	Air sampling tube with Tenax TA 20 - 35 mesh (100 mg)	Air sampling tube with Tenax TA 20 - 35 mesh (10 mg)
Detection/Analysis	Thermal adsorption cryogenic trapping GC - FID	Thermal adsorption cryogenic trapping GC - FID

66

TABLE 3.2: (cont.)

Differences between the dynamic and aerodynamic test methods

	DYNAMIC METHOD	AERODYNAMIC METHOD
Textile evaluation	1 - 5 layers	1 layer
Test temperature (°C)	20 and 40°C	22°C
Test concentration (g/cm³)	124×10^{-9} and 20×10^{-9}	124×10^{-9}
Superficial velocity (cm/s)	0.50 and 0.15	$V_n = 2.3$ m/s (13.2 cm/s - 10.6 cm/s*)

* Velocity of air permeating through textile.

c. Aerodynamic test setup

A dynamic method and an aerodynamic method were used in which the challenge method of organic chemical to the textile differs greatly. The aerodynamic test setup is illustrated in Figure 3.3.

67
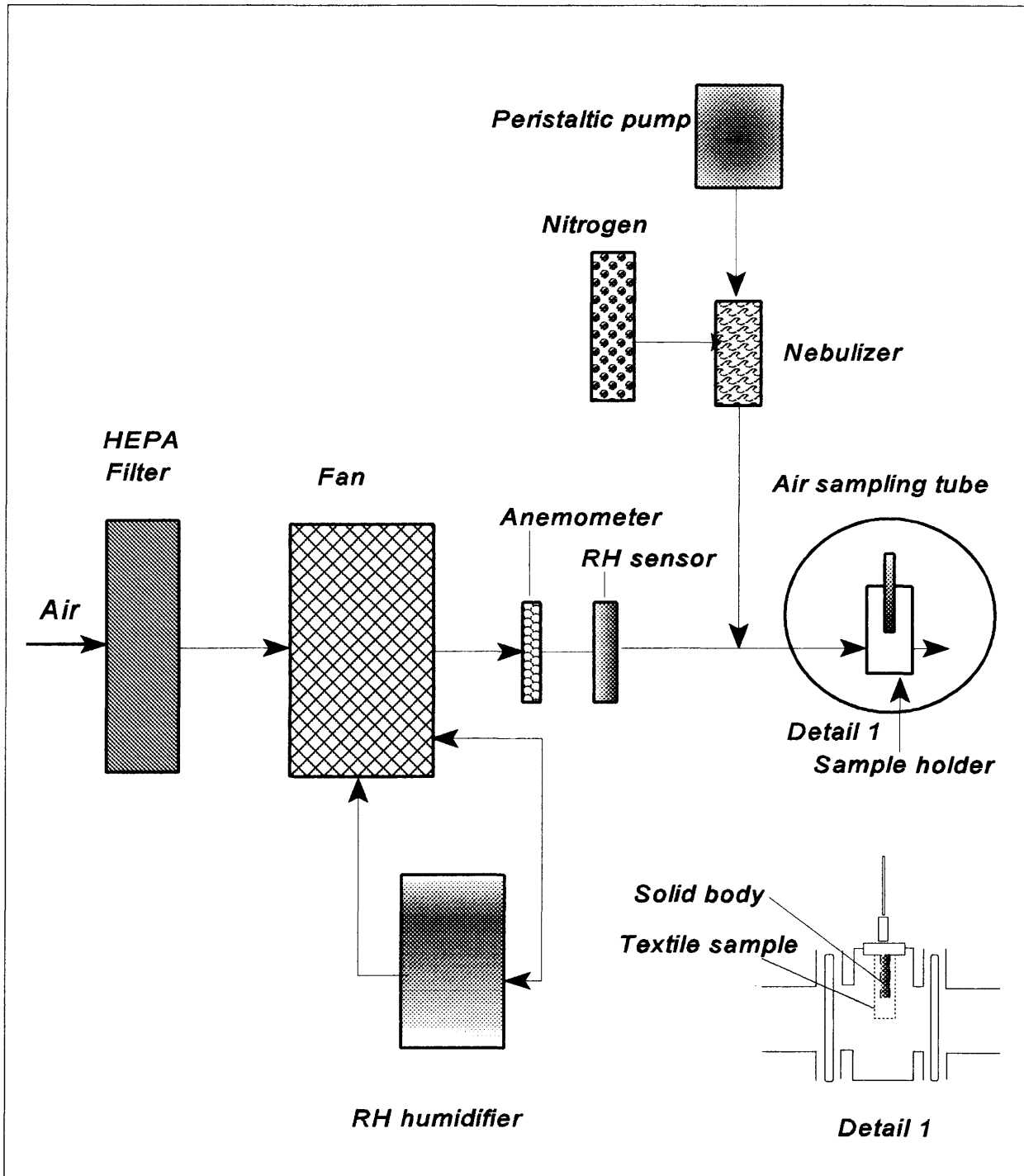
FIGURE 3.3:

Aerodynamic test setup.

3.5.3 Results and discussions

a. Dynamic test method

Textiles were exposed to HD vapour and the breakthrough curves for the different textiles were determined for one to five textile layers *(W)*. The results are displayed in Figures 3.4, 3.5 and 3.6.

FIGURE 3.4:

Breakthrough curves for the PUCP textiles with the dynamic test method at the test conditions: 40 °C, 124 μg HD/l, and an air velocity of 0.50 cm/s (1, 2 and 3 layers represent the number of the textile layers used).

69
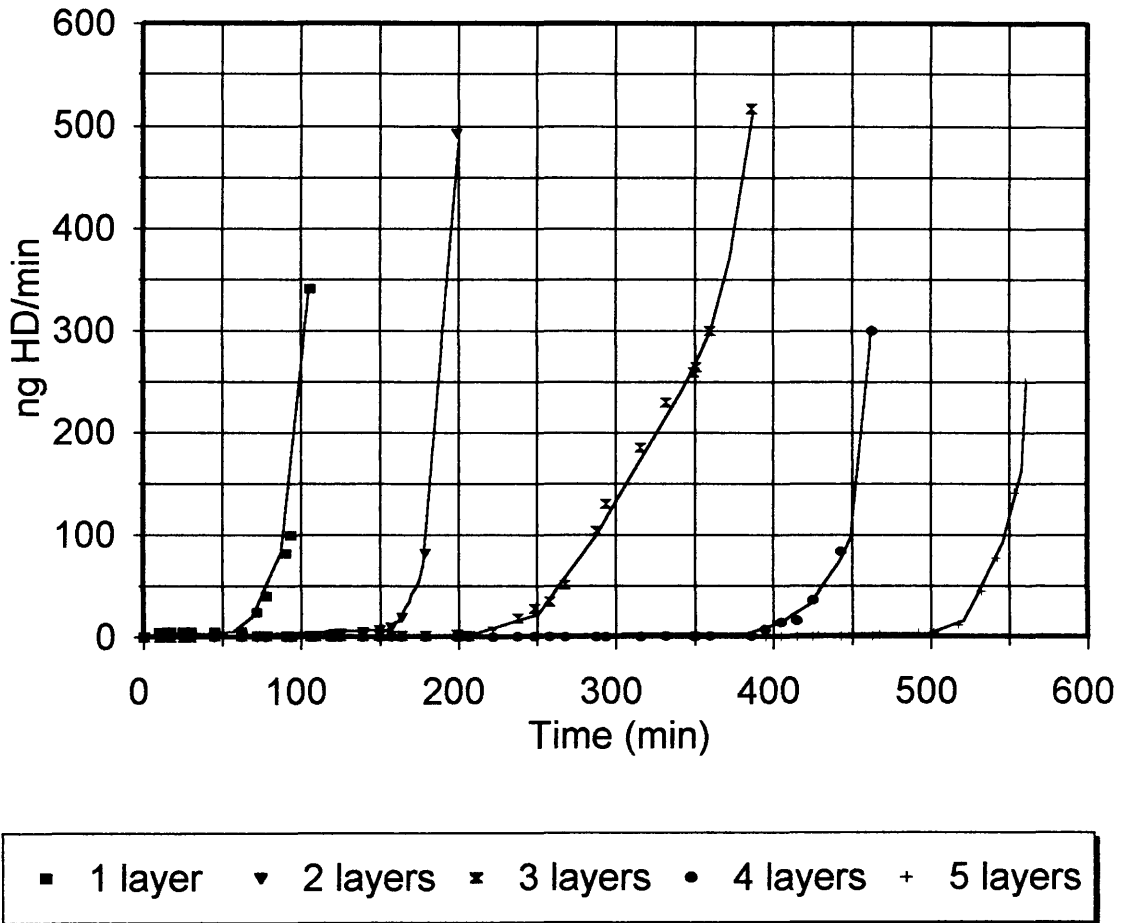
FIGURE 3.5:

Breakthrough curves for the CC textiles with the dynamic test method at the test conditions: 40 °C, 124 μg HD/l, and an air velocity of 0.50 cm/s (1, 2,..,5 layers represent the number of the textile layers used).
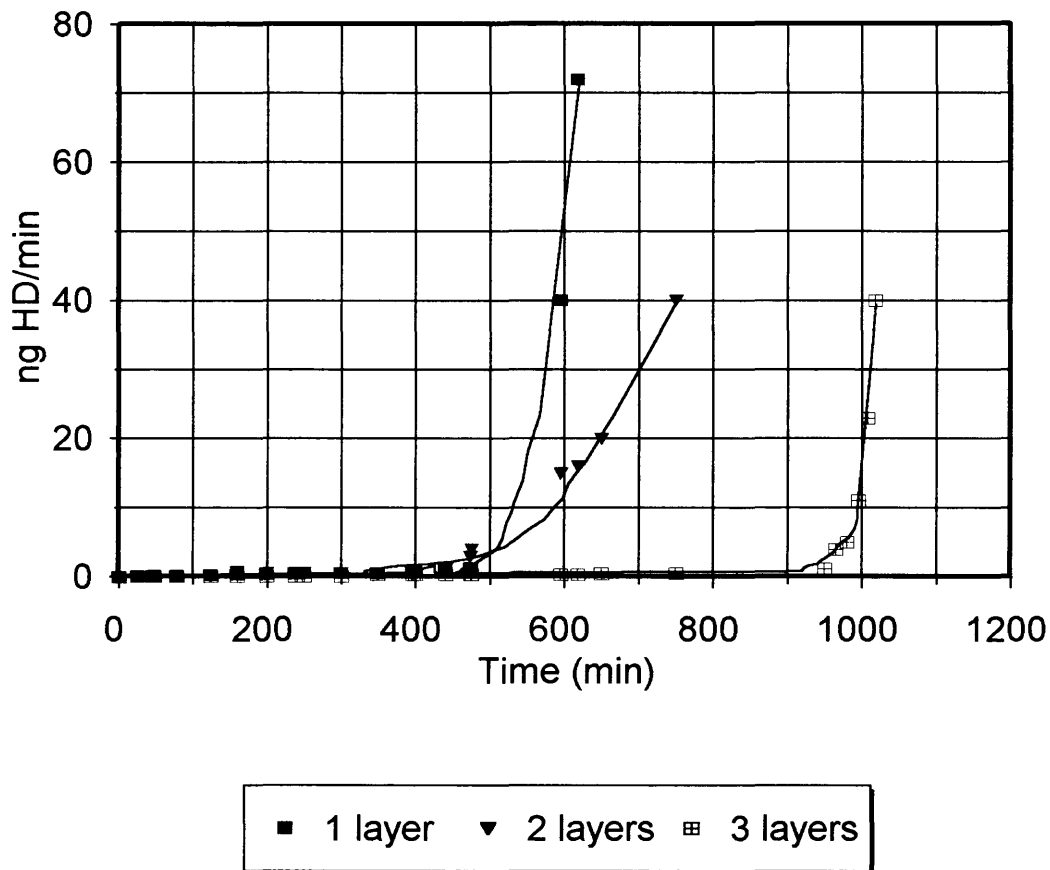
70
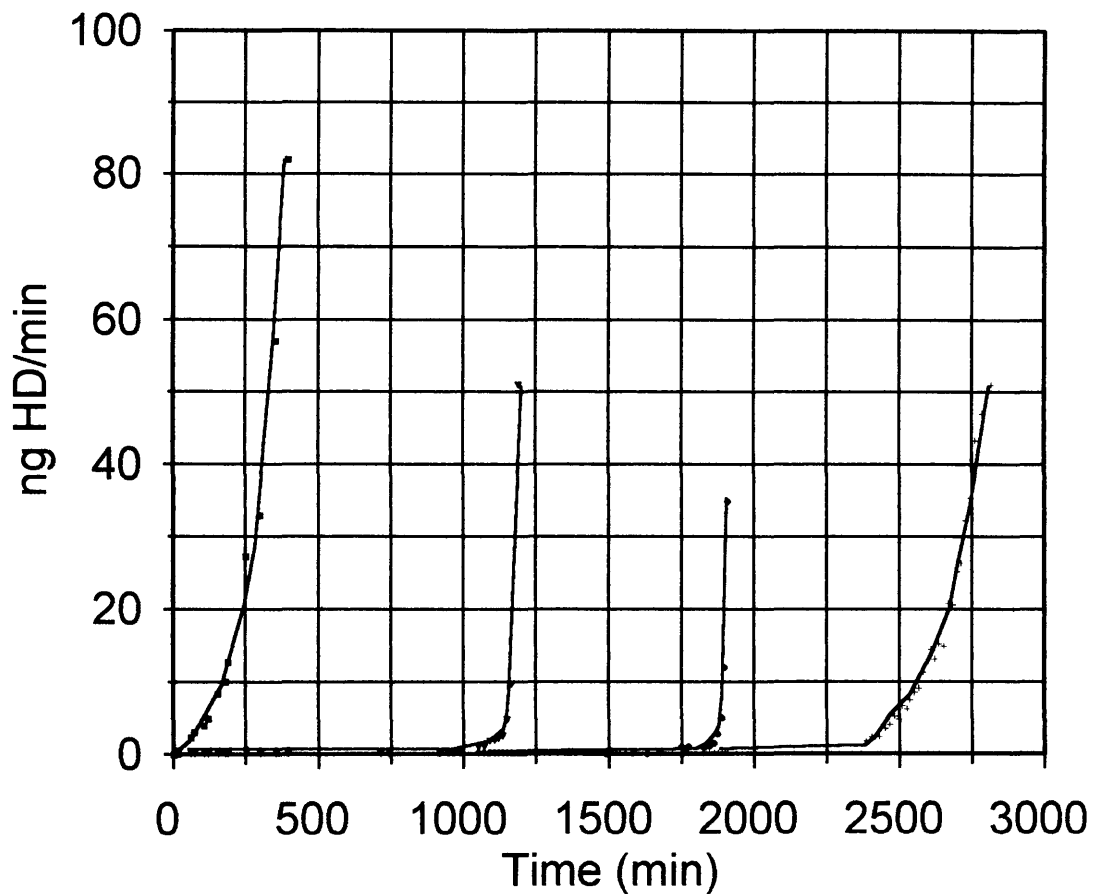
FIGURE 3.6:

Breakthrough curves for the C-spheres textile with the dynamic test method at the test conditions: 40 °C, 124 μg HD/l, and an air velocity of 0.50 cm/s (1, 2,..,4 layers represent the number of the textile layers used).

b. Aerodynamic test method
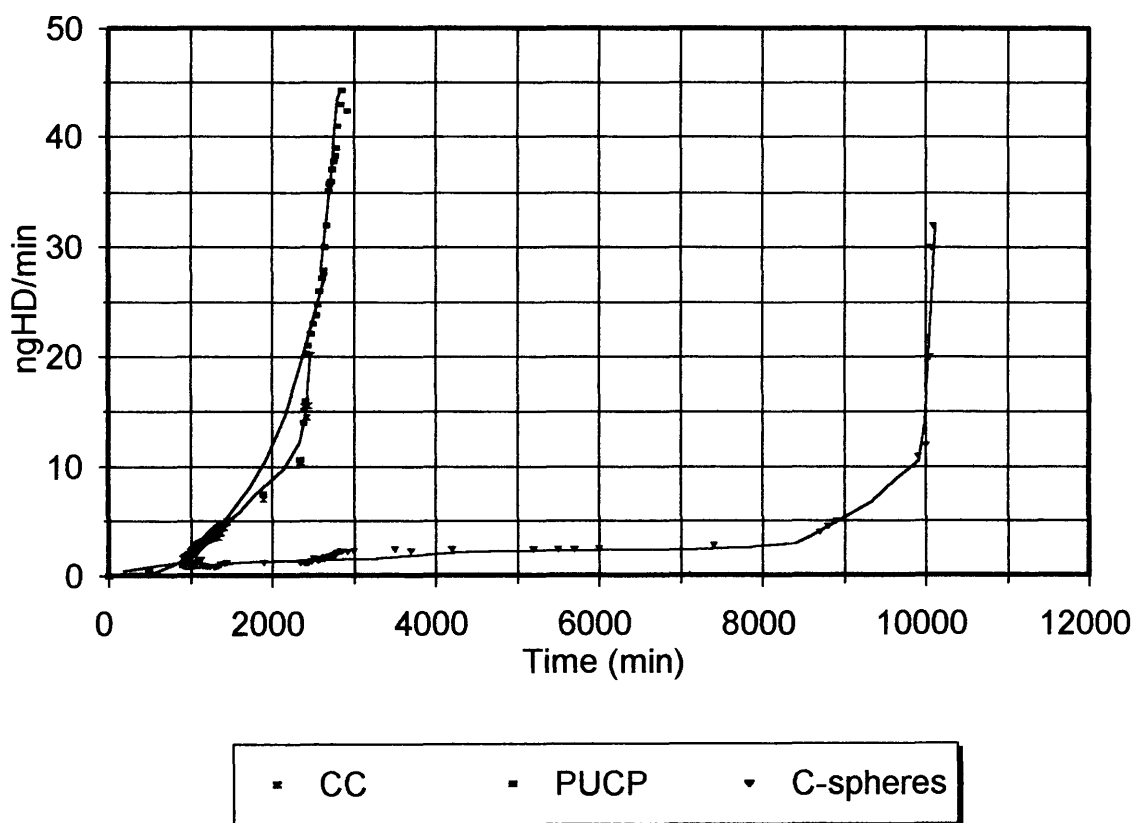
FIGURE 3.7:

HD breakthrough through textiles with the aerodynamic test method at the test conditions: 24 °C, 124 μg HD/l and an exposure air velocity of 2.2 m/s.

Figure 3.7 illustrates the breakthrough curves obtained for the three textiles with the aerodynamic breakthrough test setup. It was difficult to measure adsorption rate constants for HD vapour on the three different textiles using the Wheeler equation with the aerodynamic test method. The duration of the breakthrough experiment was seven days (10 000 min) and the air permeability through multiple layers will decrease drastically, influencing the permeation of HD vapour through the textiles in the aerodynamic test method. Consequently it was not attempted to calculate the adsorption rate constant and capacity with this method. It

72

will also be necessary to change the contaminant HD to a more volatile chemical, e.g. dimethyl methylphosphonate or carbon tetrachloride (DMMP or CCl_4), for future determinations, thus ensuring a shorter breakthrough time.

3.6 ANALYTICAL TECHNIQUES

a. Calibration of the gas chromatograph

Standards were prepared by diluting a mother solution of HD in ethanol (AR). The HD was synthesized with a well-known method from thionyl chloride and dithioglycol *[10]*. The HD is double-distilled to remove all impurities. The mother solution was prepared by pipetting 3 ml HD with an A-grade pipette into a 100 ml volumetric flask and filling it to the mark with ethanol. Three dilutions were prepared by pipetting 1 ml, 2 ml and 3 ml of the mother solution into 100 ml volumetric flasks. 0.1 µl of the dilution was injected into the thermal desorption unit with a 1 µl syringe. The injection per concentration was done in triplicate. The external standard method was used to calculate the response factor. The retention time for HD was 1.31 min. The detection limit for HD was 9 ng.

b. Sampling

Sampling the HD vapour, for calibration of the test setup and determination of the breakthrough through textiles, was done with air sampling tubes. The tubes consist of a glass tube packed with 100 mg Tenax TA (20-35 mesh). Free fatty acid (FFAP) was first used but the desorption efficiency was low. The 80-100 mesh Tenax was initially used but the pressure drop across the sampling tube was too high due to the fine particles. A plug of glass wool was placed on both sides to retain the Tenax in the tube. A restriction at the one end of the tube also aids the retention of the Tenax during sampling and desorption.

73

c. Analysis

Air sampling through the textile sample can be conducted as a function of time, or sampling can be conducted continuously over a set period of time, for example 6 hours.

The sampling technique is well known however, the method used for the analysis of the air sampling tube was a relatively new method, namely thermal desorption. The adsorbent in the air sampling tubes are normally unpacked and analysis is conducted by solvent extraction of the adsorbed vapours from the adsorbent with a suitable solvent, evaporation of the solvent to concentrate the sample is followed by injection into the GC. With this method losses may be experienced during solvent evaporation due to the volatility of the trapped chemical vapours. The mustard gas is however not volatile. To ensure complete desorption the air sampling tubes were desorbed at 270°C for 10 minutes. During desorption the trapped sample in the tube was concentrated by cryogenic cooling of the sample in a cold trap at -100°C. After desorption was completed, the cold trap was flash-heated to 250°C in 15 seconds and the temperature kept constant for 5 minutes. The time for complete desorption of the HD from the sampling tube was determined experimentally by determining the amount of HD not removed from the tube with a second desorption of the tube. The sample was injected onto a gas chromatograph (GC) column, separated and detected by a flame ionization detector.

The analysis was conducted on a CHROMPACK CP 9000 gas chromatograph, with a thermal cryogenic trap injector (TCT) connected to the injection block. A 10 m nonpolar column with CP Sil 5 CB as stationary phase, which is equivalent to OV 101, was used. The film thickness (d_f) was 1.2 μm and the maximum working temperature of the column was 350°C. An isothermal temperature programme was used.

74

The TCT-GC-FID working conditions are summarized in Table 3.3.

TABLE 3.3:

TCT-GC-FID operational conditions

TCT-GC-FID OPERATIONAL CONDITIONS FOR THE ANALYSIS OF THE AIR SAMPLING TUBES USED FOR THE DETECTION OF MUSTARD GAS BREAKTHROUGH THROUGH TEXTILES		
COLUMN	10 m x 0.75 mm fused silica WCOT CP-Sil 5CB (d_f = 1.2 μm)	
OVEN TEMPERATURE	120°C, isothermal	
CARRIER GAS	N_2 (high purity), 15 ml/min	
DETECTOR	FID, 250°C	
FLAME GASES	synthetic air, 250 ml/min	
	H_2 (high purity), 30 ml/min	
INJECTOR	TCT	
	Pre-cool time	1 min
	Desorption time	10 min
	Desorption temperature	270 °C
	Vented desorption flow	5 ml/min
	Injection time	5 min
	Injection temperature	250°C
	Capillary trap	0.75 mm ID fused silica WCOT CP-Sil 5CB (d_f = 1.2 μm)
	Trap cooling temperature	-100°C
	Injection block temperature	250°C

Data integration and analysis were done on a Spectra Physics Model

75

SP6469 integrator.

The increase of mustard gas in the N_2 flow downstream of the textile sample in the test setup was an indication of a breakthrough, and was monitored as a function of time. The challenge concentration was known. Thus a mass balance was used to calculate the mass of mustard gas adsorbed on the textile as a function of time.

The repeatability of the breakthrough curve for a specific set of conditions was determined for the polyurethane carbon containing textile. The deviation between the breakthrough curves was between 5% and 8%. This could be due to mainly two reasons: impregnation of the charcoal powder is not homogeneous throughout the polyurethane foam rubber, and the desorption of the mustard gas from the adsorbent in the air sampling tube is 95% efficient. 5% or less of the HD was still detected on the tube after a second desorption cycle.

76

REFERENCES

1. "*Interim Technical Report*", DAAK -84 -C-0019, Winfield Manufacturing Co., 1985. pA-10

2. "*Ontwikkeling van Nieuwe Textielbeschermstukturen Tegen Toxische Gassen*", unpublished work, Seyntex.

3. D. Griffiths, "*The Mark IV: State-of-the-art in British NBC Protection*", NBC Defense & Technology Int. 1987 Yearbook.

4. R. F. Goldman, "*Tactical Implications of the Physiological Stress imposed by Chemical Protective Clothing Systems*", US Army Research Inst. For Environmental Medicine, 1987.

5. J. Medema, "*Protective Clothing, Comparison of 17 Materials*", Unpublished work.

6. "*Interim Technical Report*", DAAK -84 -C-0019, Winfield Manufacturing Co., 1985. p2-6

7. Ibid. pA-14.

8. J. Klotz, "*Alternative Test Methods for Textiles*", Proc. of Second Int. Symp. on Protection Against Chemical Warfare Agents, Stockholm, Sweden. 1986.

9. P.D. Fedele, *"Model of Aerosol Protection offered by Permeable Protective Garments"*, Performance of Protective Clothing, ASTM STP 1133, Fredricksburg, 1992. p4.

10. S. Franke, *"Manual of Military Chemistry, Vol I, Chemistry of Chemical Warfare Agents"*, Report no AD849 866, Berlin, 1967. p116.

CHAPTER 4

CHARACTERISATION

4.0 INTRODUCTION

The objective of the characterisation was to determine the differences in pore volume and pore distribution between the three different textiles. The active surface areas were determined with the ASAP 2010 by nitrogen adsorption at 77K. The micropore volume was determined by the t-plot and the pore distribution was determined by the density functional theory.

A scanning electron microscope from the Botany Department, University of Pretoria, was used to obtain the electron micrographs for the different textiles.

4.1 RESULTS AND DISCUSSION

4.1.1 Electron microscope studies

a. Charcoal cloth (CC)

Figure 4.1 illustrates a fibre from the CC, magnified 10 000 times. The carbon particles bonded to the textile fibre with binder can be seen in this figure. The porous structure of the carbon cannot be seen as a higher magnification is needed for viewing micropores.

78
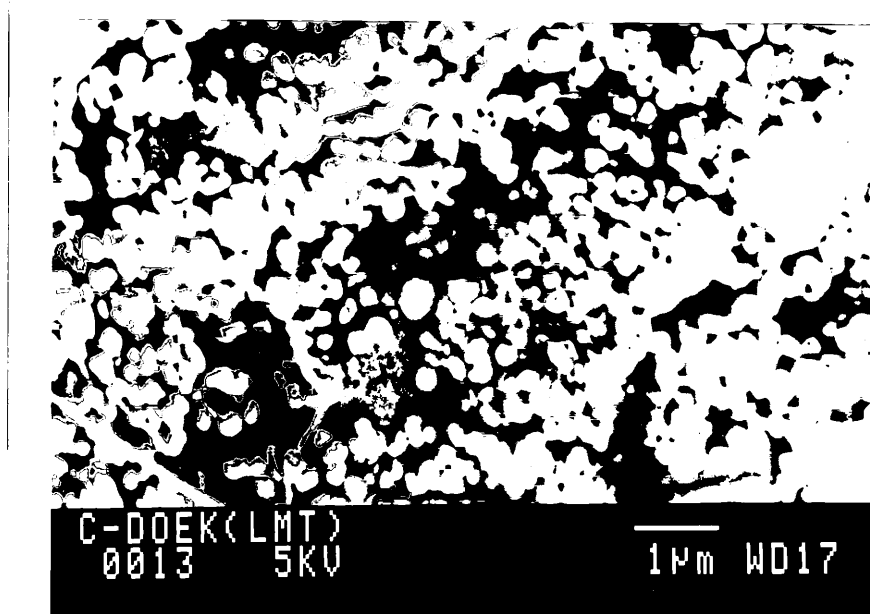
FIGURE 4.1:

Electron micrograph of the CC (10 000X magnification).

b. Polyurethane foam rubber impregnated with charcoal powder (PUCP)

Figure 4.2 is a 5 000 times magnification of the carbon impregnated in the polyurethane foam rubber. The porous structure, although at this magnification only macropores, can be seen.

FIGURE 4.2:

Electron micrograph of the PUCP (5 000X magnification).

c. Spherical carbon (C-spheres)

Figure 4.3 is a 100 times magnification of a carbon sphere of the C-sphere. The porous structure is only visible on spheres which are broken. The spheres, which are perfectly round, have a smooth surface and appear to be covered by a substance which could be the binders used to point bond the spheres to the woven support textile.

80

FIGURE 4.3:

Electron micrograph of the C-spheres (100X magnification).

4.1.2 ACTIVE SURFACE AREA DETERMINATION

a. CC

The isotherm, illustrated in Figure 4.4, is a closer representation of a Type II isotherm which is usually obtained from a carbon containing micro- and mesoporosity [1]. The CC showed the smallest equilibrium adsorption uptake. This can be due to a small active surface area and a small micropore volume.

The isotherm displays a sharp rise in adsorption volume up to $p/p^0 \leq 0.2$, which indicates the presence of micropores. The inflection point is not sharply defined and the plateau of this isotherm is not horizontal like the isotherms obtained with

the foam rubber textile and carbon spheres. Adsorption continued to increase after $p/p^0 \approx 0.2$, which further indicated the pressence of mesopores. It was also observed that the adsorption line turned upwards approaching the saturation pressure line $p/p^0 = 1$ asymptotically displaying possible wetting of the previous adsorbed film by the adsorbate condensing in the pores [2]. A hysteresis loop, although small, was observed for the desorption line, thus indicating that in this region there are two relative pressure values corresponding to a given value adsorbed; the lower value always residing on the desorption isotherm. Many theories exists for the hysteresis: Zigsmondy postulated that the hysteresis was caused by contact from a different angle during adsorption and desorption, while McBain accounted for hysteresis by assuming pores containing a narrow opening [3]. The characteristics measured for the CC are summarised in Table 4.1.

b. PUCP

The adsorption isotherm for N_2 adsorption on the charcoal impregnated into foam rubber, illustrated in Figure 4.4, displayed Type I isotherm characteristics [1]. The PUCP showed larger equilibrium adsorption uptake than the CC. This can be ascribed to a fairly large active surface area and micropore volume. The isotherm displays a sharp rise in adsorption volume up to $p/p^0 \leq 0.2$, which further indicates the presence of micropores. The inflection point is well defined. A flat plateau region was developed early in the isotherm at $p/p^0 \approx 0.2$. The plateau is parallel to the relative pressure axis, which indicates no further adsorption. The adsorption line cuts the $p/p^0 = 1$ line at a definite angle, which indicates that the liquid condensing in the pores does not completely wet the previous adsorbed film [2]. A hysteresis loop is present. The adsorption characteristics measured are summarised in Table 4.1.

b. C-spheres

The isotherm for the N_2 adsorption on the C-spheres, illustrated in Figure 4.4, displayed a Type I isotherm with an almost horizontal line for adsorption at p/p^0

82

$\approx$ 0.1 [1]. The C-spheres showed, relative to the other two textiles, a large equilibrium adsorption uptake. This can be ascribed to a fairly large active surface area and micropore volume. The adsorption line did not turn upwards approaching the saturation pressure line $p/p^0 = 1$ but approached the line at 90°. No hysteresis was displayed at the plateau. The BET and Langmuir surface area plots showed linear characteristics at low relative pressures according to Henry's law. The results are summarised in Table 4.1.

From the nitrogen adsorption studies on the textiles containing charcoal, it may be concluded that the position of the inflection point and the inclination of the saturation plateau to the relative pressure axis can provide a significant amount of information on the porous structure of the adsorbents.

TABLE 4.1:

Physical adsorption characteristics of the textiles

ADSORPTION CHARACTERISTICS	CC	PUCP	C-SPHERES
BET SINGLE POINT SURFACE AREA (m^2 / g)	146.2524	334.2515	389.0793
BET SURFACE AREA (m^2 / g)	152.1981	330.9075	383.7623
LANGMUIR SURFACE AREA (m^2 / g)	159.4861	499.6667	514.0886
TOTAL PORE VOLUME (cm^3/ g)	0.0929	0.1659	0.1834
t-plot MICROPORE AREA (m^2 / g)	124.5955	311.7151	372.5563
t-plot MICROPORE VOLUME (cm^3 / g)	0.0577	0.1444	0.1716
AVERAGE PORE DIAMETER (Å)	24.41	20.06	19.11
BET C-VALUE	+115.418	-150.83	-125.92

From Table 4.1 it follows that the CC has a small surface area compared to

83

the two other textiles. The differences measured between the single point surface determination and the BET multipoint determination were within experimental error. The total pore volume of the CC is relatively small, and the micropore volume indicates that there is a large distribution of meso- or macropores present in the carbon. The average pore diameter indicates more mesopores present. From the BET C value it could be concluded that a monolayer was formed.
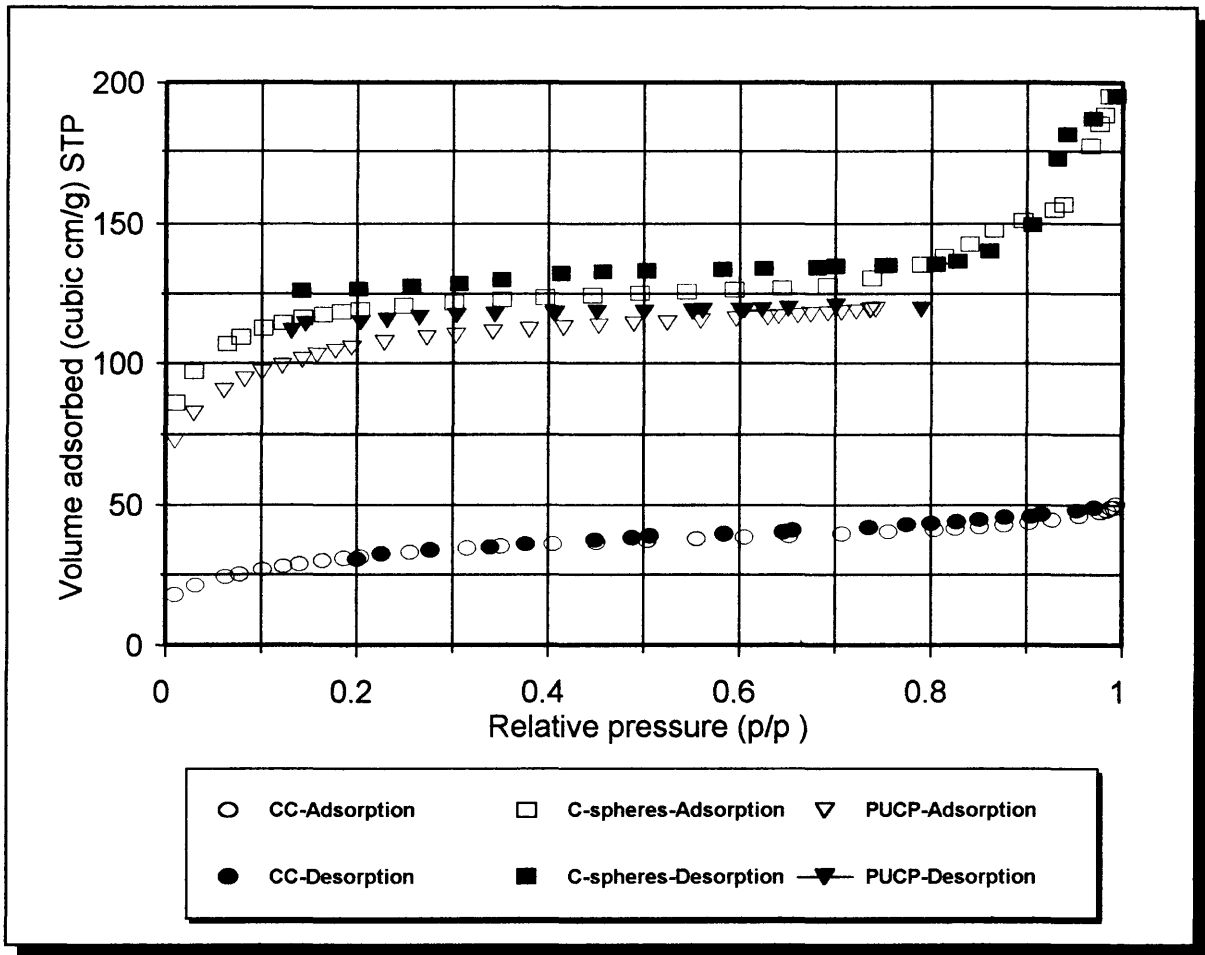
FIGURE 4.4:

Adsorption isotherm of N_2 on the three different textiles

4.1.3 Micropore volume - t-plot

a. CC

The shape of the t-plot is associated with a small surface area and therefore, a small micropore volume. The curvature between the two parts of the V_A - t plot indicates a fairly wide distribution of micropore diameters.

b. PUCP

The shape of the t-plot is associated with microporosity. The curvature between the two parts of the V_A - t plot indicates a fairly wide distribution of micropore diameters.

c. C-spheres

The shape of the t-plot is associated with microporosity. The curvature between the two parts of the V_A - t plot indicates a fairly narrow distribution of micropore diameters.

4.1.4 Pore distribution

The pore size distribution of the three different textiles, determined with the density functional theorie (DFT), is summarised in Table 4.2 and illustrated in Figure 4.5.

TABLE 4.2:

Pore size distribution determined by the DFT

PORE WIDTH (Å)	INCREMENTAL VOLUME CC (cm³/g)	INCREMENTAL VOLUME PUCP (cm³/g)	INCREMENTAL VOLUME C-SPHERES (cm³/g)
MICROPORES			
< 14.83	0.0252	0.0898	0.1042
14.83 - 20.02	0.0139	0.0279	0.0382
MESOPORES			
21.62 - 200.69	0.0293	0.0155	0.0094

From Table 4.2 and Figure 4.5 it follows that the CC has a very small micropore volume compared to the two other textiles. The CC also has a wider distribution of both micropores and mesopores than the other two textiles. From Table 4.1 it follows that 32% of the total pore volume for the CC is mesopores, compared with only 9% and 5% for the PUCP and the C-spheres respectively.
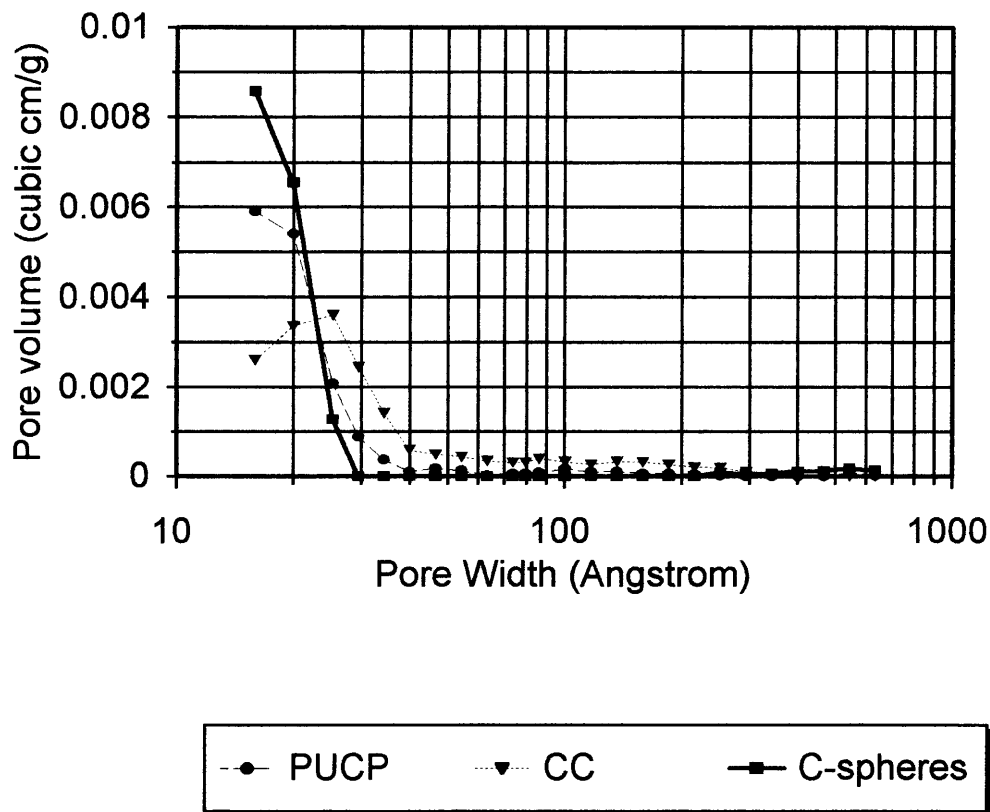
FIGURE 4.5:

Pore size distribution determined with the DFT.

REFERENCES

1. S.J.Gregg and K.S.W.Sing, "*Adsorption Surface Area and Porosity*", Academic press, NY, 1967. p198

2. S. Lowell and J.E. Shields, "*Powder Surface Area and Porosity*", 2nd Ed., Chapman and Hall, London, UK, 1984. p57

3. Ibid., p58

CHAPTER 5

# SORPTION RATE CONSTANTS

5.0 INTRODUCTION

Protective textiles containing activated charcoal are compared with each other on the basis of the protection time against an organic vapour [1]. For CBW protective textiles the protection time against HD vapour is usually compared. The protection time can however be increased by increasing the carbon loading, which has negative influences on the heat load experienced by the wearer and also increases the cost. An alternative method had to be found to evaluate and compare textiles.

The rate of vapour adsorption by the textiles containing activated carbon was studied in terms of the functional dependence of the pseudo first-order adsorption rate constant. HD was used as the adsorbate vapour, and the PUCP, the C-spheres and the CC as the respective adsorbents. The dynamic test method was used to blow a constant HD concentration through the textiles, at a constant linear velocity and temperature. The breakthrough time was taken as the time it took until 1% of the inlet concentration was detected in the outlet air stream. By applying the Wheeler; Yoon and Nelson; and Ackley kinetic equations to the experimental results, graphs of breakthrough time as a function of carbon mass (Wheeler), $ln(C_0 - C_x/C_x)$ as a function of breakthrough time (Yoon and Nelson), and bed residence time as a function of breakthrough time (Ackley) were drawn and pseudo first-order adsorption rate constants were determined. The influence of HD concentration (varied between 20 x 10^{-9} g / cm^3 and 124 x 10 $^{-9}$g / cm ^{3}) and temperature (varied between 20°C and 50°C) on the adsorption rate constant and adsorption capacity was investigated for the three textiles. The results showed that the rate constant is a more effective parameter to compare the protective textiles containing charcoal than the protection time.

5.1 EXPERIMENTAL

The three different textiles were evaluated. These textiles were exposed to different

89

challenge concentrations of HD vapour. The exposure temperatures were also varied. The breakthrough time was measured and was considered to be the time it took for the outlet flow to reach a concentration equal to 1% (0.01 times) of the inlet concentration (C_0). The dynamic test method, described in detail in Chapter 3, was used for this study. To study the influence of the variation of the mass of adsorbent on the breakthrough time the number of textile layers were increased. See Chapter 3 for the breakthrough curves for the different textiles at 40°C, 124 μg HD/l and 0.5 cm/s. The influence of different test conditions on the W_e and k_v of HD adsorption on the different textiles were also investigated. The test results are illustrated in Figures 5.1 to 5.13.
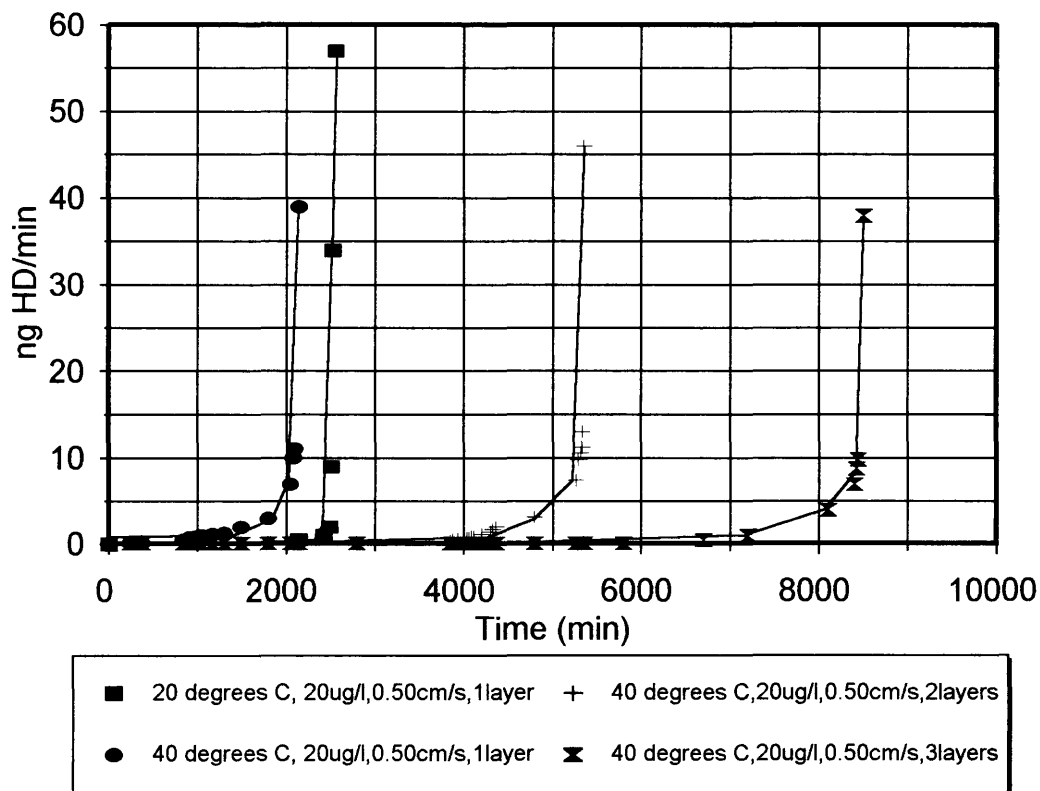
Figure 5.1:

Breakthrough curves for the PUCP textiles with the dynamic test method at test conditions: 20 °C and 40 °C, 20 μg HD/l, and an air velocity of 0.50 cm/s (1, 2 and 3 layers represent the number of the textile layers used).

90
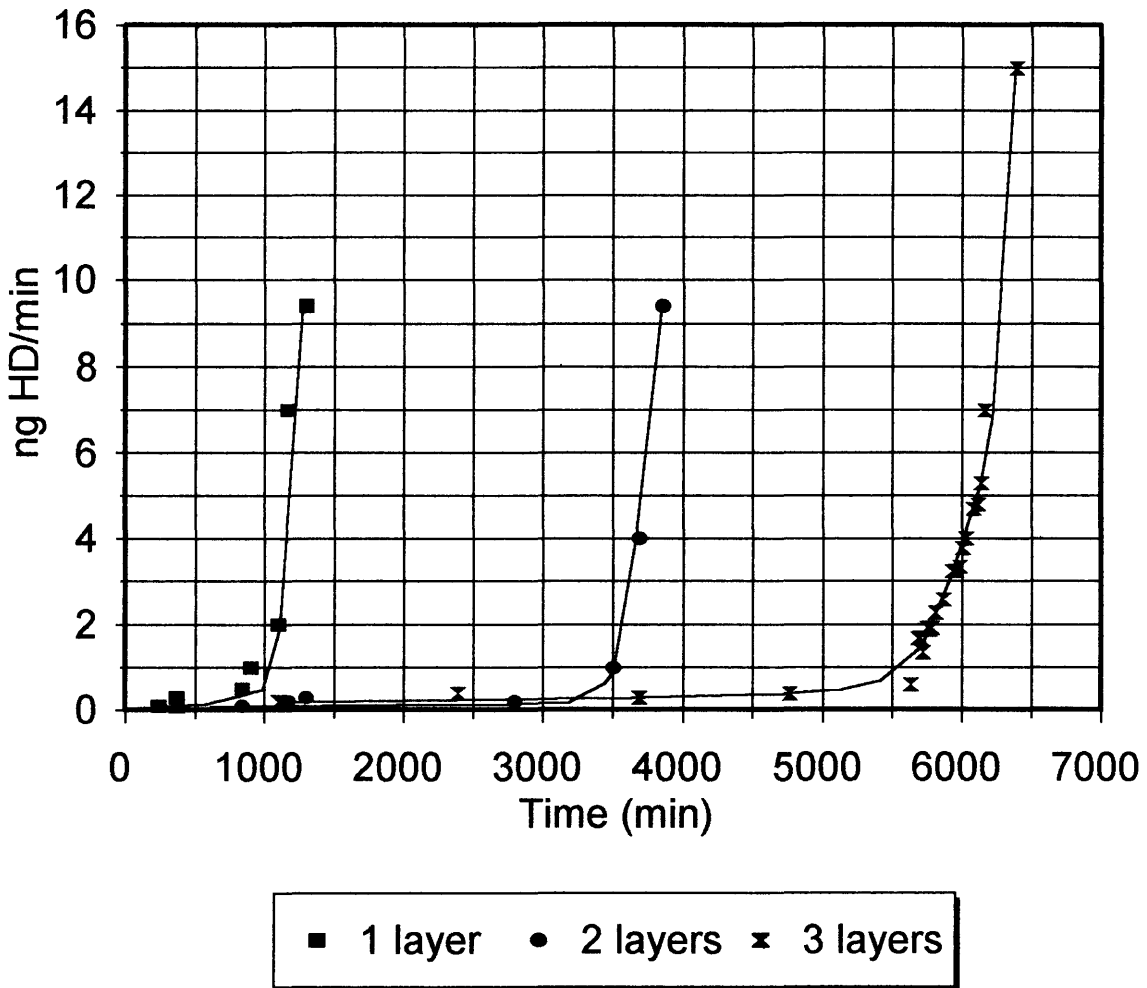
Figure 5.2:

Breakthrough curves for the PUCP textiles with the dynamic test method at
test conditions: 40 °C, 47 μgHD/l, and an air velocity of 0.50 cm/s (1, 2 and 3
layers represent the number of the textile layers used).

Figure 5.3:

Breakthrough curves for the PUCP textiles with the dynamic test method at test conditions: 40 °C, 79 μgHD/l, and an air velocity of 0.50 cm/s (1, 2 and 3 layers represent the number of the textile layers used).
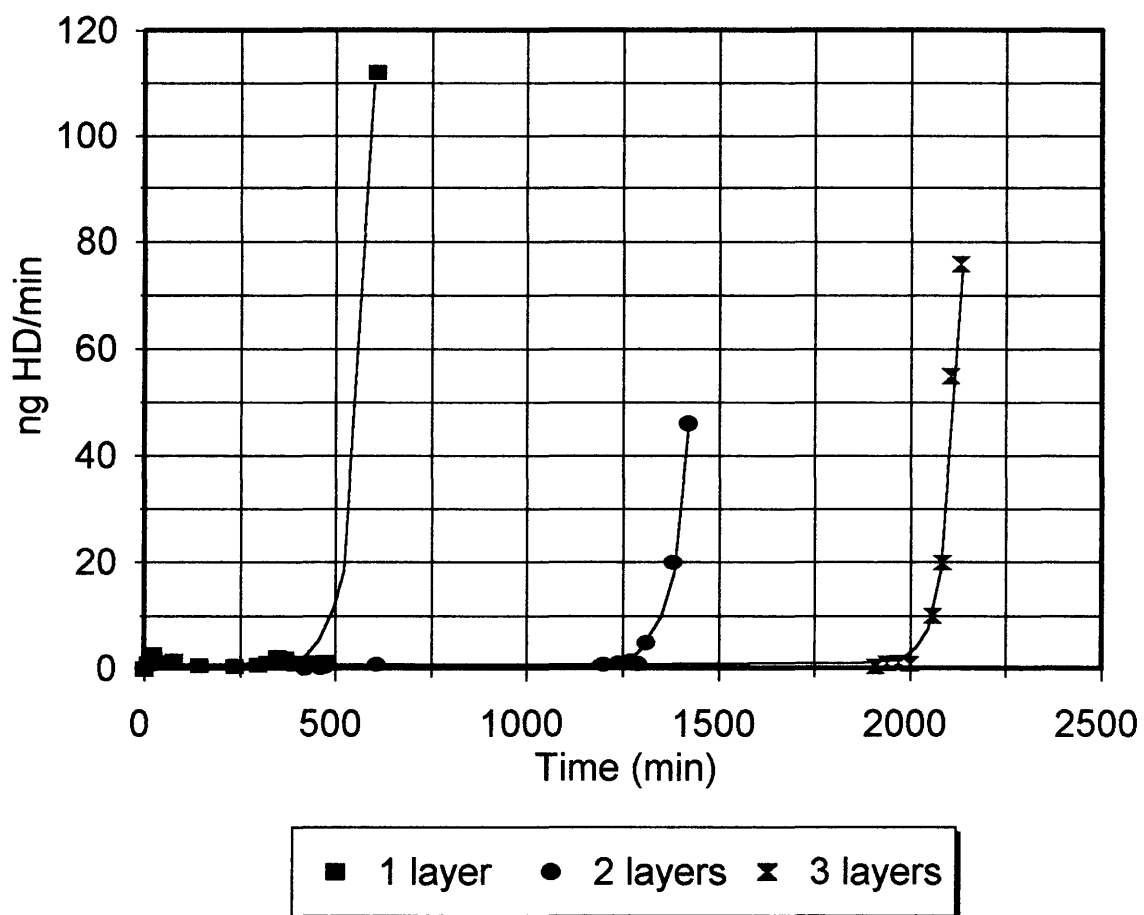
Figure 5.4:

Breakthrough curves for the PUCP textiles with the dynamic test method at test conditions: 40 °C, 124 μgHD/l, and an air velocity of 0.15 cm/s (1, 2 and 3 layers represent the number of the textile layers used).

93

Figure 5.5:

Breakthrough curves for the PUCP textile as function of temperature with the dynamic test method at test conditions: 124 μg HD/l, and an air velocity of 0.50 cm/s.
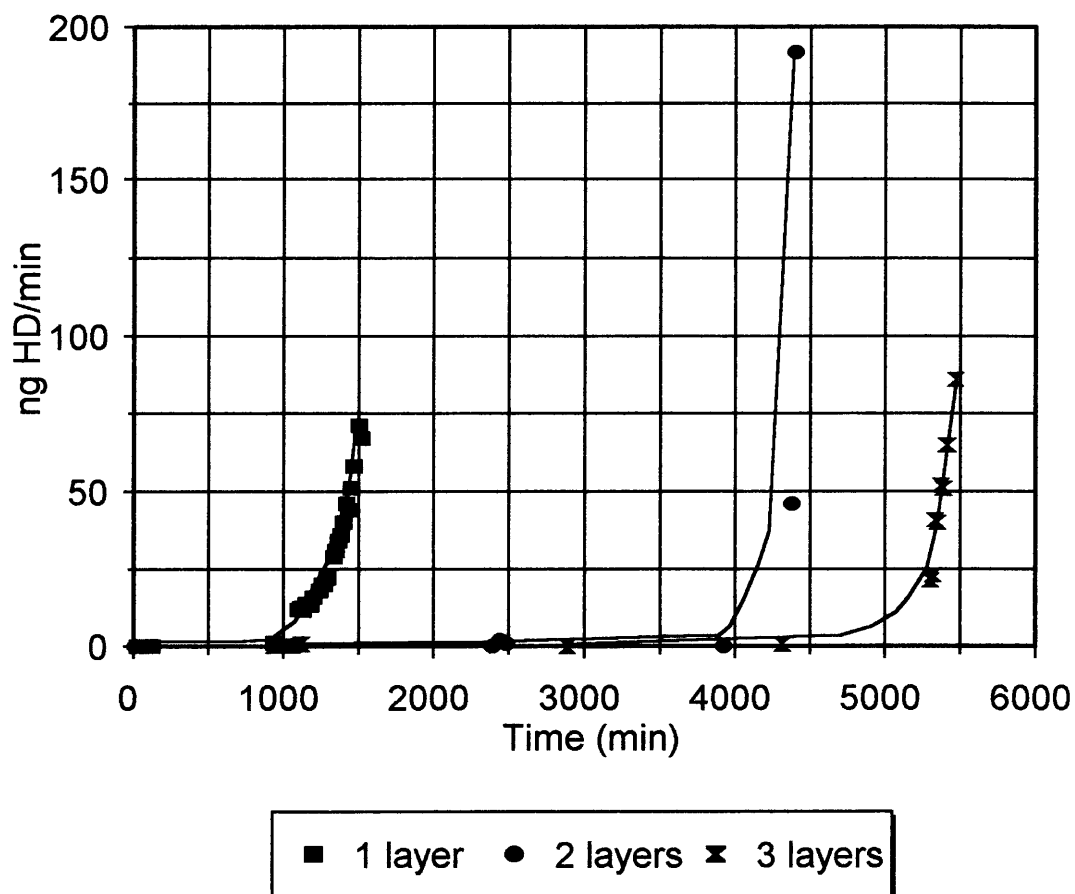
Figure 5.6:

Breakthrough curves for the CC textiles with the dynamic test method at test conditions: 20 °C, 20 μgHD/l, and an air velocity of 0.50 cm/s (1 and 2 layers represent the number of the textile layers used).
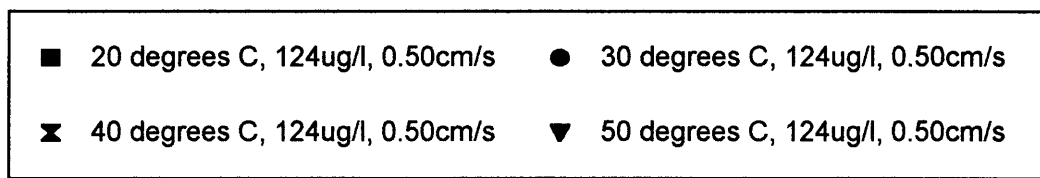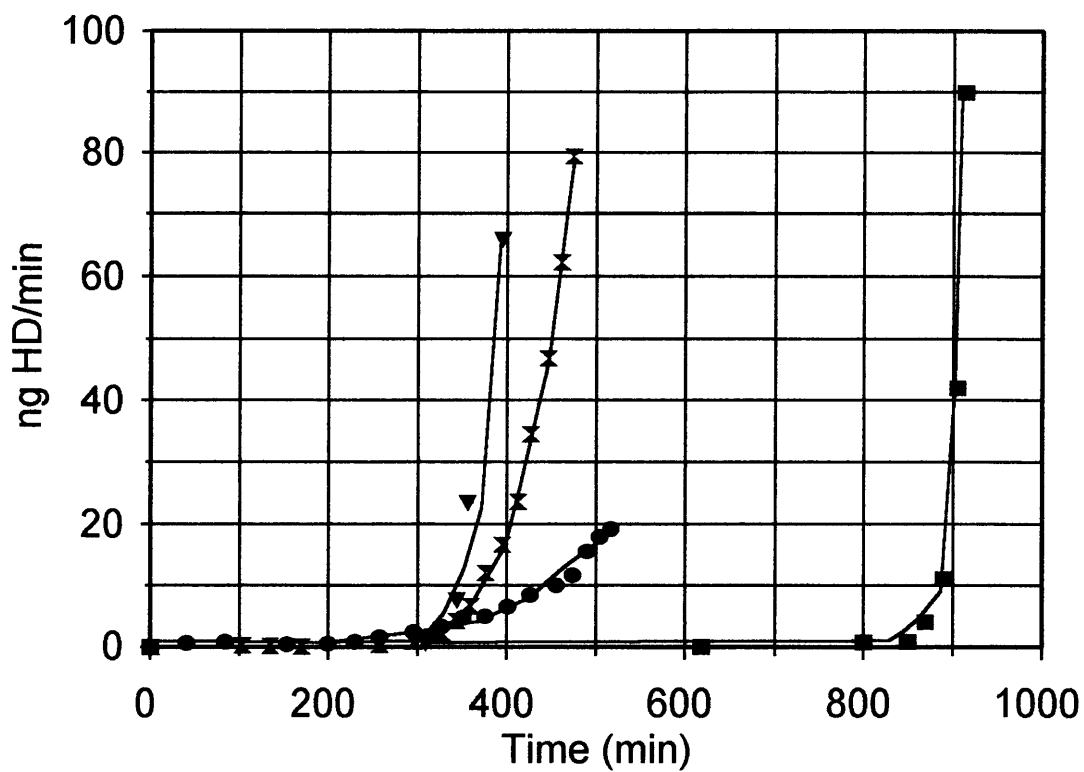
Figure 5.7:

Breakthrough curves for the CC textiles with the dynamic test method at test
conditions: 40 °C, 20 μgHD/l, and an air velocity of 0.50 cm/s (1, 2 and 3 layers
represent the number of the textile layers used).

Figure 5.8:

Breakthrough curves for the CC textiles with the dynamic test method at test conditions: 40 °C, 59 μgHD/l, and an air velocity of 0.50 cm/s (1, 2 and 3 layers represent the number of the textile layers used).
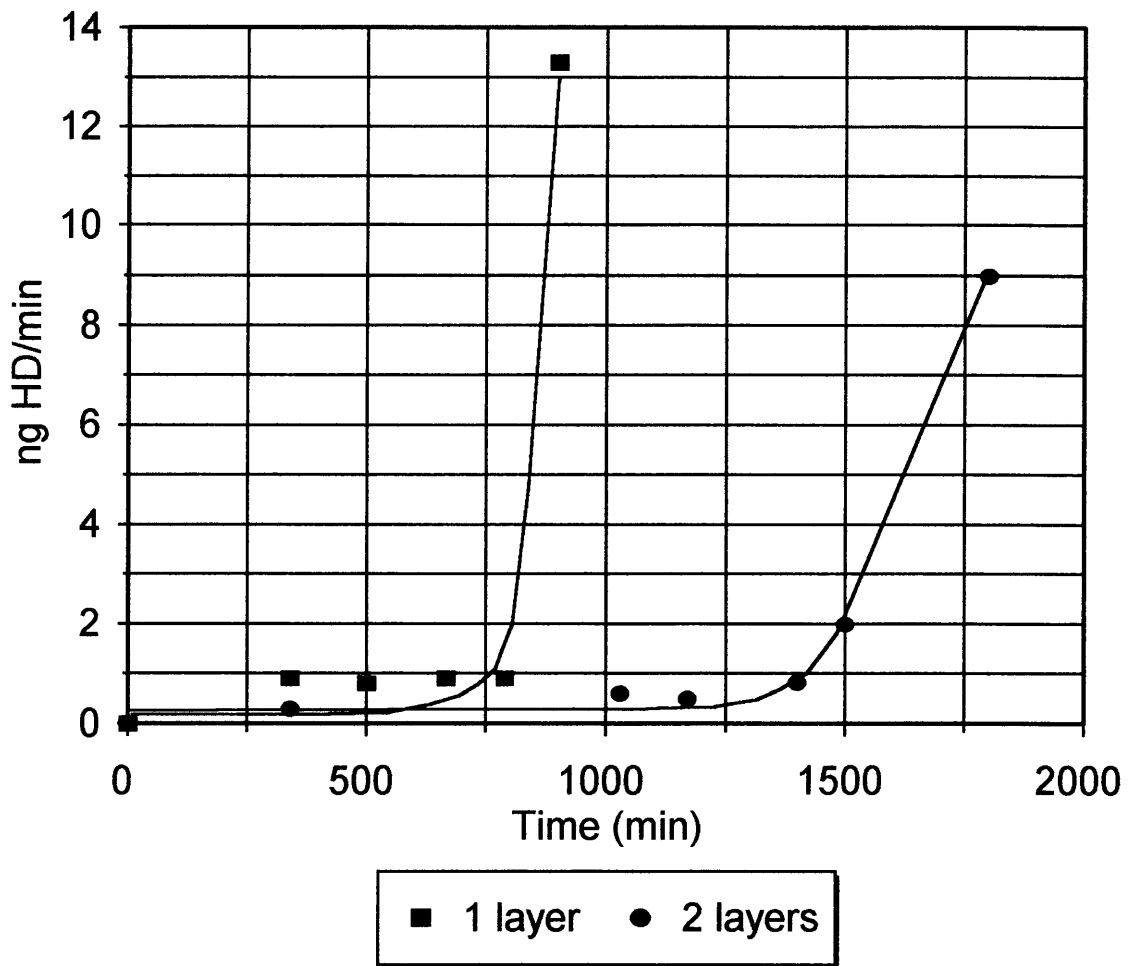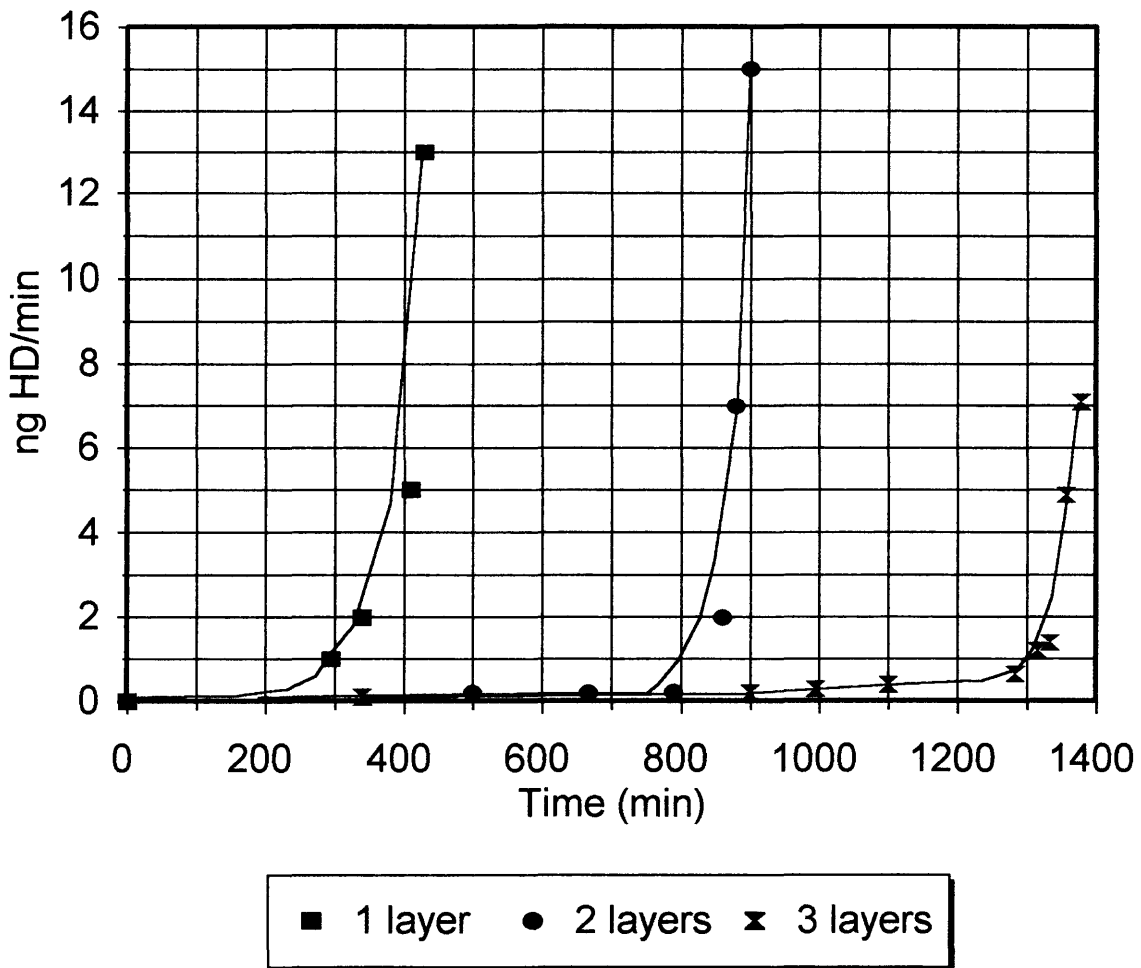
Figure 5.9:

Breakthrough curves for the CC textiles with the dynamic test method at test conditions: 40 °C, 124 μgHD/l, and an air velocity of 0.15 cm/s (1 and 2 layers represent the number of the textile layers used).

98

Figure 5.10:

Breakthrough curves for the C-spheres textiles with the dynamic test method at test conditions: 20 °C, 20 μgHD/l, and an air velocity of 0.50 cm/s (1 and 2 layers represent the number of the textile layers used).

Figure 5.11:

Breakthrough curves for the C-spheres textiles with the dynamic test method

at test conditions: 40 °C, 20 μgHD/l, and an air velocity of 0.50 cm/s (1, 2 and 3

layers represent the number of the textile layers used).

100
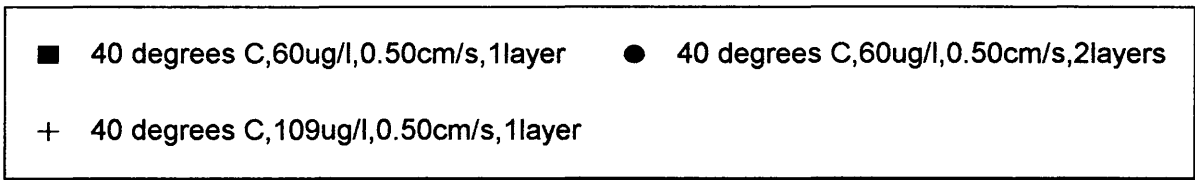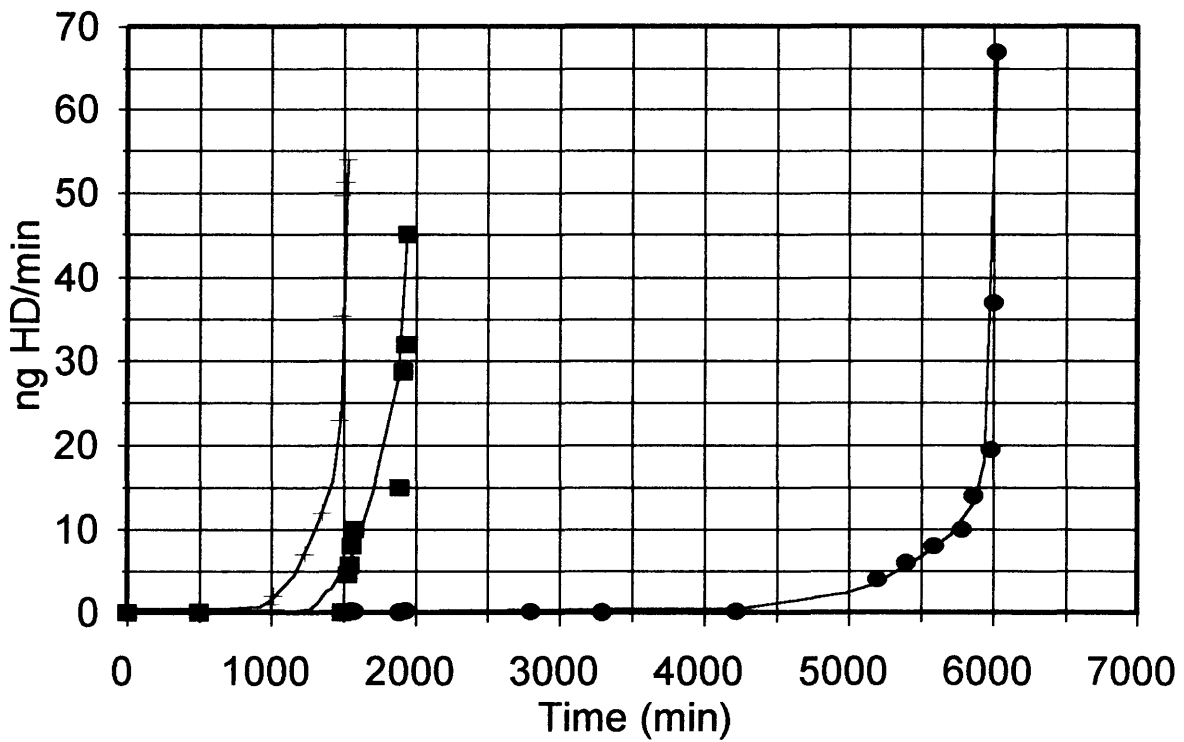
Figure 5.12:

Breakthrough curves for the C-spheres textiles with the dynamic test method at test conditions: 40 °C, 60 and 109 μg HD/l, and an air velocity of 0.50 cm/s (1 and 2, and 1 layers, respectively represent the number of the textile layers used).
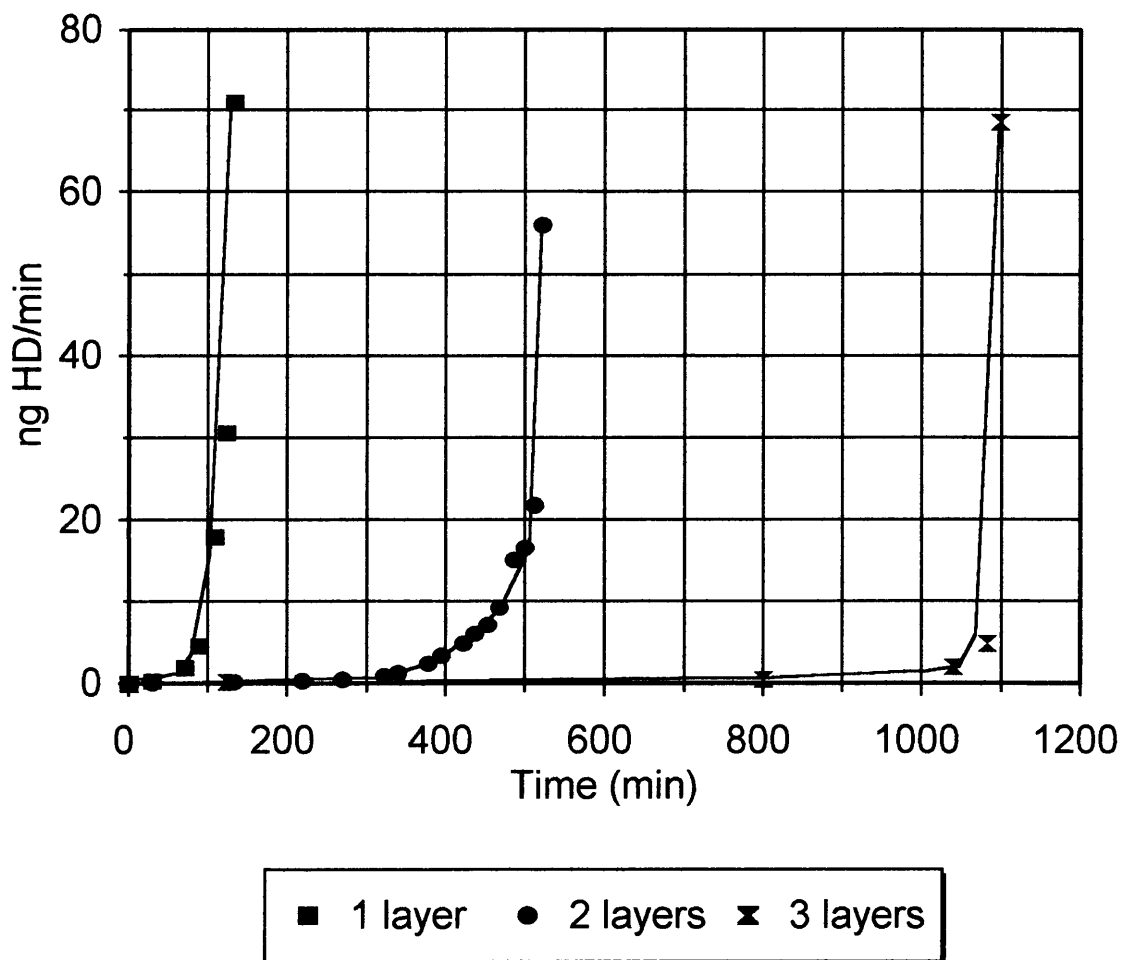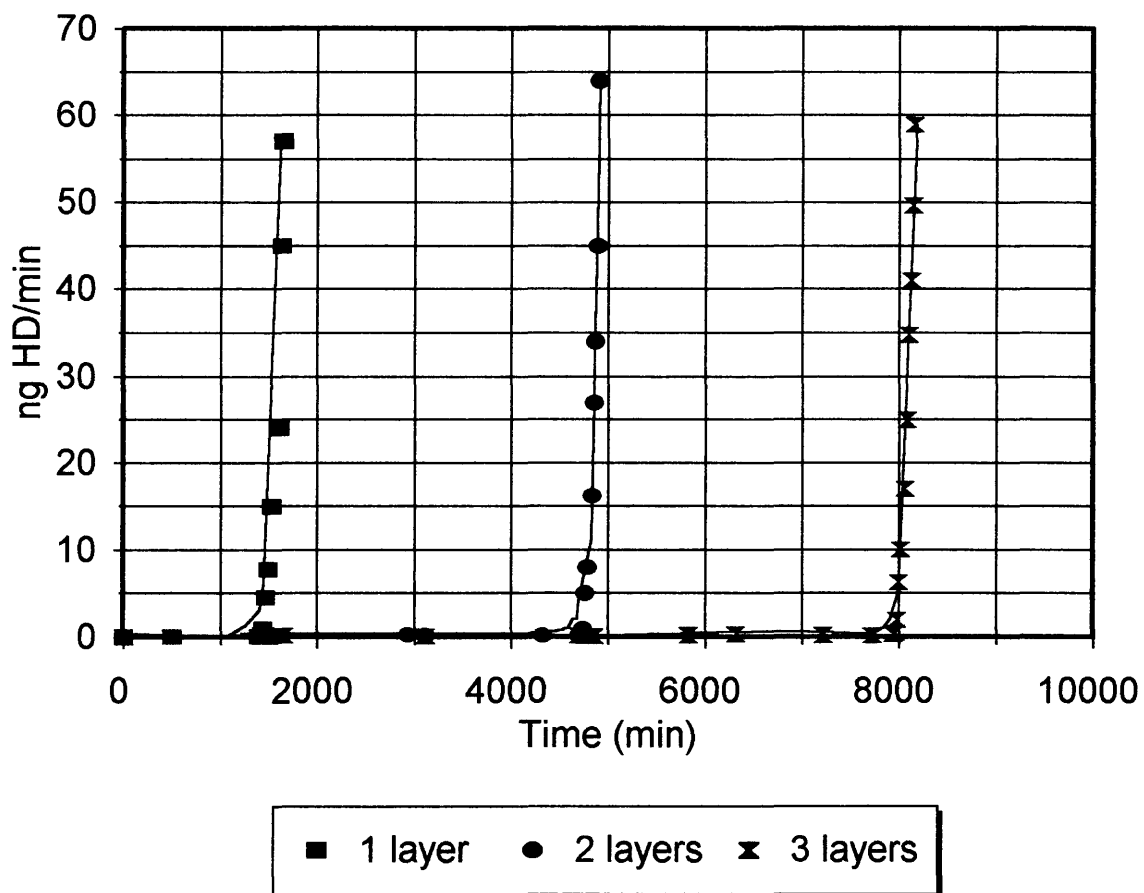
Figure 5.13:

Breakthrough curves for the C-spheres textiles with the dynamic test method

at test conditions: 40 °C, 124 μg HD/l, and an air velocity of 0.15 cm/s (1, 2 and

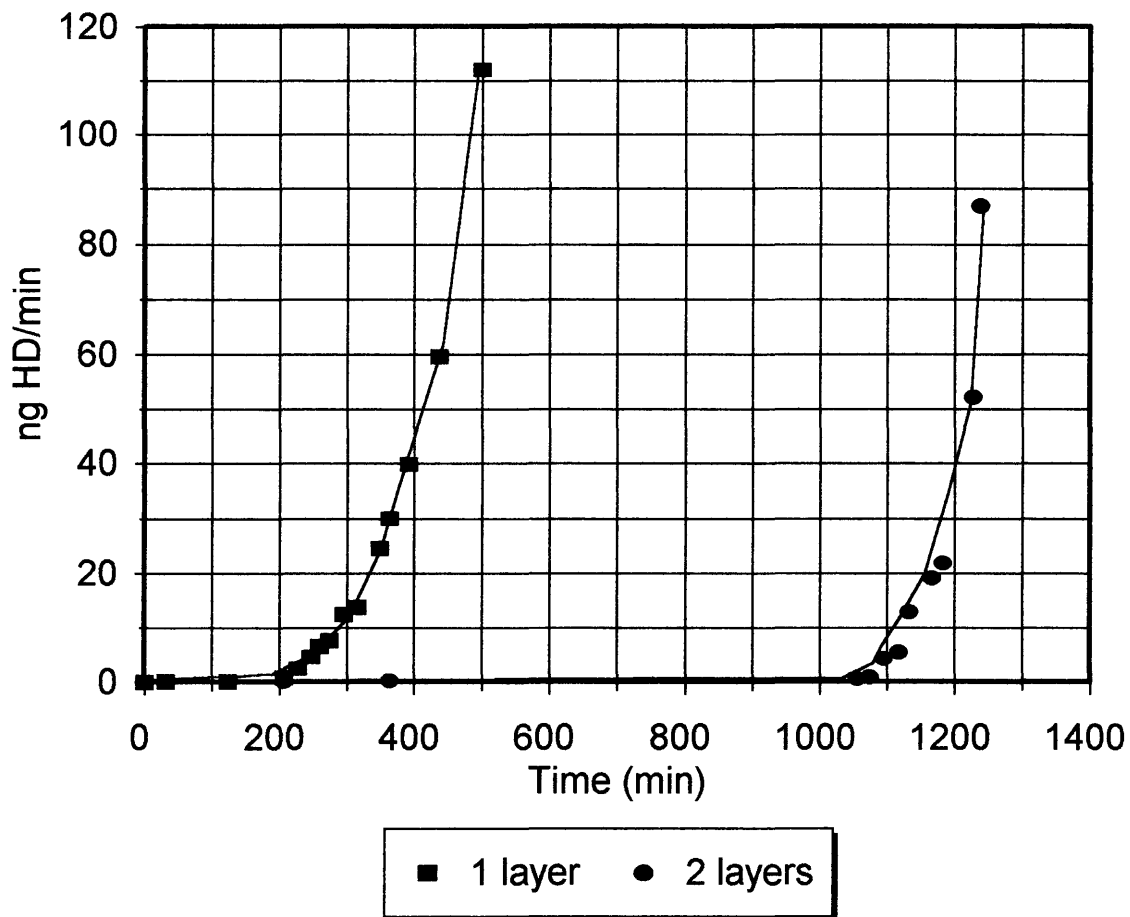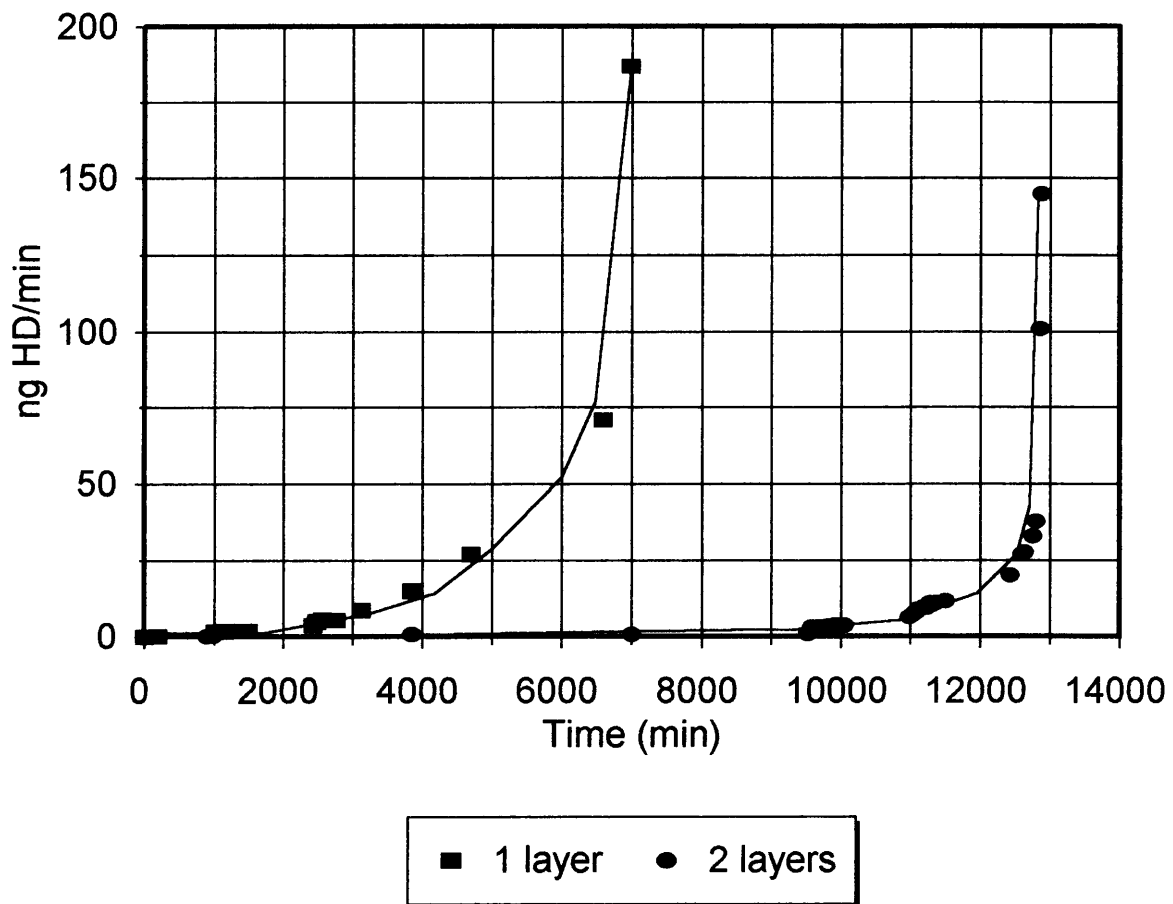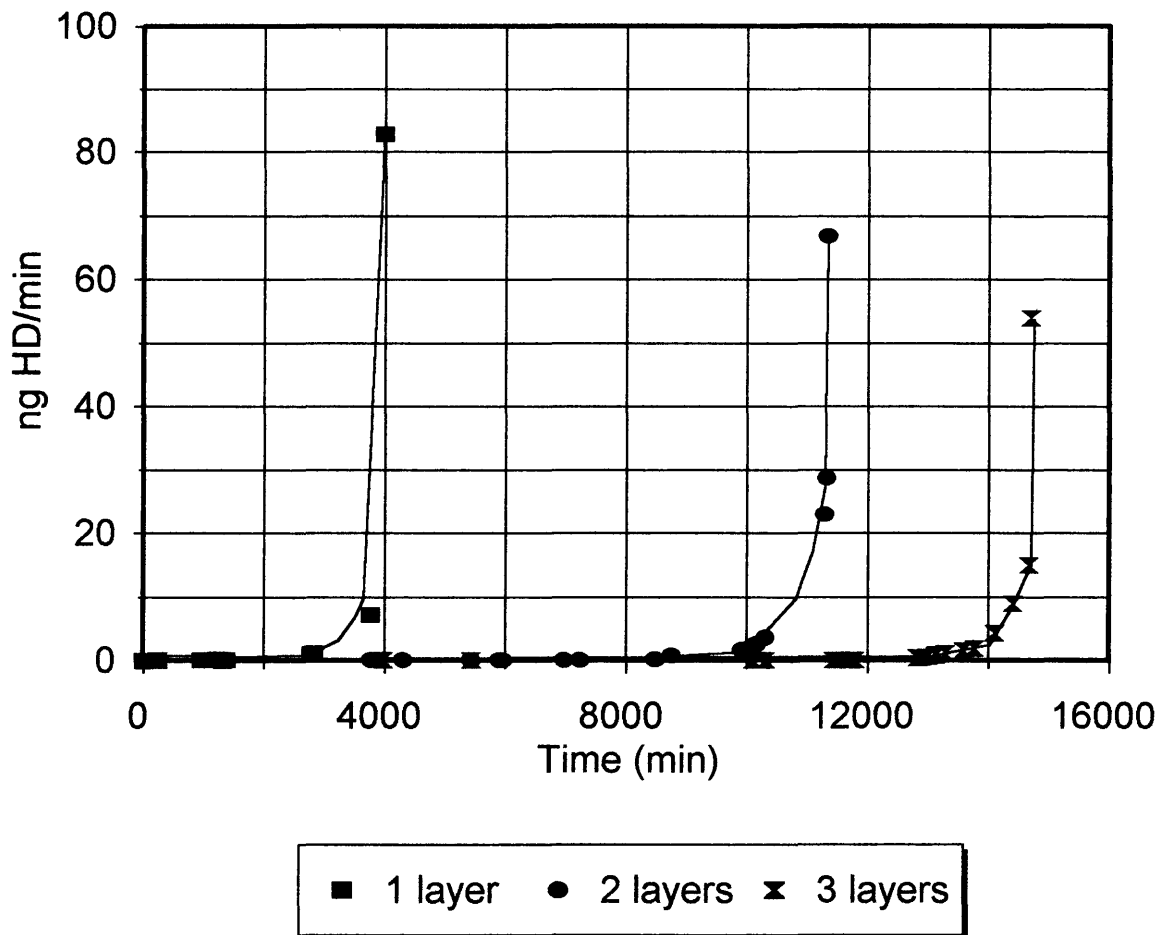3 layers represent the number of the textile layers used).

5.2 RESULTS AND DISCUSSIONS

The results were interpreted by using the Wheeler *(2.37)*, Yoon and Nelson *(2.40)* and Ackley *(2.43)* equations respectively. The rate constants, capacity for HD and critical mass were calculated with these equations.

5.2.1 Kinetic equations

a. Wheeler

Graphs similar to Figure 2.3 were obtained for the breakthrough time (t_b) of the HD through the textiles as a function of mass (W) of activated carbon in the three different textiles under different test conditions. These graphs are shown in Figures 5.14 to 5.16. Straight lines were obtained in most cases. The equations obtained from the linear regression are summarised in Table 5.1. The high coefficients of correlation for the regression equations indicate a high degree of confidence that the straight line equations accurately represent the data points.
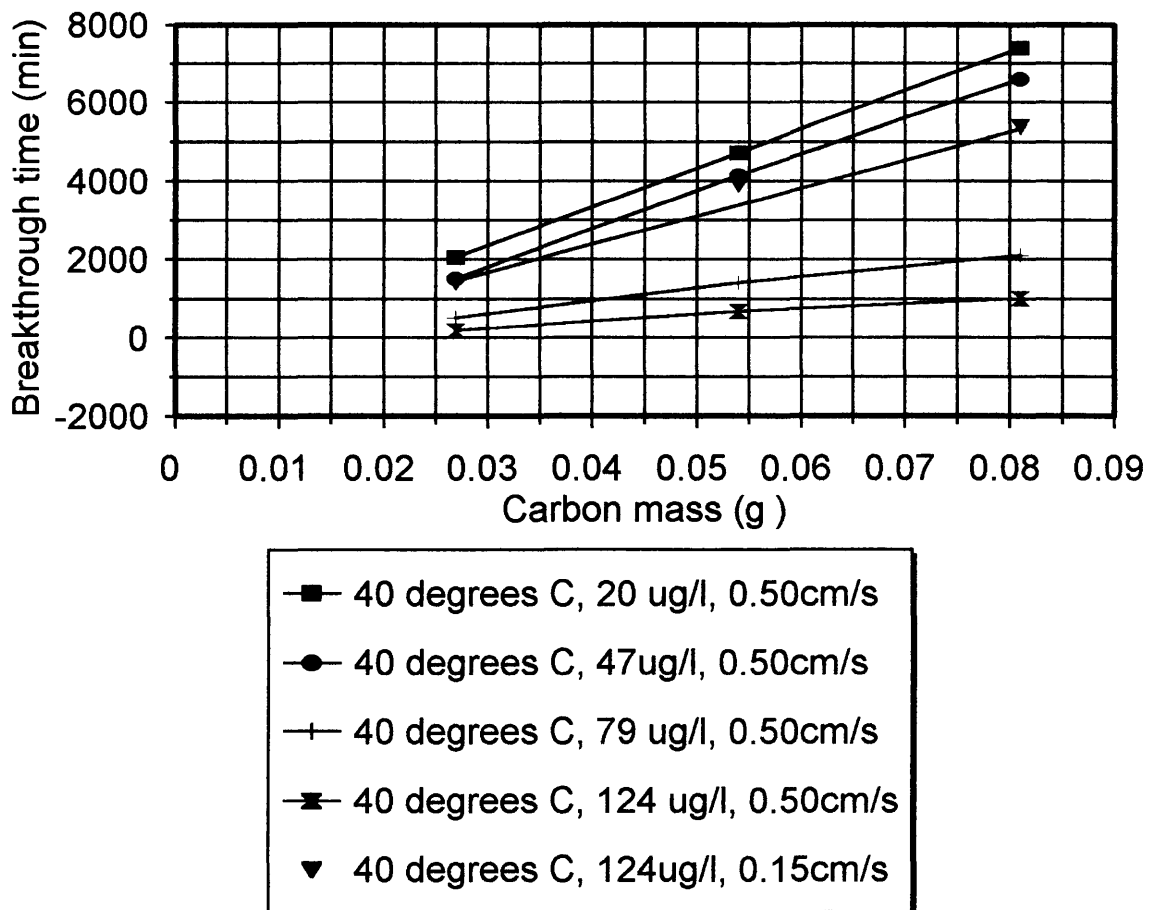
Figure 5.14:

Adsorption data for HD vapour on the PUCP. A plot of the t_b versus carbon mass impregnated into the textile layers shows a linear relationship as predicted by the Wheeler equation (2.37)
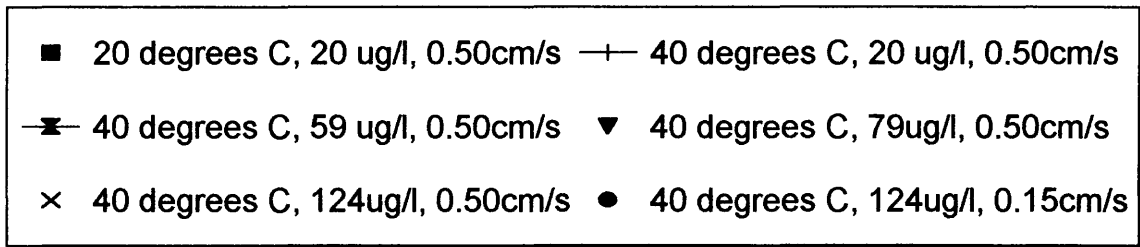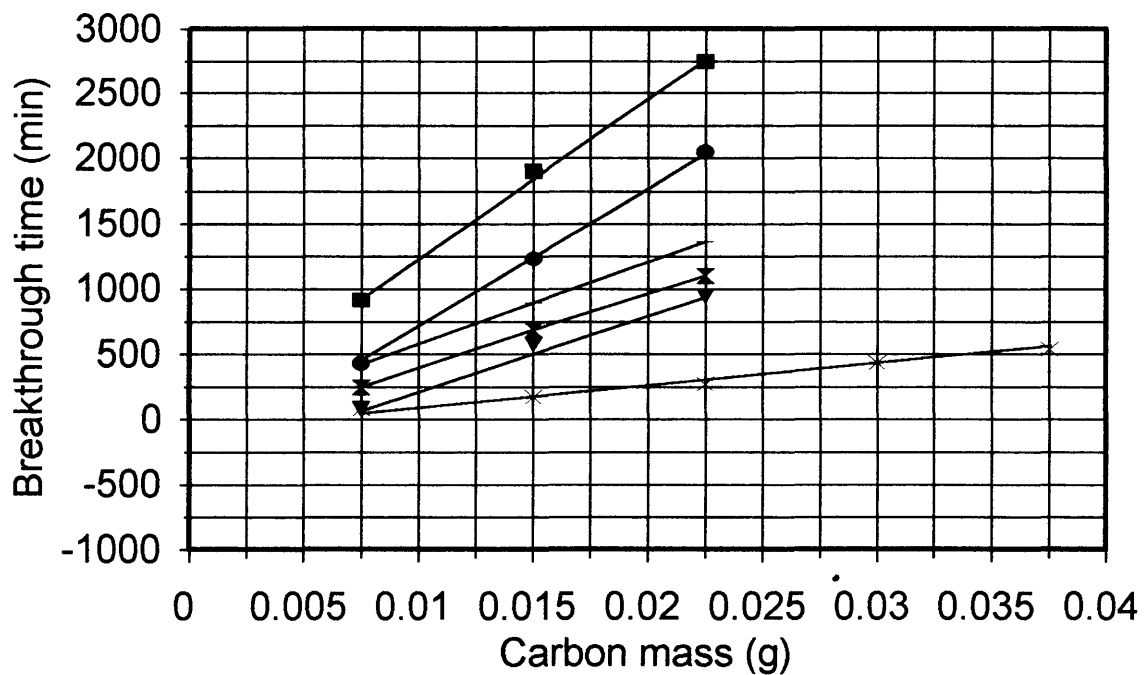
Figure 5.15:

Adsorption data for HD vapour on the CC. A plot of the t_b versus carbon mass impregnated into the textile layers shows a linear relationship as predicted by the Wheeler equation (2.37)
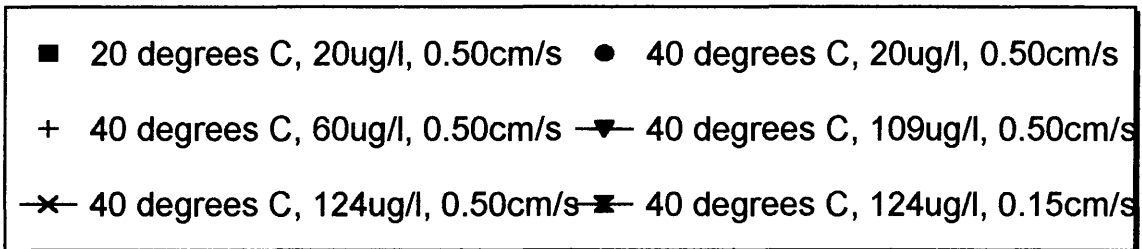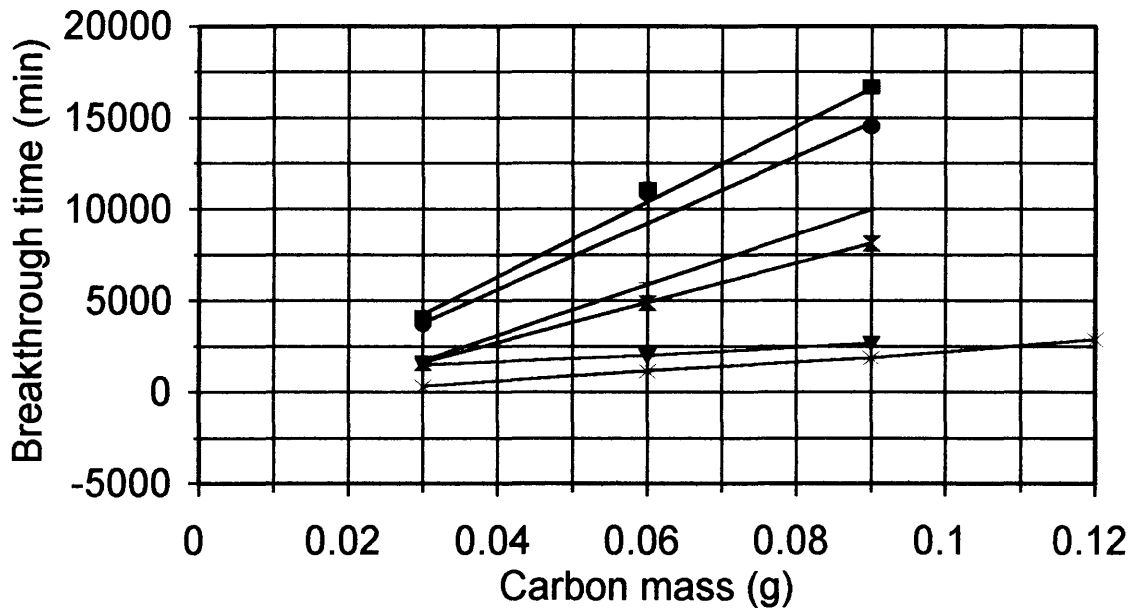
Figure 5.16:

Adsorption data for HD vapour on the C-spheres. A plot of the t_b versus carbon mass impregnated into the textile layers shows a linear relationship as predicted by the Wheeler equation (2.37)

From similarity considerations between the regression equations and equation *(2.37)*, adsorption capacity (W_e) values were calculated from the slope, which equalled $W_e / C_0 Q$ and adsorption rate (k_v) from the y-axis intercept, which equalled $-W_e \rho_B \ln(C_0 / C_x) / C_0 k_v$. The critical bed mass (W_c), or the mass of carbon just sufficient to reduce the inlet concentration to the arbitrarily chosen exit concentration, was calculated from $\rho_B \ln(C_0 / C_x)/k_v$ and are summarized in Tables 5.2, 5.3 and 5.4. The values calculated for k_v and W_e are summarised in Tables 5.2, 5.3 and 5.4 for the PUCP, the CC and the C-spheres respectively. The critical bed residence time (τ_c), or the time the HD vapour molecules have to spent in the carbon bed for complete adsorption was read from the graphs in Figures 5.26, 5.27 and 5.28 and are summarized in Tables 5.2, 5.3 and 5.4.

Table 5.1:

Linear regression of results with the Wheeler equation

TEXTILES	THEORETICAL REGRESSION EQUATION	COEFFICIENT OF CORRELATION (THEORETICAL)
20 °C, 20 µg/l, 0.50 cm/s		
CC	$t_b = 125\ 533.3\ W - 9$	0.999
C-spheres	$t_b = 226\ 083.3\ W - 3251.67$	0.989
40 °C, 20 µg/l, 0.50 cm/s		
CC	$t_b = 63\ 000\ W - 49.33$	0.999
C-spheres	$t_b = 180\ 000\ W - 1066.67$	0.995
PUPC	$t_b = 99\ 259.3\ W - 629$	0.999
40 °C, 60 µg/l, 0.50 cm/s		
CC	$t_b = 64\ 666.67\ W - 385.67$	0.988
PUCP	$t_b = 94\ 574.07\ W - 1\ 023.67$	0.989
40 °C, 124 µg/l, 0.50 cm/s		
CC	$t_b = 15\ 666.67\ W - 49.5$	0.989
C-spheres	$t_b = 27\ 833.3\ W - 500$	0.996
PUCP	$t_b = 15\ 351\ W - 198.67$	0.989
40 °C, 124 µg/l, 0.15 cm/s		
CC	$t_b = 107\ 800\ W - 378.3$	0.999
C-spheres	$t_b = 108\ 666.7\ W - 1620$	0.965
PUCP	$t_b = 71\ 759\ W - 125$	0.928

b. Yoon and Nelson

The inlet concentration (C_o), outlet concentration (C_x) and breakthrough times (t_b) were used to plot graphs similar to Figure 2.4. These graphs are illustrated in Figures 5.17 to 5.25. The results were subjected to linear regression. The gradient and y-intercept were calculated and used for the calculation of k_v and W_e. The values are also summarised in Tables 5.2, 5.3 and 5.4 for the different textiles. Different values for k_v and W_e were obtained for each textile layer

108

calculated with the Yoon and Nelson equation as the k_v and W_e are dependent on the sorbent mass.
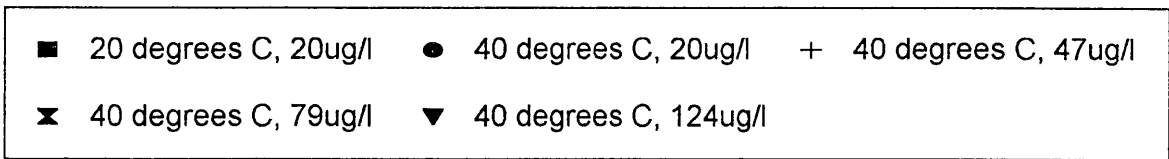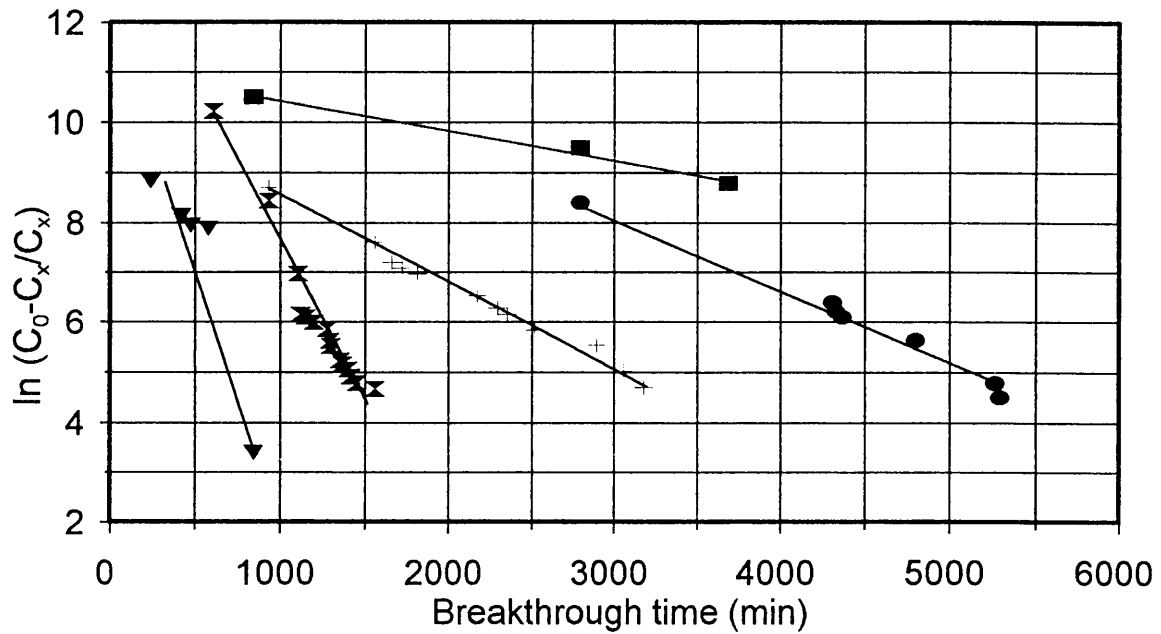
Figure 5.17 :

Adsorption data for HD vapour on the PUCP. A plot of ln $(C_0 - C_x / C_x)$ versus t_b shows a linear relationship as predicted by the Yoon and Nelson equation (2.40). The results were obtained with one textile layer. The air velocity (v) was constant for all test conditions namely, 0.50 cm/s

109
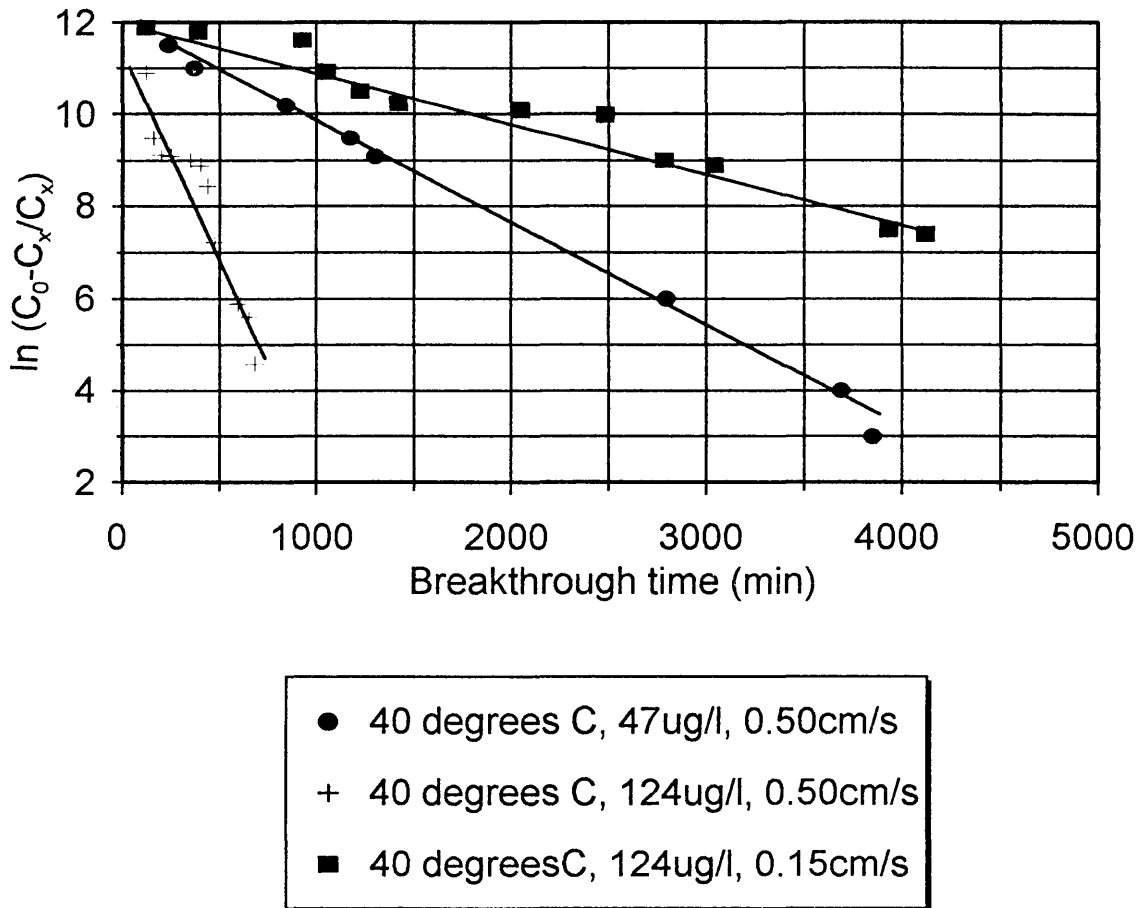
Figure 5.18 :

Adsorption data for HD vapour on the PUCP. A plot of $\ln (C_0 - C_x / C_x)$ versus t_b
shows a linear relationship as predicted by the Yoon and Nelson equation
(2.40). The results were obtained with two textile layers.

110

Figure 5.19:

Adsorption data for HD vapour on the PUCP. A plot of $\ln (C_0 - C_x / C_x)$ versus t_b shows a linear relationship as predicted by the Yoon and Nelson equation (2.40). The results were obtained with three textile layers.

Figure 5.20:

Adsorption data for HD vapour on the CC. A plot of $\ln (C_0 - C_x / C_x)$ versus t_b shows a linear relationship as predicted by the Yoon and Nelson equation (2.40). The results were obtained with one textile layer.

Figure 5.21:

Adsorption data for HD vapour on the CC. A plot of In $(C_0 - C_x / C_x)$ versus t_b shows a linear relationship as predicted by the Yoon and Nelson equation (2.40). The results were obtained with two textile layers.

113
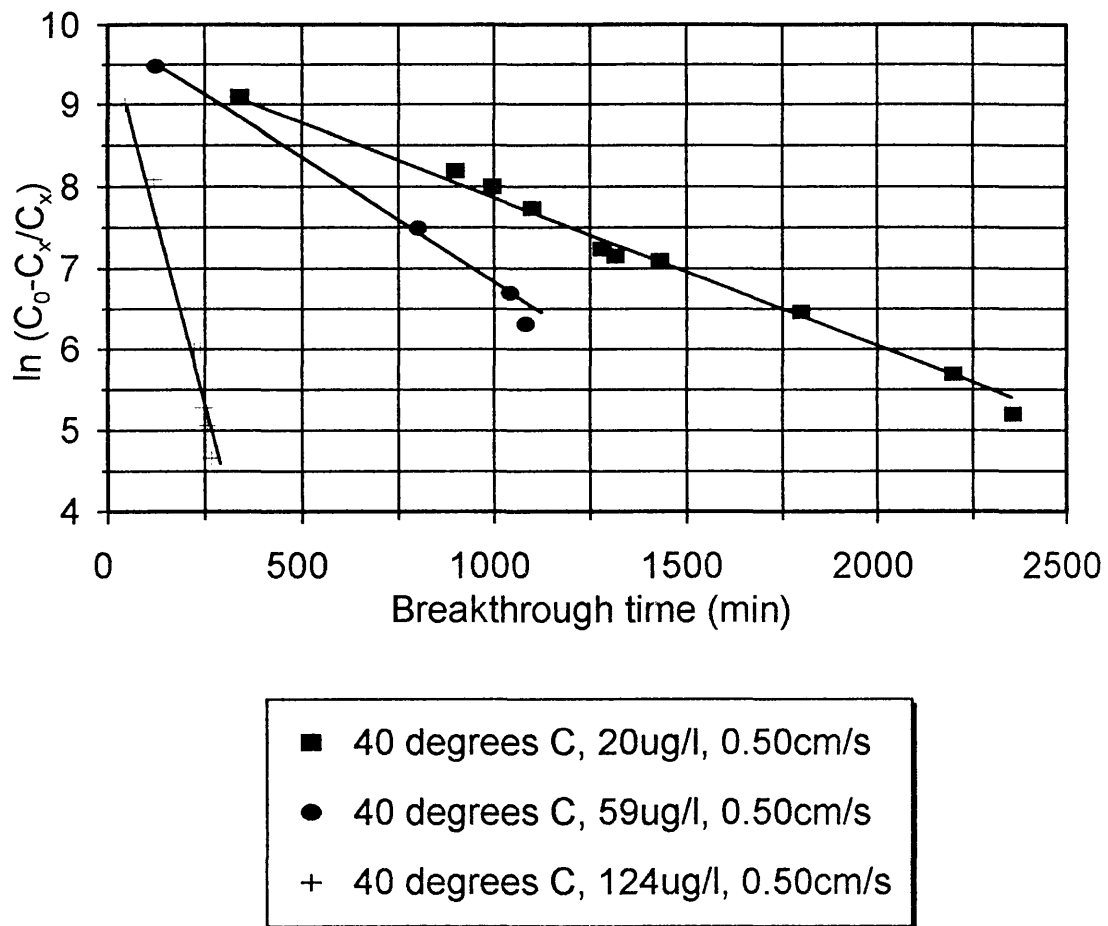
Figure 5.22:

Adsorption data for HD vapour on the CC. A plot of $\ln(C_0 - C_x / C_x)$ versus t_b shows a linear relationship as predicted by the Yoon and Nelson equation (2.40). The results were obtained with three textile layers.
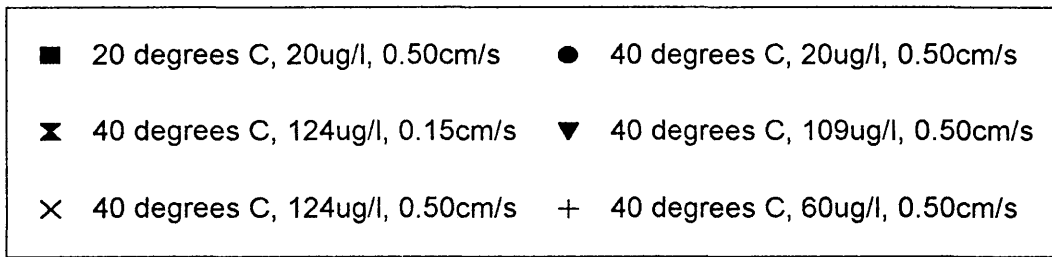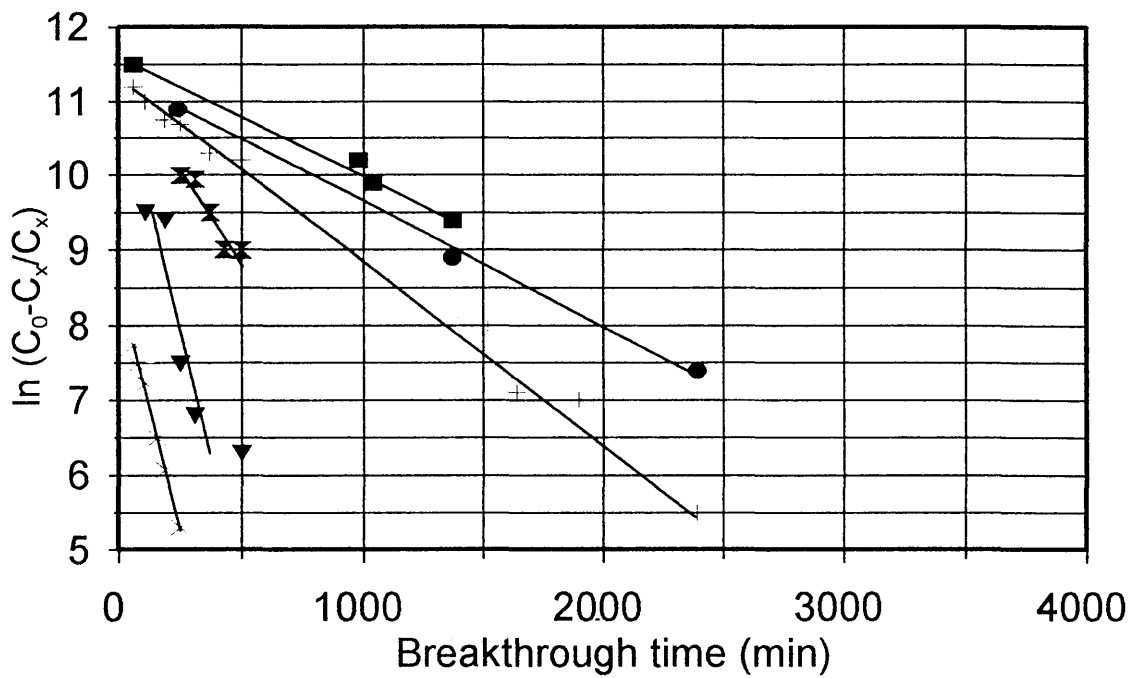
Figure 5.23:

Adsorption data for HD vapour on the C-spheres. A plot of $\ln(C_0 - C_x / C_x)$ versus t_b shows a linear relationship as predicted by the Yoon and Nelson equation (2.40). The results were obtained with one textile layer.

115
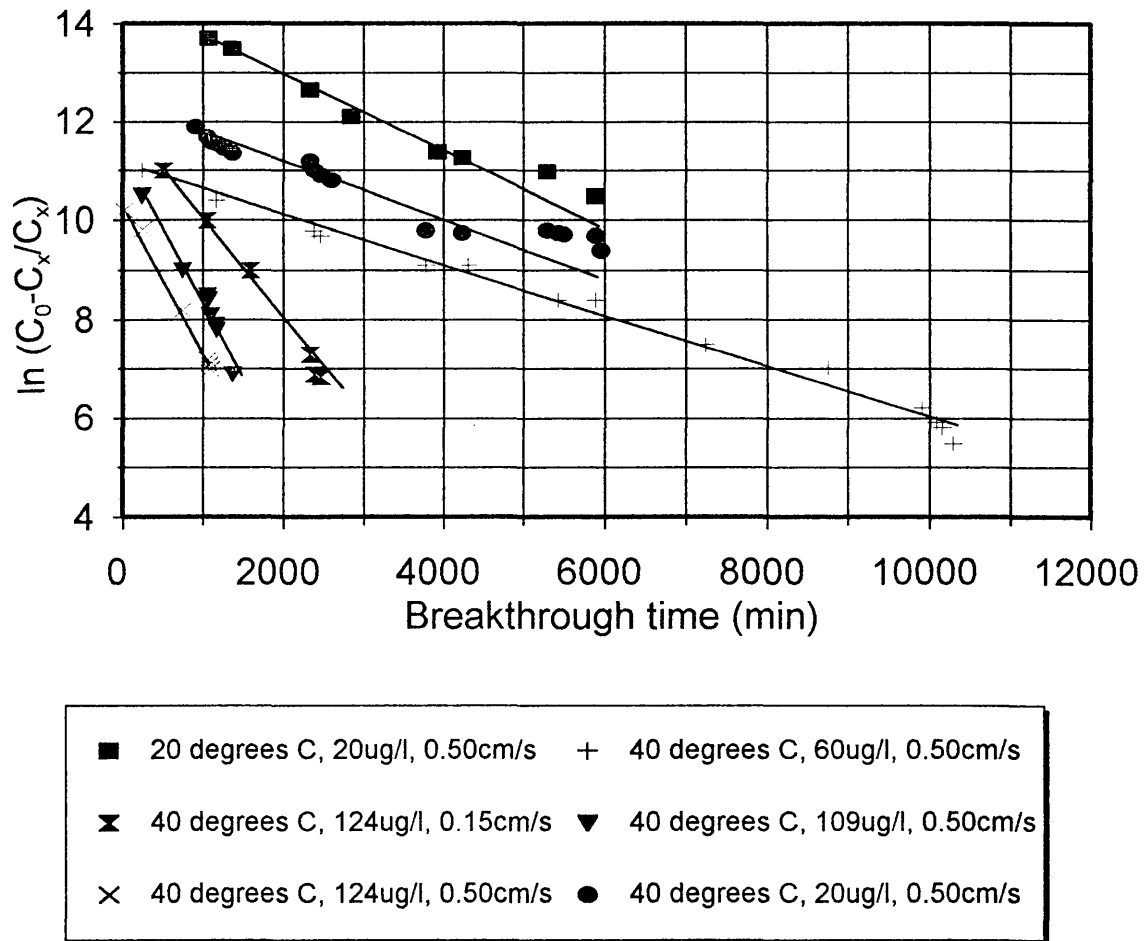
Figure 5.24:

Adsorption data for HD vapour on the C-spheres. A plot of $\ln (C_0 - C_x / C_x)$ versus t_b shows a linear relationship as predicted by the Yoon and Nelson equation (2.40). The results were obtained with two textile layers.
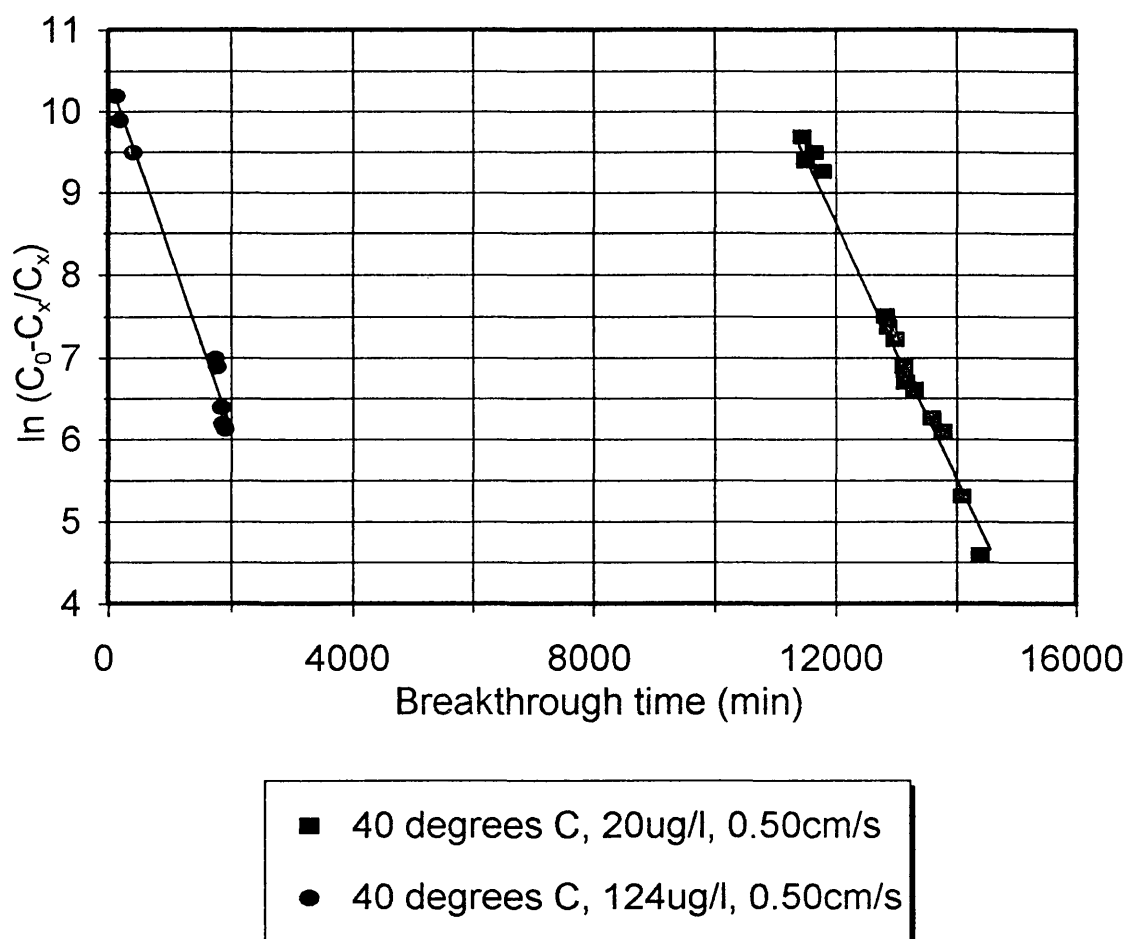
Figure 5.25:

Adsorption data for HD vapour on the C-spheres. A plot of ln $(C_0 - C_x / C_x)$

versus t_b shows a linear relationship as predicted by the Yoon and Nelson

equation (2.40). The results were obtained with three textile layers.

c. Ackley

The residence time (τ) was calculated with the three different methods, d_b / V_f, V/Q and $W/Q\rho_B$. Similar plots, to Figure 2.5, for τ as function of t_b were obtained for the different textiles under different test conditions. These graphs are illustrated in Figures 5.26 to 5.28. Straight lines were obtained and the gradients and y-intercepts were used to calculate the k_v and W_e. The values were summarised in Tables 5.2, 5.3 and 5.4.
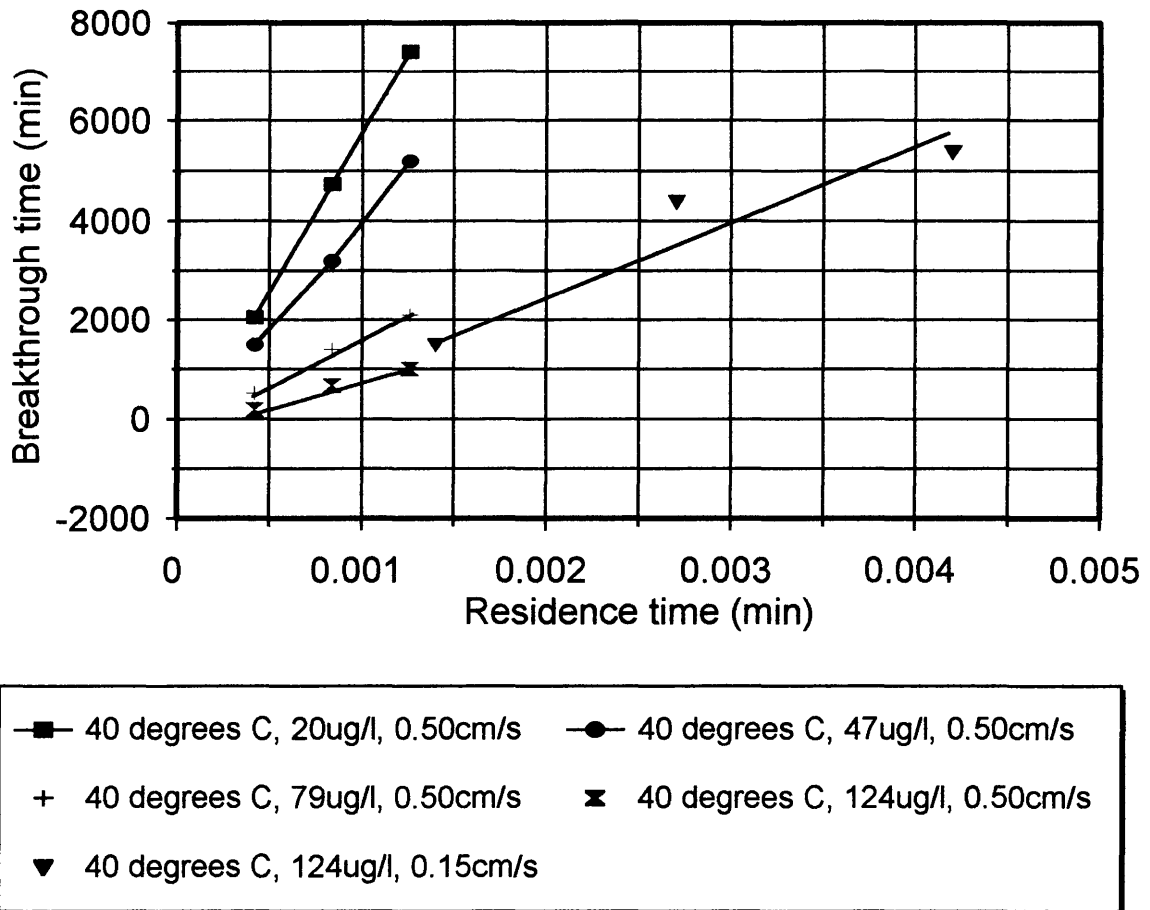
Figure 5.26:

Adsorption data for HD vapour on the PUCP. A plot of τ versus the t_b shows a linear relationship as predicted by the Ackley equation (2.43).

119
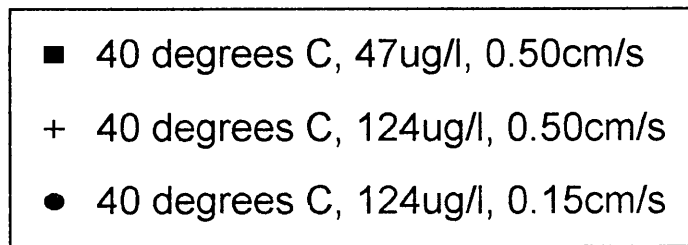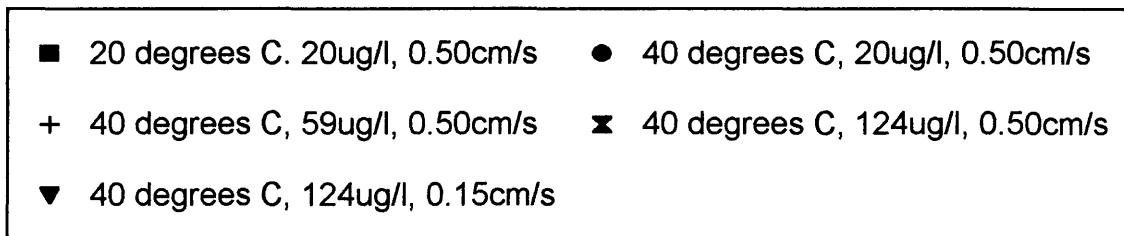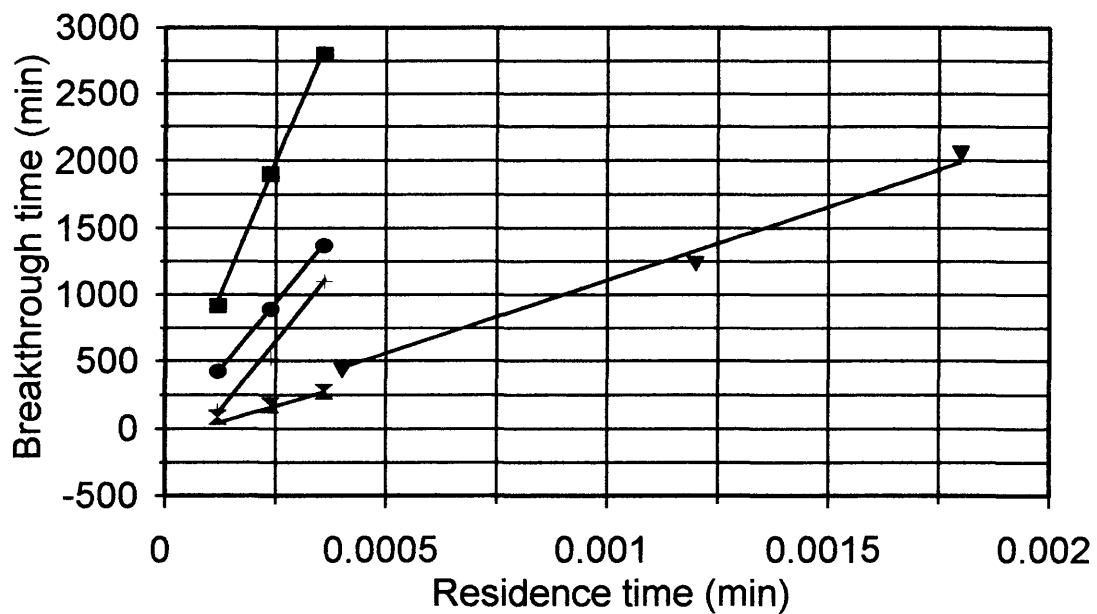
Figure 5.27:

Adsorption data for HD vapour on the CC. A plot of τ versus the t_b shows a linear relationship as predicted by the Ackley equation (2.43).
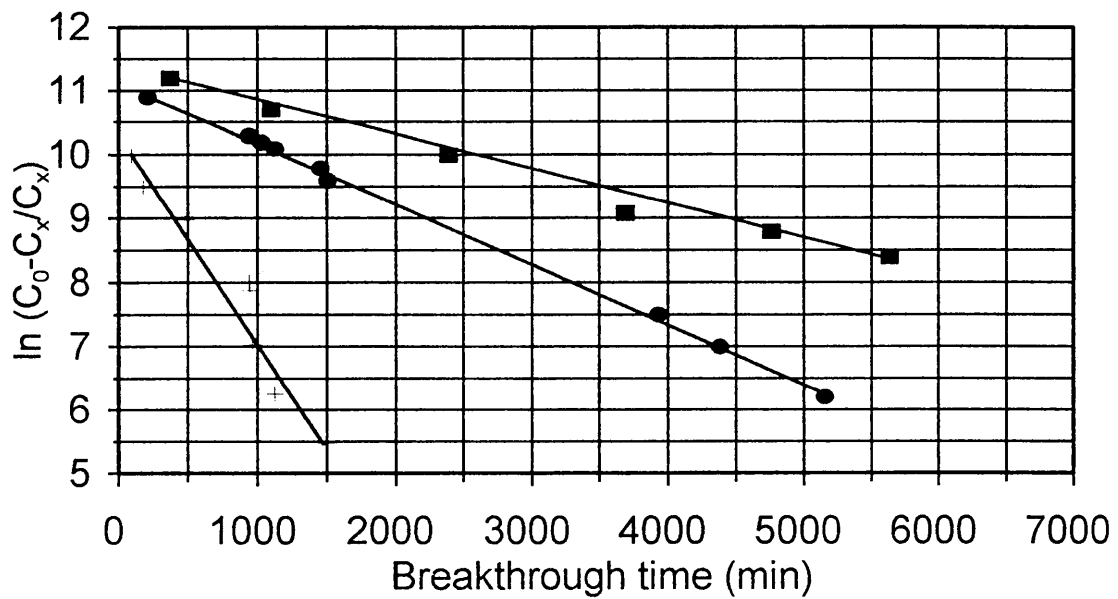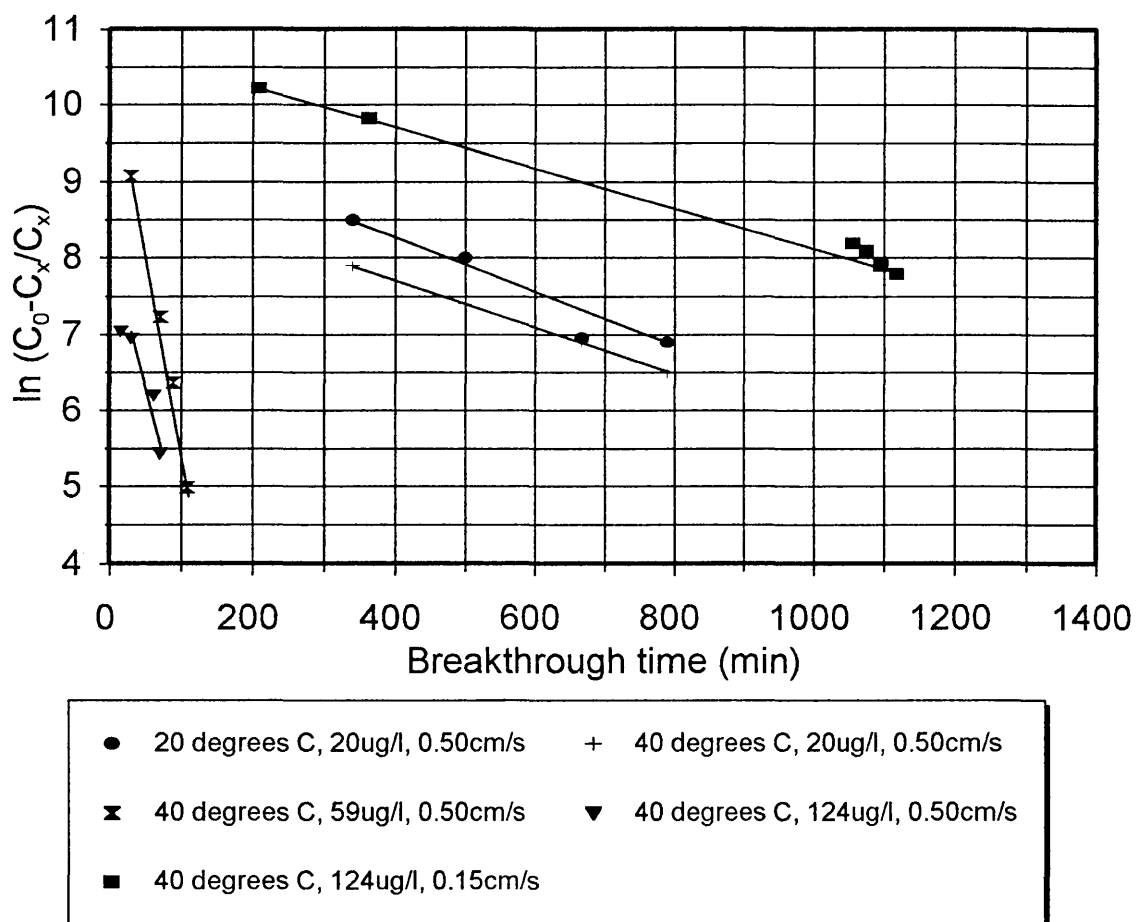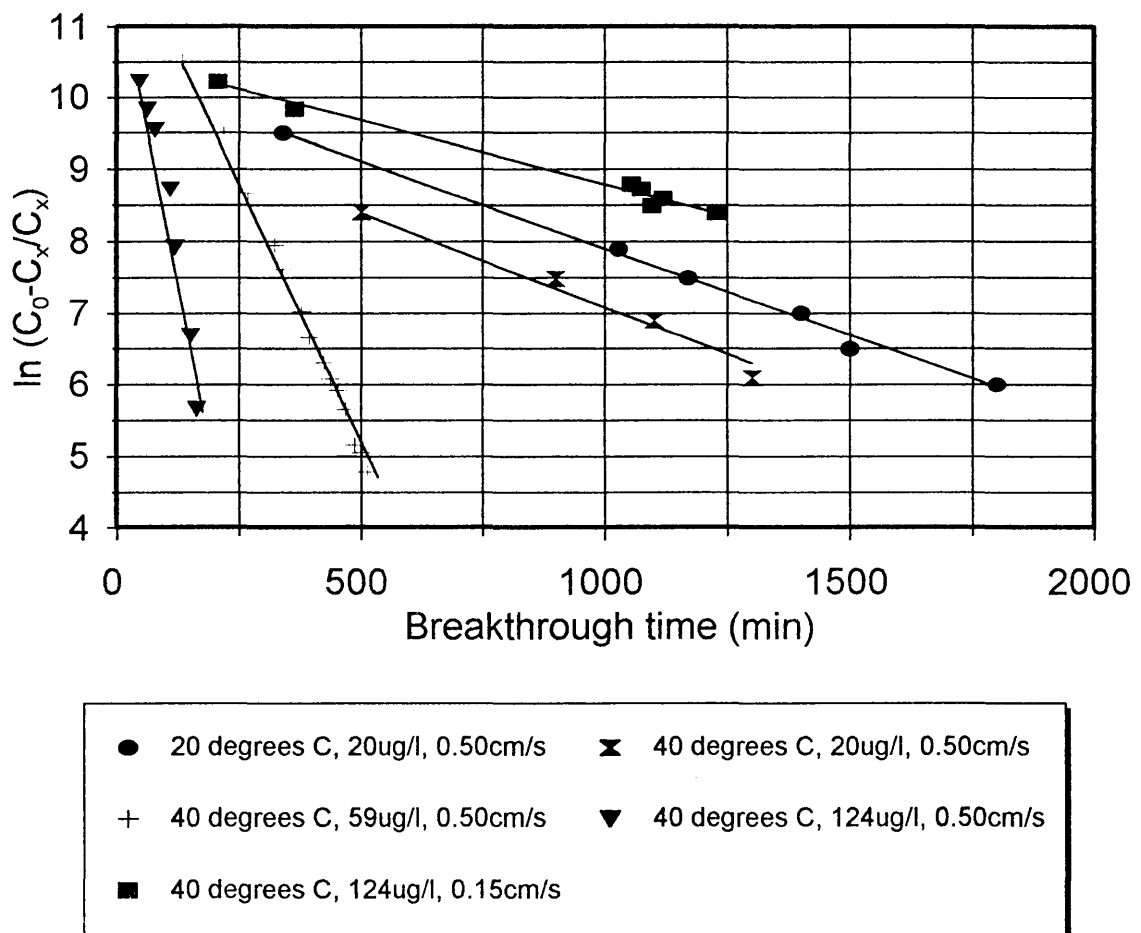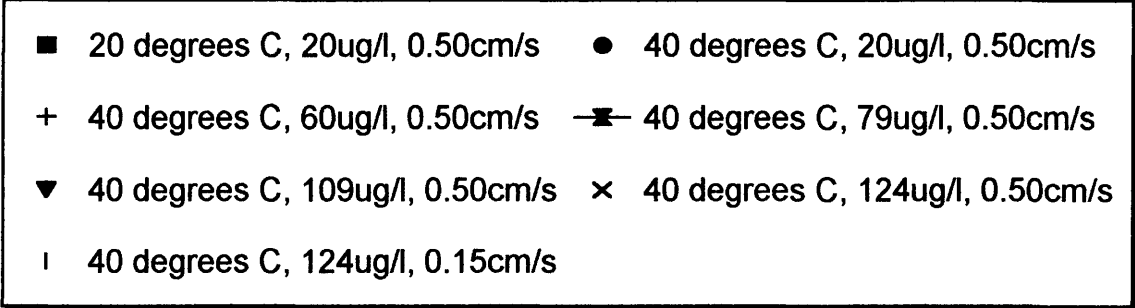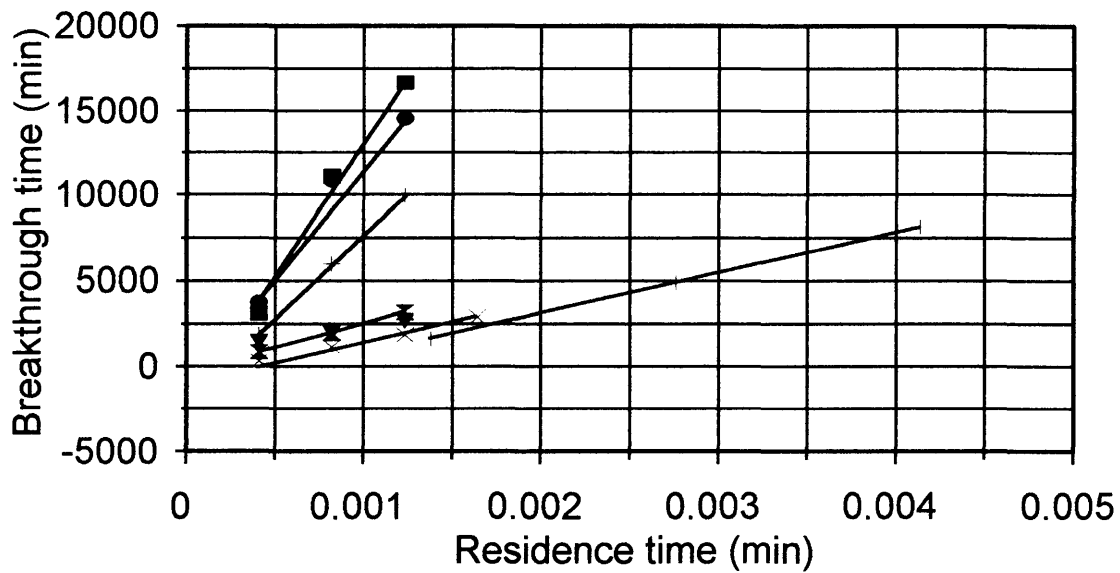
Figure 5.28:

Adsorption data for HD vapour on the C-spheres. A plot of τ versus the t_b shows a linear relationship as predicted by the Ackley equation (2.43).

The values for k_v and W_e differed much from the values calculated with the Wheeler and Yoon and Nelson equations. The thicknesses of the textiles (d_b) were measured with a textile thickness gauge as 0.086 cm, 0.076 cm and 0.093 cm for the CC, the C-spheres and the PUCP respectively. These thicknesses were used to calculate the residence times.

The residence time, calculated with the carbon mass impregnated in the textile ($W/Q\rho_B$), was substituted into the equation $\tau = d_b / V_f$, using the linear air velocity, the bed depths (d_b) for the different textiles were calculated as: CC = 0.0036 cm, PUCP = 0.0127 cm and C-spheres = 0.0124 cm. The calculated bed depth was used to calculate the k_v and W_e. These calculated values compared very well with the values calculated with the Wheeler equation, whereas the values calculated with the measured thicknesses in some cases could not be compared (and are therefore not summarised in Tables 5.2, 5.3 and 5.4). Only one value was obtained for the k_v and W_e with the Wheeler and Ackley equations at each set of test conditions, respectively.

Table 5.2:

Rate constants, HD capacity and critical masses for the PUCP at different challenge conditions

	WHEELER	YOON & NELSON			ACKLEY
		1 layer	2 layer	3 layer	$\tau = d_b/v_f$
20 °C, 20 µg/l, 0.50 cm/s					
$k_v(min^{-1})$	*	24 835.3 ± 1211.6			
$W_o (g/gC)$		0.214 ± 0.002			
40 °C, 20 µg/l, 0.50 cm/s					
$k_v(min^{-1})$	46 094.6 ± 732.4	36 732.5	34 134	40 475	46 614 ± 696.7
$W_o (g/gC)$	0.089 ± 0.001	0.243	0.213	0.198	0.090 ± 0.001
$W_c(g)$	0.006	-	-	-	-
$\tau_c(s)$	-	-	-	-	0.0059
40 °C, 79 µg/l, 0.50 cm/s					
$k_v(min^{-1})$	37 605.9 ± 292.1	21 656	20 321.2	21 436.2	37 889.9 ± 296.4
$W_o (g/gC)$	0.100 ± 0.019	0.434	0.315	0.259	0.101 ± 0.030
$W_c(g)$	0.008	-	-	-	-
$\tau_c(s)$	-	-	-	-	0.0073
40 °C, 124 µg/l, 0.50 cm/s					
$k_v(min^{-1})$	22 742.9 ± 1722.0	30 841.7	17 110.1	38 470.3	22 826 ± 1711
$W_o (g/gC)$	0.086 ± 0.001	0.151	0.105	0.078	0.086 ± 0.011
$W_c(g)$	0.0129	-	-	-	-
$\tau_c(s)$	-	-	-	-	0.013
50 °C, 124 µg/l, 0.50 cm/s					
$k_v(min^{-1})$	*	21 000.3			
$W_o (g/gC)$		0.084			
40 °C, 124 µg/l, 0.15 cm/s					
$k_v(min^{-1})$	49 097.8 ± 5934.8	9 512.3	7 504.0	13 495.4	26 780.9 ± 3236.7
$W_o (g/gC)$	0.118 ± 0.001	0.128	0.147	0.116	0.120 ± 0.001
$W_c(g)$	0.0017	-	-	-	-
$\tau_c(s)$	-	-	-	-	0.015

* - only one textile layer was evaluated

123

Table 5.3:
Rate constants, HD capacity and critical masses for the CC at different challenge conditions

	WHEELER	YOON & NELSON			ACKLEY
		1 layer	2 layer	3 layer	$\tau = d_b/v_f$
20 °C, 20 µg/l, 0.50 cm/s					
k_v(min^{-1})	2.95x10^6 ± 1.5x10^6	124 415	45 624.1	-	4.01x10^6 ± 2.01x10^5
W_e (g/gC)	0.113 ± 0.001	0.303	0.368	-	0.113 ± 0.001
W_c(g)	0.0007	-	-	-	-
τ_c(s)	-	-	-	-	0.00007
40 °C, 20 µg/l, 0.50 cm/s					
k_v(min^{-1})	377 488.7 ± 78 115.5	60 119.7	41 217.2	27 985.7	366 994.9 ± 75 943
W_e (g/gC)	0.057 ± 0.001	0.217	0.406	0.349	0.057 ± 0.001
W_c(g)	0.0008	-	-	-	-
τ_c(s)	-	-	-	-	0.00075
40 °C, 59 µg/l, 0.50 cm/s					
k_v(min^{-1})	48 184.7	89 140.8	46 920.2	39 993.3	48 150.0
W_e (g/gC)	0.059	0.144	0.325	0.452	0.172
W_c(g)	0.006	-	-	-	-
τ_c(s)	-	-	-	-	0.0057
40 °C, 124 µg/l, 0.50 cm/s					
k_v(min^{-1})	93 531.9 ± 19 285.9	58 917.9	46 451.2	46 621.1	311 715 ± 64 271
W_e (g/gC)	0.087 ± 0.001	3.335	0.198	0.091	0.071 ± 0.001
W_c(g)	0.0032	-	-	-	-
τ_c(s)	-	-	-	-	0.0015
40 °C, 124 µg/l, 0.15 cm/s					
k_v(min^{-1})	23 665.6 ± 625.7	31 380.9	40 272.7	-	24 551 ± 648
W_e (g/gC)	0.174 ± 0.001	0.243	0.292	-	0.181 ± 0.001
W_c(g)	0.0035	-	-	-	-
τ_c(s)	-	-	-	-	0.0112

Table 5.4:

Rate constants, HD capacity and critical masses for the C-spheres at different challenge conditions

	WHEELER	YOON & NELSON			ACKLEY
		1 layer	2 layer	3 layer	$T = d_b/v_f$
20 °C, 20 µg/l, 0.50 cm/s					
$k_v(min^{-1})$	23 134.4 ± 71.1	17 815	10 159	-	22 376 ± 68
W_e (g/gC)	0.204 ± 0.001	0.267	0.201	-	0.205 ± 0.011
$W_c(g)$	0.0144	-	-	-	-
$\tau_c(s)$	-	-	-	-	0.0114
40 °C, 20 µg/l, 0.50 cm/s					
$k_v(min^{-1})$	56 151.1	43 925.0	21 196.1	23 949.8	56 737.3
W_e (g/gC)	0.162 ± 0.001	0.136	0.228	0.171	0.162 ± 0.033
$W_c(g)$	0.0059	-	-	-	-
$\tau_c(s)$	-	-	-	-	0.0049
40 °C, 124 µg/l, 0.50 cm/s					
$k_v(min^{-1})$	18 527.1 ± 370.6	20 267.6	84 398.4	99 138.6	18 716 ± 373
W_e (g/gC)	0.155 ± 0.001	0.135	0.119	0.124	0.156 ± 0.005
$W_c(g)$	0.0179	-	-	-	-
$\tau_c(s)$	-	-	-	-	0.0147
40 °C, 124 µg/l, 0.15 cm/s					
$k_v(min^{-1})$	6 447.2 ± 39.8	8 247.6	12 157.5	20 248.1	6 701 ± 41
W_e (g/gC)	0.175 ± 0.001	0.155	0.117	0.135	0.181 ± 0.001
$W_c(g)$	0.0149	-	-	-	-
$\tau_c(s)$	-	-	-	-	0.0408

The critical mass needed to reduce the outlet concentration to 1% of the inlet concentration was less than the impregnated carbon mass for the PUCP, CC

125

and C-spheres, namely 0.027 g, 0.0075 g and 0.03 g respectively. The critical residence time (τ_c) needed to reduce the outlet concentration to 1% of the inlet concentration was in all cases less than the residence time (τ) of the HD molecule in the PUCP, CC and C-spheres textile namely, 0.0254 s, 0.0072 s and 0.0248 s, respectively at an air velocity of 0.50 cm/s.

The results showed that the parameters calculated with the Wheeler and Ackley equations are in good agreement. The k_v and W_e have single values for the different test conditions because the equations do not take account of the bed depth. Different values for k_v and W_e were obtained for the different textile layers with the Yoon and Nelson equation due to the different adsorbent masses which were used in the calculation.

In general, the rate constant showed that the CC had a higher adsorption rate than the PUCP, which in turn had a higher adsorption rate than the C-spheres. This could be due to the small particles of the CC and the powder impregnated into the polyurethane foam rubber, compared with the large particles of the C-spheres. The adsorption capacity of the C-spheres was the highest, followed by the W_e of the PUCP and the CC, due to the large micropore volume of the C-spheres.

The W_e and k_v calculated with *(2.37)*, *(2.40)* and *(2.43)* in Tables 5.2, 5.3 and 5.4 were used to calculate t_b and were compared with the experimentally measured t_b's. The values for the test conditions 40 °C, 124 μg/l and 0.50 cm/s are summarized in Table 5.5. The percentage deviation of the calculated from the experimental value is also summarized in Table 5.5.

The results in Table 5.5 show a small deviation from the experimental data calculated with the Wheeler equation. The t_b's calculated with the Ackley equation showed small deviations from the experimental data for one layer of the PUCP and one, two and three layers of the CC textiles. At higher adsorbent

masses the percentage deviation exceeded 10%. The percentage deviation from the experimental data for the C-spheres was high. The t_b's calculated with the Yoon and Nelson equation showed small percentage deviations from the experimental data for two and three layers of the PUCP. The percentage deviations for the other textiles were high.

Table 5.5:

Comparison of the t_b's calculated with equations (2.37), (2.40) and (2.43) and the experimentally measured t_b's.

Adsorbent mass (g)	t_b (exp) (min)	t_b (Wheeler) (min)	% deviation	t_b (Yoon&Nelson) (min)	% deviation	t_b (Ackley) (min)	% deviation
PUCP							
0.027	191	217	13.6	473	147.6	194	1.6
0.054	680	633	-6.9	694	2.1	587	-13.7
0.081	1020	1049	2.8	1025	0.5	979	-4.1
CC							
0.0075	85	69	-18.8	1573	1750.6	83	-2.4
0.015	175	185	5.7	313	78.9	178	1.7
0.0225	275	302	9.8	275	0	274	-0.4
0.03	440	419	-4.8	-		369	-16.1
0.0375	540	536	-0.7	-		464	-14.1
C-spheres							
0.03	350	334	4.6	701	100.3	690	97.1
0.06	1200	1167	-2.8	1572	31	1550	29.2
0.09	1900	2001	5.3	2443	28.6	2410	26.8
0.12	2900	2834	-2.3	-		3270	12.8

5.2.2 Influence of the challenge concentration on the adsorption capacity

a. PUCP

The adsorption capacity *(W_e)* as calculated with the Wheeler equation, was plotted as a function of the HD concentration at constant temperature (40°C) and linear velocity (0.50 cm/s), as illustrated in Figure 5.29.

128
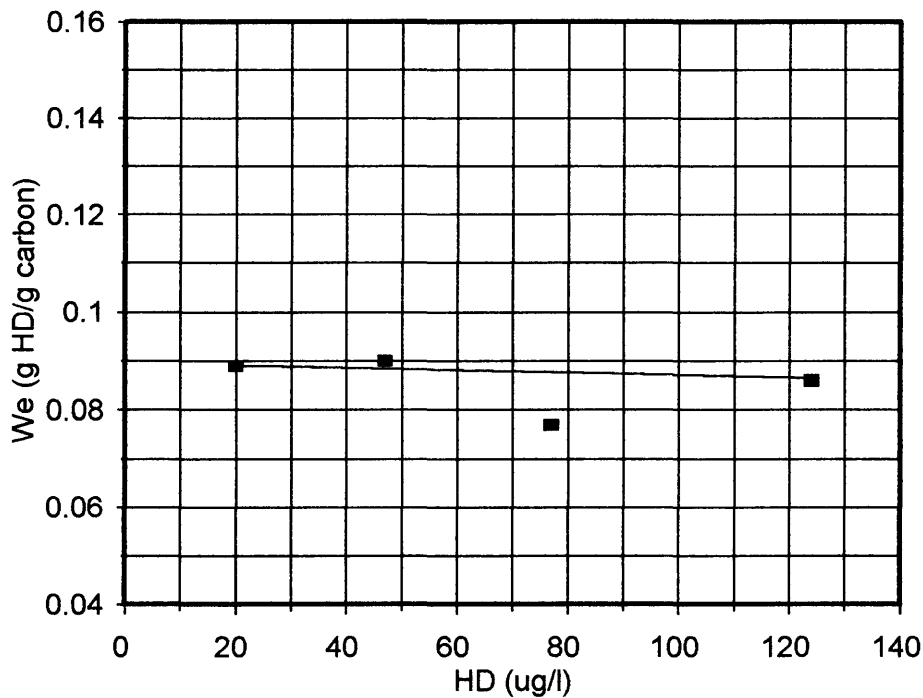
FIGURE 5.29:

Adsorption capacity of the PUCP as a function of the challenge concentration.

According to Figure 5.29 the adsorption capacity stayed constant over the concentration range studied due to a decreasing rate constant. At lower concentrations the capacity is high due to a large micropore volume and the number of HD molecules per bed volume is sufficiently low to be adsorbed within the residence time of the molecules in the carbon bed. At higher exposure concentrations the capacity remains the same. Although a larger number of HD molecules are available for adsorption, the adsorption rate is not sufficiently high for a larger number of molecules to be adsorbed. From the micropore volume studies discussed in Chapter 4, it follows that the capacity for nitrogen at 77 K is $0.083 \text{ cm}^3 \text{ N}_2$ /g of carbon. An average capacity of 0.086 g HD/ g carbon was measured over the concentration range, which is equal to 0.068 cm^3 HD/ g carbon at a HD density of ρ = 1.274 kg/l, or 80.7% occupancy of the micropore

129

volume of the PUCP.

The W_e was calculated experimentally with the breakthrough times (t x challenge concentration / carbon mass), with the Wheeler equation (2.37) and with the Ackley equation (2.43) and are listed in Table 5.6.

TABLE 5.6 :

HD adsorption capacity for the PUCP

$W_e(t_b)$ (g HD/g carbon)	W_e(Wheeler) (g HD/g carbon)	W_e(Ackley) (g HD/g carbon)
40°C, 20 μg/l, 0.50 cm/s		
0.077 ± 0.007	0.089 ± 0.001	0.090 ± 0.001
40°C, 124 μg/l, 0.50 cm/s		
0.070 ± 0.001	0.086 ± 0.001	0.086 ± 0.011
40°C, 124 μg/l, 0.15 cm/s		
0.118 ± 0.017	0.116 ± 0.001	0.120 ± 0.001

The capacity and micropore volume correlates, namely a high capacity is found for the PUCP with a large micropore volume. The HD capacities calculated with the experimentally measured t_b were in general lower than the values calculated with equations (2.37) and (2.43), this could be due to the 80% occupation of the micropore volume only. The capacities obtained for these two equations were obtained from linear regression of the experimental results for at least one, two and three textile layers, respectively.

A sensitivity analysis was conducted on the W_e values calculated from the Wheeler equation. The test condition: 20 °C, 20 μg/l and a linear velocity of 0.50 cm/s, was taken as the reference test condition. The percentage variation from the reference W_e was calculated for the other conditions. The reference

130

condition for the PUCP was chosen as 40 °C, 20 μg/l and a linear velocity of 0.50 cm/s. The results are illustrated in Figure 5.30.

Variables

■	40 degrees C, 20ug/l, 0.50cm/s
□	40 degrees C, 124ug/l, 0.50cm/s
▨	40 degrees C, 124ug/l, 0.15cm/s
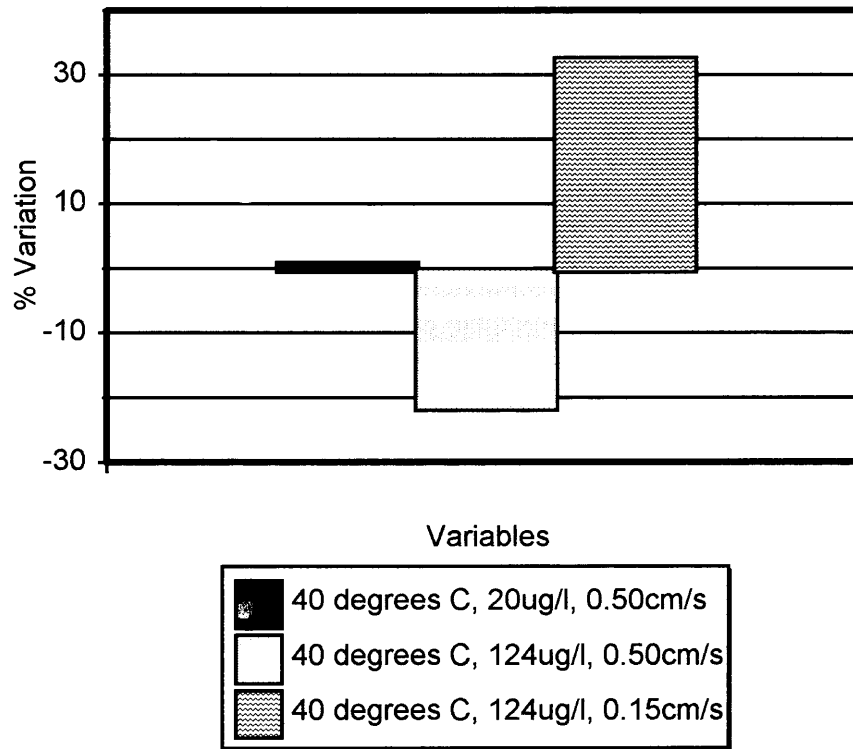
FIGURE 5.30:

% variation of W_e of the PUCP calculated with the Wheeler equation.

The decrease for W_e of HD adsorption on the PUCP is not linear with the increase in the exposure concentration as an 21.1% decrease in the W_e was measured for an increase of 520% in the exposure concentration. The decrease measured for W_e could be due to an overloading of the carbon or too short a residence time in the carbon bed as was illustrated with the reduction in the linear velocity. The W_e increased by 32% for a decrease in the linear velocity from 0.50 cm/s to 0.15 cm/s in spite of the large increase in the inlet concentration. This could be due to increased residence time of the HD vapour in the textile.

b. CC

The HD capacity of the CC was expressed as a function of HD concentration at constant temperature (40 °C) and linear velocity (0.50 cm/s), as illustrated in Figure 5.31.
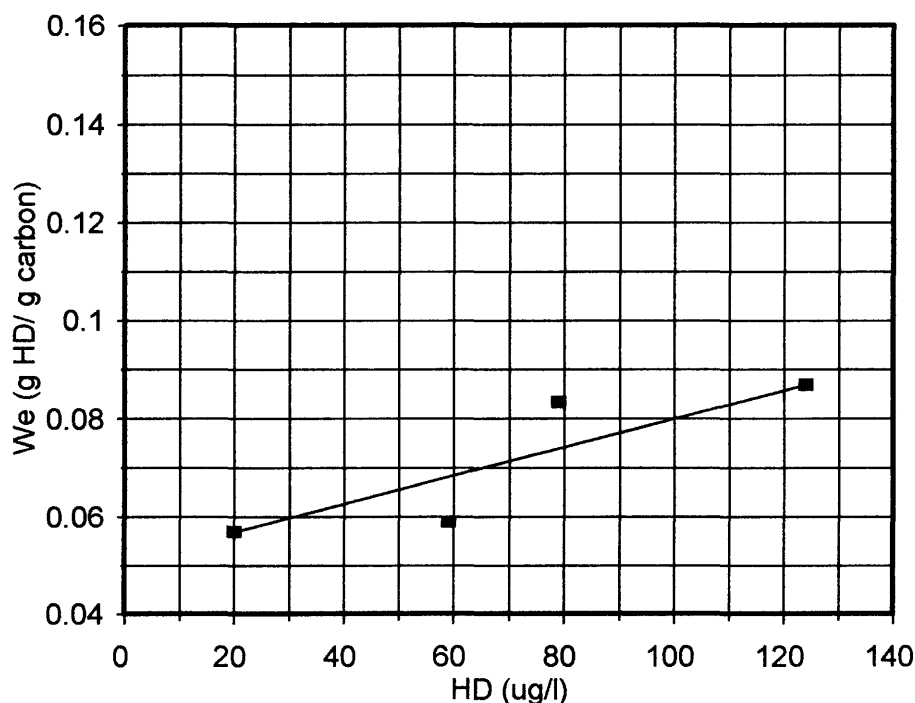
FIGURE 5.31:

Adsorption capacity of the CC as a function of the challenge concentration.

From Figure 5.31 the capacity (W_e) increased as a function of the HD concentration. At a HD concentration of 124 μg/l the maximum capacity for the CC was measured, namely 0.087 g HD/g carbon or 0.069 cm³ HD/g carbon. According to the micropore volume for nitrogen at 77K of 0.043 cm³ N_2/g carbon, calculated with the t-plot in Chapter 4, the micropore capacity was exceeded by approximately 61.4%. This could be due to pore filling of the mesopores of the CC.

The HD adsorption capacities calculated experimentally (t_b) and theoretically with equations **(2.37)** and **(2.43)** are listed in Table 5.7.

132

TABLE 5.7:

HD adsorption capacity for the CC

$W_e(t_b)$ (g HD/g carbon)	W_e(Wheeler) (g HD/g carbon)	W_e(Ackley) (g HD/g carbon)
20 °C, 20 μg/l, 0.50 cm/s		
0.112 ± 0.002	0.113 ± 0.001	0.113 ± 0.001
40 °C, 20 μg/l, 0.50 cm/s		
0.054 ± 0.001	0.057 ± 0.001	0.057 ± 0.001
40 °C, 124 μg/l, 0.50 cm/s		
0.072 ± 0.008	0.087 ± 0.001	0.071 ± 0.001
40 °C, 124 μg/l, 0.15 cm/s		
0.184 ± 0.127	0.174 ± 0.001	0.181 ± 0.001

The capacity and micropore volume correlates, namely a low capacity is found for the CC with a small micropore volume. The HD capacities calculated with the experimentally measured t_b correlated with the values calculated with equations (2.37) and (2.43).

Similar to the PUCP a sensitivity analysis was conducted on the W_e results obtained for the CC. The reference condition for this textile was similar to the NATO standard, namely 20 °C, 20 μg/l and a linear velocity of 0.50 cm/s. The results are depicted in Figure 5.32.

133

Variables

▨	20 degrees C, 20ug/l, 0.50cm/s
▨	20degreesC,20ug/l,0.50cm/s,2 layers
■	40 degrees C, 20ug/l, 0.50cm/s
□	40 degrees C, 124ug/l, 0.50cm/s
▨	40 degrees C, 124ug/l, 0.15cm/s

FIGURE 5.32:

% variation of W_e of the CC calculated with the Wheeler equation.

An increase in the carbon mass at the reference experimental condition (20 °C, 20 μg/l and 0.50 cm/s) did not improve the capacity markedly, which indicated that the carbon mass is sufficient to offer protection at this exposure concentration, or that the residence time in the single layer is long enough for complete adsorption, or that the rate of adsorption is high enough for effective adsorption. The capacity decreased by 49.5% for a 20 °C increase in the temperature. This could be due to an increase in the volatility of HD. (The volatility of HD increases from 610 mg/m³ at 20 °C to 2851 mg/m³ at 40 °C [2].) HD is physically adsorbed and physical adsorption is affected negatively by an increase in temperature and thus volatility. The decrease in capacity measured at increased exposure temperature and concentration (40 °C and 124 μg/l) was smaller than the decrease measured for increased exposure temperature alone (23%). This could be explained by an increase in the number of HD molecules available for adsorption. For a decrease in the linear velocity through the textile

134

an increase in the capacity supports the fact that the residence of the molecule in the carbon bed is longer which aids adsorption.

c. C-spheres

The HD capacity of the C-spheres was expressed as a function of HD concentration at constant temperature (40 °C) and linear velocity (0.50 cm/s) and the results are illustrated in Figure 5.33. The experimental and theoretical values calculated are depicted in Table 5.4. According to Figure 5.33, the adsorption capacity stayed constant over the HD concentration range (20 - 124 μg/l). The HD capacity measured for the C-spheres is higher than the capacities measured for the PUCP and CC textiles. This could be explained by the large micropore volume which was measured (Chapter 4). The capacity remained constant over the concentration range due to a decreasing rate constant. At lower concentrations the capacity is high due to a large micropore volume and the number of HD molecules per bed volume is sufficiently low to be adsorbed within the residence time of the molecules in the carbon bed. At higher exposure concentrations the capacity remains the same. Although a larger number of HD molecules are available for adsorption, the adsorption rate is not sufficiently high for a larger number of molecules to be adsorbed. From the micropore volume studies discussed in Chapter 4, it follows that the capacity for nitrogen at 77 K is 0.132 cm^3 N$_2$ /g of carbon. An average capacity of 0.155 g HD/ g carbon was measured over the concentration range, which is equal to 0.122 cm^3 HD/ g carbon at a HD density of ρ = 1.274 kg/l, or 92.4% occupancy of the micropore volume of the C-spheres.

135
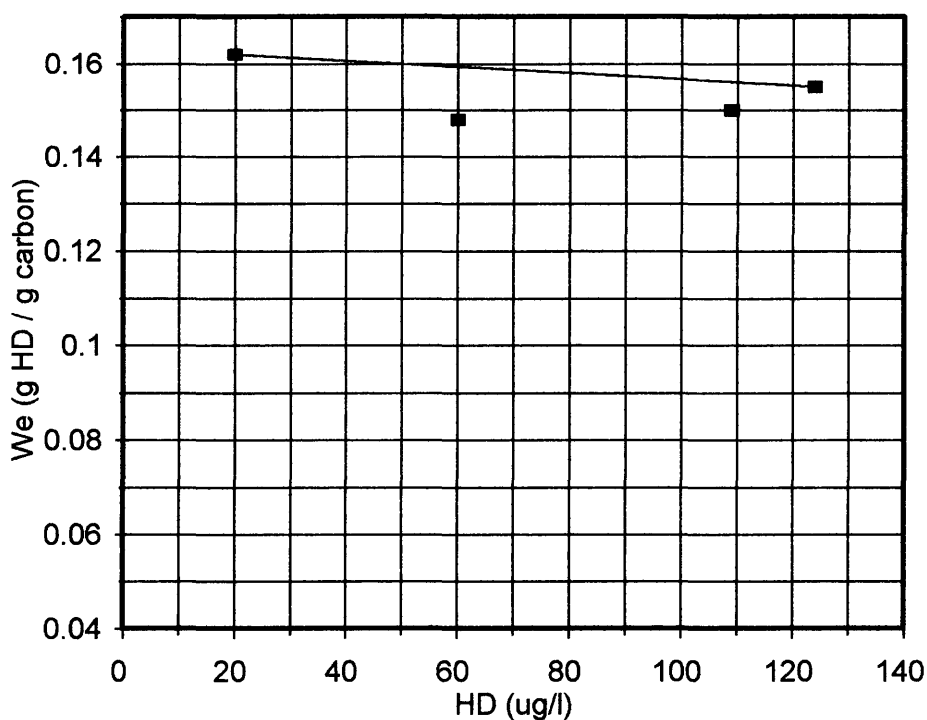
FIGURE 5.33:

Adsorption capacity of the C-spheres as a function of the challenge concentration.
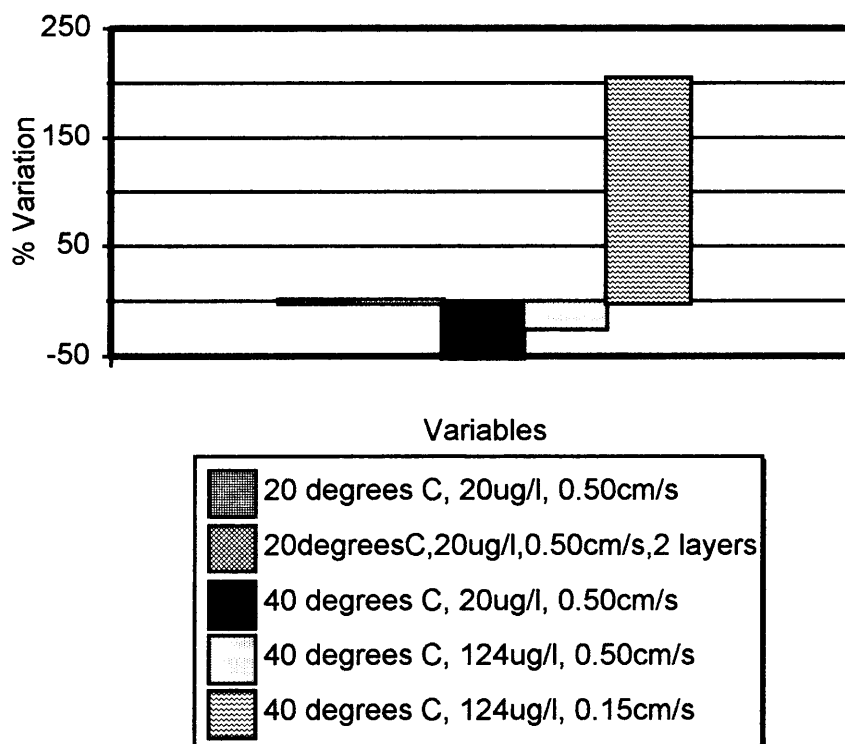
The HD adsorption capacities calculated experimentally (t_b) and theoretically with equations **(2.37)** and **(2.43)** are listed in Table 5.8. The capacities and micropore volumes correlate, namely a high capacity is found for the C-spheres with a large micropore volume. The HD capacities calculated with the experimentally measured t_b were in general lower than the values calculated with equations **(2.37)** and **(2.43)**. This could be due to a low carbon load in a single layer of the textile. The capacities obtained for these two equations were obtained from linear regression of the experimental results for at least one, two and three textile layers, respectively.

136

TABLE 5.8:

HD adsorption capacity for the C-spheres

$W_e(t_b)$ (g HD/g carbon)	W_e(Wheeler) (g HD/g carbon)	W_e(Ackley) (g HD/g carbon)
20 °C, 20 μg/l, 0.50 cm/s		
0.167 ± 0.001	0.204 ± 0.001	0.205 ± 0.011
40 °C, 20 μg/l, 0.50 cm/s		
0.154 ± 0.012	0.162 ± 0.001	0.162 ± 0.033
40 °C, 124 μg/l, 0.50 cm/s		
0.115 ± 0.004	0.155 ± 0.001	0.156 ± 0.005
40 °C, 124 μg/l, 0.15 cm/s		
0.139 ± 0.010	0.175 ± 0.001	0.181 ± 0.001

Results of the sensitivity analysis for the C-spheres are illustrated in Figure 5.34. An increase in the carbon mass at the reference experimental condition did not improve the capacity markedly which indicated that the carbon mass is sufficient to offer protection at this exposure concentration, or that the residence time in the single layer is long enough for complete adsorption, or that the rate of adsorption is high enough for effective adsorption. A 20 °C increase in the test temperature lead to a 20% decrease in the capacity. This could be explained by an increase in the volatility of the HD. The volatility of the HD will be higher at a higher temperature and it is expected that physisorption will be negatively influenced. A 24% decrease in capacity for the increased exposure temperature and concentration indicated that an increase in the volatility of the HD and an increase in the number of HD molecules available for adsorption, influenced the adsorption negatively. It could be argued that the diffusion into the micropores is not fast enough to adsorb the large number of HD molecules at the present residence time. An increase of 8% in the W_e at a slower linear velocity showed that a longer residence time aids the adsorption process.

137
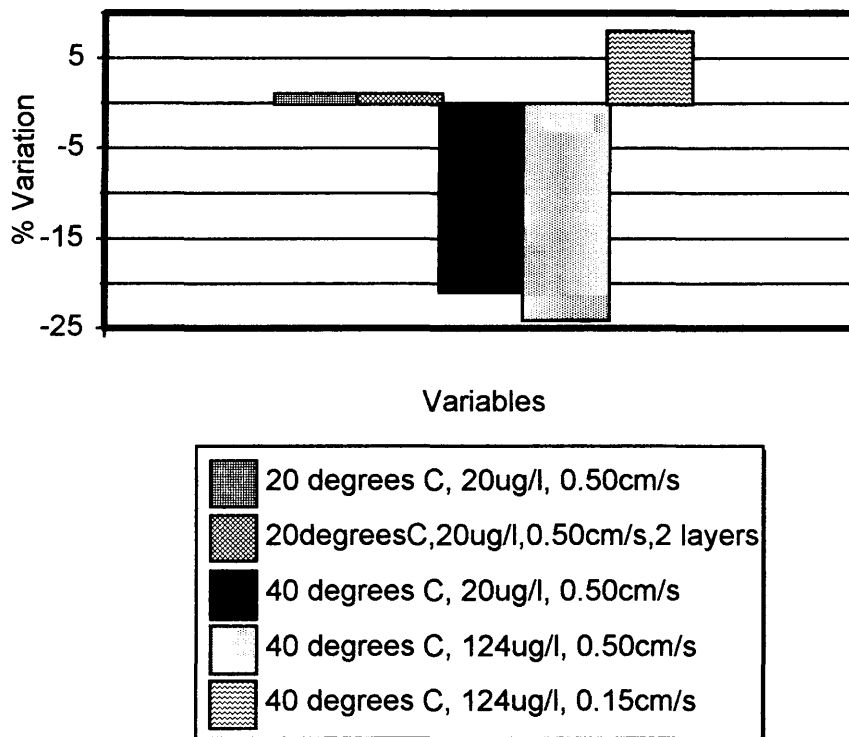
FIGURE 5.34:

% variation of W_e of the C-spheres calculated with the Wheeler equation.

The results indicated that exposure of the textiles to a higher temperature lead to a decrease in adsorption capacity (and protection) of 50%. Thus, increased temperature has a more negative effect on the protection offered against HD vapour by textiles containing activated carbon than an increase in the exposure concentration. From the results in Figures 5.30, 5.32 and 5.34 it could be concluded that the specification for protective textiles contemplated to be used for protective clothing in desert and subtropical climates, with higher temperature, should be different from the specifications for protective clothing to be used in milder climates. The protective textiles to be used in hot climates should at least be qualified at another set of test conditions, preferably at a higher temperature.

5.2.3 Influence of the challenge concentration on the adsorption rate constant

a. PUCP

The adsorption rate constant k_v calculated with equation *(2.37)* was expressed

138

as a function of HD concentration at constant temperature (40 °C) and air velocity (0.50 cm/s) and illustrated in Figure 5.35. The rate constants for the adsorption of HD on the carbon powder were very high. This could be due to the small diameter of the charcoal powder which, according to D.L. Griffiths, was 14μm [3]. According to Rehrmann and Jonas the rate constant is a function of the particle diameter [4]. Thus a relatively short distance had to be covered by the HD molecules before adsorption could take place in the micropores. From Figure 5.35 it follows that k_v decreased with an increase in the HD concentration. For a bed depth of 0.0127 cm and a linear velocity of 0.50 cm/s, the mean residence time is 0.0381 s. For an HD exposure concentration of 20 μg/l the rate constant of 46 094.6 min^{-1} (768 s^{-1}) was calculated. In accordance with the first-order reaction concept, an amount of 768 volumes of HD-nitrogen mixtures (containing 20x10^{-9} g HD/ cm^3) equal to the volume of the carbon bed (0.0191 cm^3) can be adsorbed by the carbon per second. Therefore the HD in each volume of HD-N$_2$ mixture was adsorbed in 0.0013 s (1/k_v). At higher HD concentrations (47 - 124 μg/l) the decrease in the k_v could be explained by the increase in the number of HD molecules per HD-N$_2$ volume as the HD concentration was increased, while the mass of carbon or active surface area available for adsorption remained constant. Thus the number of volumes which could be adsorbed in a certain residence time decreased, and consequently a decrease in the adsorption rate was measured.

139
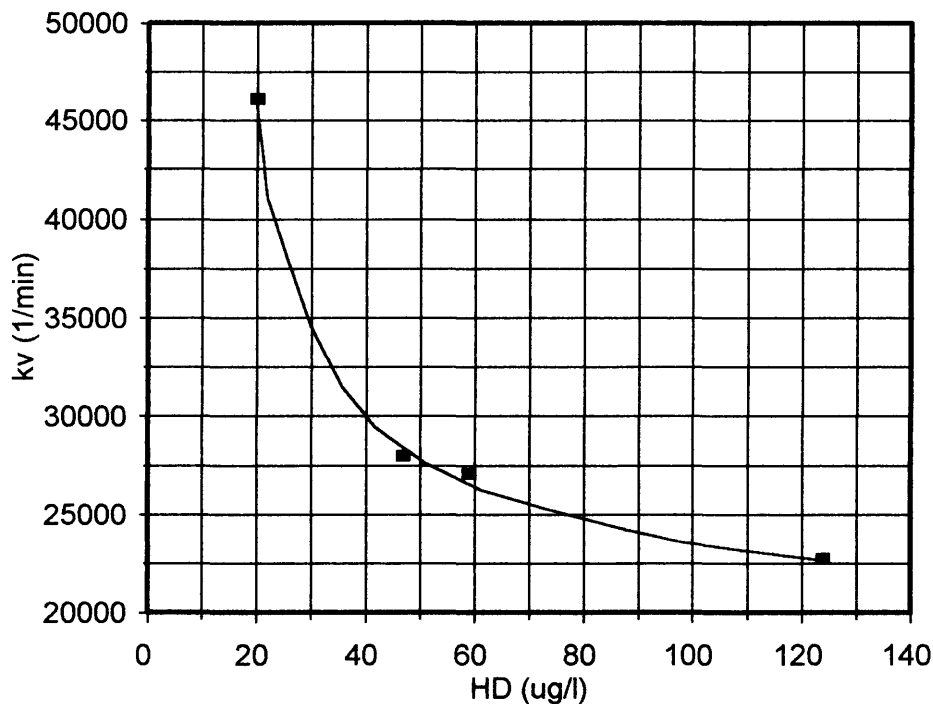
FIGURE 5.35:

The adsorption rate constant of the PUCP as a function of the challenge concentration.

b. CC

The adsorption rate constant k_v was calculated with equation *(2.37)* and the variation with HD concentration at constant temperature (40 °C) and air velocity (0.50 cm/s) is illustrated in Figure 5.36. From Figure 5.36 it follows that the rate of adsorption was the highest for the CC when compared with the other two textiles. This could be ascribed to the small diameter of the CC particles, namely 20 μm **[3]**. Thus the HD molecule had to travel a short distance in a CC particle before reaching the micropores where adsorption could take place. The decrease in the rate constant with an increase in the HD concentration can also be explained, as for the PUCP, in that the available adsorption area remains

140

constant as the HD concentration is increased.
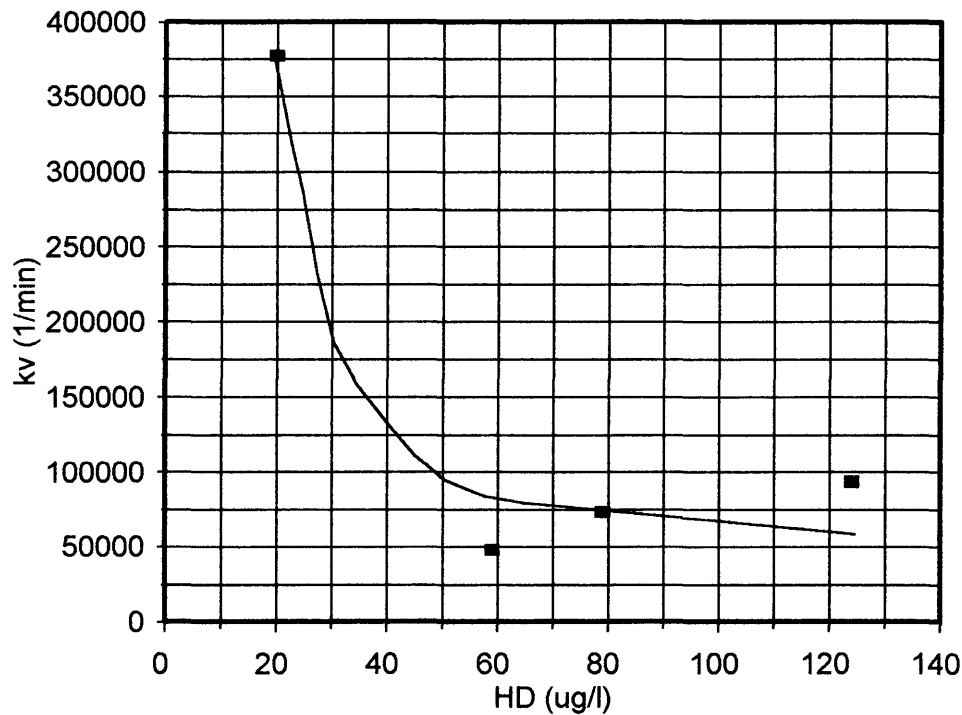
FIGURE 5.36:

Adsorption rate constant of the CC as a function of the challenge concentration.

c. C-spheres

The adsorption rate constant *(k $_v$)* calculated as function of HD concentration at constant temperature (40 °C) and air flow velocity (0.50 cm/s) for the C-spheres showed a decrease with an increase in the HD concentration (Figure 5.37). The rate constants were low compared with the k_v calculated for the other two textiles. This could be due to the large diameter of the carbon sphere, namely 0.5 mm [3,5]. Thus a relatively large distance had to be covered by the HD molecules compared with the CC and the PUCP, before the micropores were reached for adsorption to take place.

141
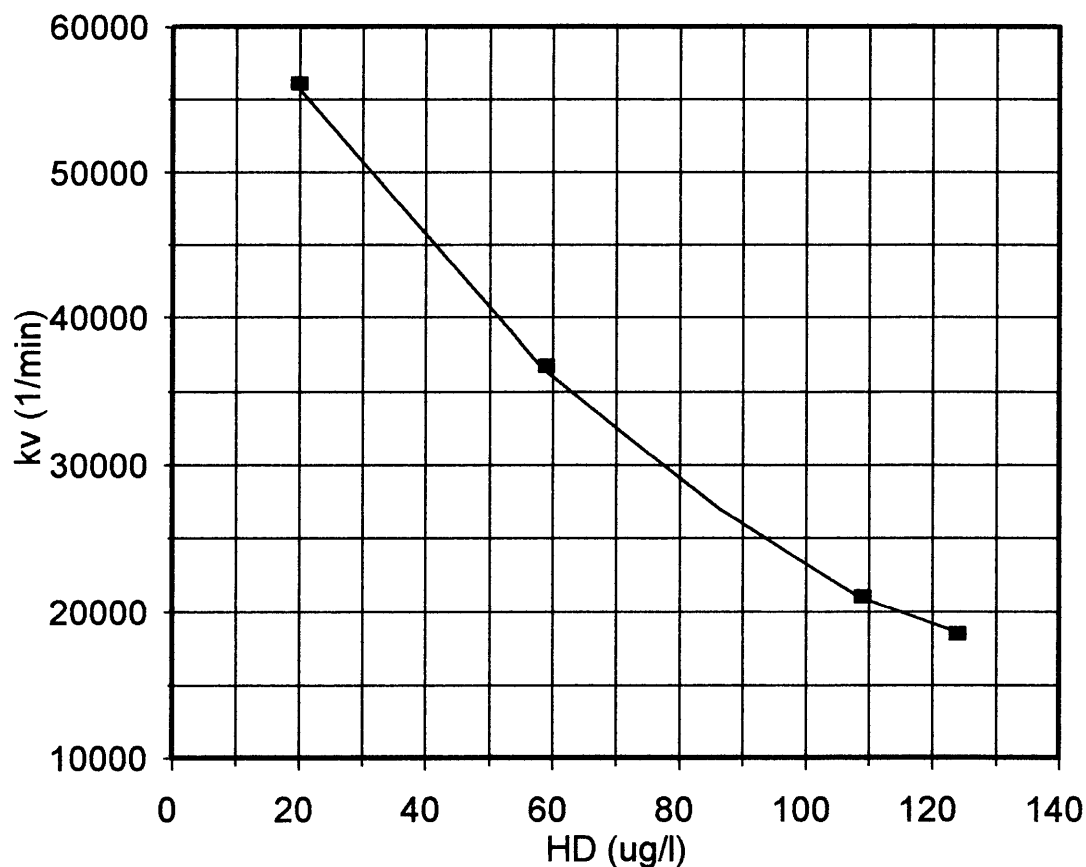
FIGURE 5.37:

Adsorption rate constant of the C-spheres as a function of the challenge concentration.

5.2.4 Influence of the environmental temperature on the adsorption capacity and the rate constant

a. PUCP

The breakthrough time as a function of the ambient temperature was also investigated for the PUCP textiles. The W_e and k_v were plotted as a function of the environment temperature at constant HD concentration and superficial velocity, 124 μg HD/l and 0.50 cm/s. It was found that the capacity of the carbon for HD vapour decreased with temperature (Figure 5.38). The high HD capacity at 20°C was due to physical adsorption of the HD molecules on the charcoal and the relatively low volatility at this temperature which aided physisorption.

142

At higher temperature, e.g. 50°C, the sorption capacity decreased due to increased volatility.

The rate constant stayed constant at 20 - 30 °C (Figure 5.39). At this temperature the volatility of the HD is sufficiently low to be adsorbed at a high rate. The adsorption rate decreased at temperatures above 30 °C. Due to the increase in the volatility a smaller number of HD molecules can be adsorbed per bed volume therefore, the rate decreased.
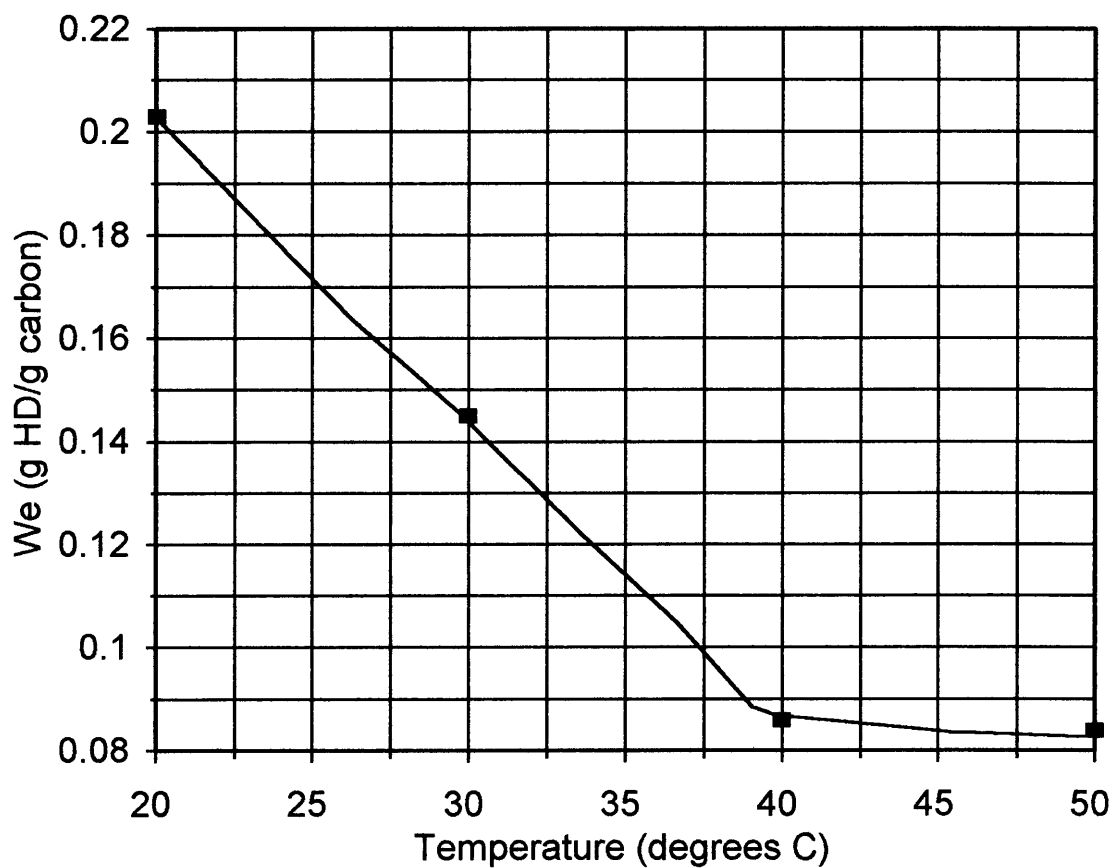
FIGURE 5.38:

Adsorption capacity of the PUCP as a function of temperature.

143
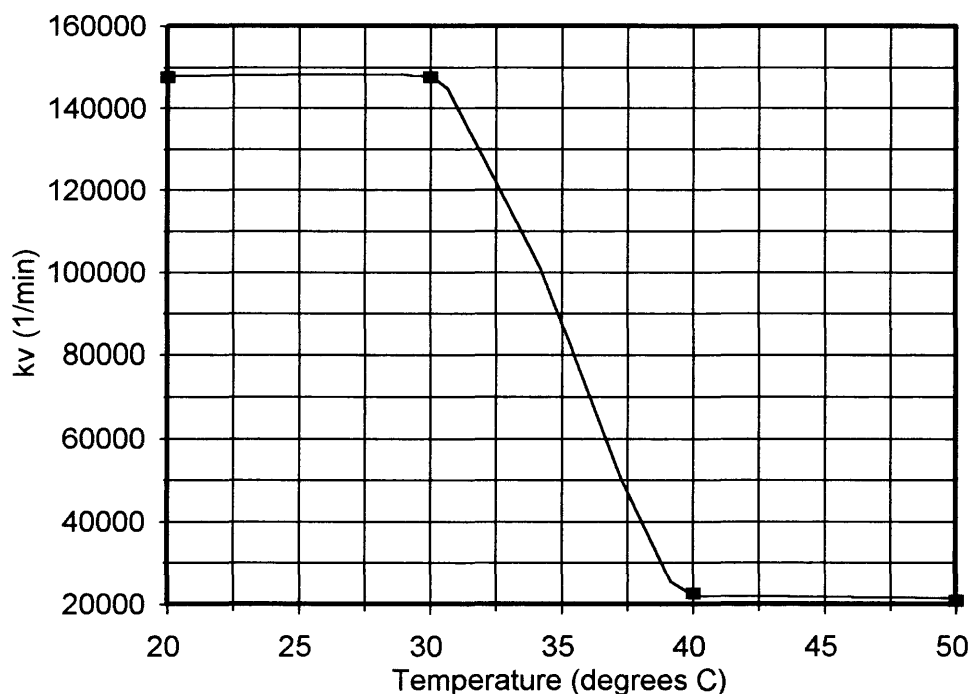
FIGURE 5.39:

Adsorption rate constant of the PUCP as a function of the temperature.

5.2.5 Residence time of the adsorbate in the carbon bed utilised for adsorption

From Table 5.2 with the adsorption rate constant k_v = 22 742.9 min^{-1} or 379.0 s^{-1} for the PUCP at conditions T = 40 °C, V_f = 0.50 cm/s, and C_o = 124 μg/l and at first-order reaction, it is perceived that 379 volumes, which is equal to the textile bed volume of 0.0191 cm^3 containing 2.368 ng HD, reacts with the carbon per second. Therefore, the HD in each bed volume of 0.0191 cm^3 of HD-air mixture were adsorbed by the textile in 0.0026 s ($1/k_v$) [5]. Even under these extreme conditions the adsorption occurred in only 10.4 % of the mean residence time, (τ = 0.0127 cm/ 0.50 cm/s) of the gaseous volume in the textile. Table 5.9 summarises the percentages of the mean residence times utilised for adsorption under the different experimental conditions for the different textiles.

TABLE 5.9:

The percentage of the residence time (τ) utilised for adsorption

TEST CONDITIONS	% x τ		
	PUCP	CC	C-spheres
50°C, 124 μg/l, 0.50 cm/s	11.2	-	-
40°C, 124 μg/l, 0.50 cm/s	10.4	8.9	13.1
40°C, 60 μg/l, 0.50 cm/s	-	17.3	6.6
40°C, 20 μg/l, 0.50 cm/s	5.1	2.2	4.3
30°C, 124 μg/l, 0.50 cm/s	1.6	-	-
20°C, 124 μg/l, 0.50 cm/s	1.6	-	-
20°C, 20 μg/l, 0.50 cm/s	9.5	0.28	10.5
40°C, 124 μg/l, 0.15 cm/s	1.4	10.6	11.3

The percentage residence time needed to lower the inlet concentration to 1% increases for the PUCP with increasing temperature, from 1.6% at 20 °C to 11.2% at 50 °C. The same increase in the τ was also measured for the CC (0.28% at 20 °C to 2.2% at 40 °C). However, a decrease was measured in the % residence time needed for the C-spheres from 10.5% at 20 °C to 4.3% at 40 °C. At low temperatures the volatility of the HD is low and a low percentage of the residence time is needed for complete adsorption of the HD vapour. At high temperatures (40 °C) the volatility of the HD is high and a larger percentage of the residence time is needed for complete adsorption. For the C-spheres the decrease in the % τ needed for complete adsorption at higher temperatures could be due to the increase in the diffusion into the micropores and therefore more effective adsorption.

The percentage residence time needed to lower the inlet concentration to 1% increases for the PUCP with increasing air velocity through the adsorbent bed, from 1.4% at 0.15 cm/s to 10.4% at 0.50 cm/s. The same tendency was measured for the C-spheres, however a decrease in the

145

percentage residence time was measured for an increase in the air velocity through the adsorbent bed for the CC, 10.6% at 0.15 cm/s to 8.9% at 0.50 cm/s.

The percentage residence time needed to lower the inlet concentration to 1% increases for the PUCP with increasing HD concentration from 5.1% at 20 μg/l to 10.4% at 124 μg/l. The same tendencies were measured for both the CC and C-spheres textiles. This could be due to a larger number of HD molecules to be adsorbed in each bed volume with an increase in the HD concentration.

Overall the percentage residence time needed to lower the inlet concentration to 1% was longer for the C-spheres textiles compared to the PUCP and CC textiles. Although the C-spheres have large micropore volumes and small average pore diameters, the spheres have relatively large diameters and are coated with the binder which blocks the macropores, preventing the HD vapour molecules from entering the micropore region. Owing to the different sizes of the spheres and the one layer of spheres only, the packing of the carbon "bed" is not optimal and it is suspected that channelling takes place. This would account for the longer time needed for adsorption and the low rate constants compared with the other two textiles.

146

REFERENCES

1. L.A. Jonas, Y.B. Tewari, E.B.Sansone, *"Prediction of Adsorption Rate Constants of Activated Carbon for Various Vapors"*, Carbon <u>17</u>,1979. p3,5,6.

2. S. Franke, *"Manual of Military Chemistry, Vol I, Chemistry of Chemical Warfare Agents",* Report no AD849 866, Berlin, 1967. p117.

3. D. L. Griffiths, "*An Extract from an Appreciation of the Major Permeable NBC Body Protection Systems in Service with World Forces in 1990*", Unpublished work, 1989.

4. Interim Technical Report, DAAK-84-C-0019, Winfield Manufacturing Co., 1985.

5. J.A. Rehrmann and L.A. Jonas, "*Dependence of Gas Adsorption Rates on Carbon Granule Size and Linear Flow Velocity*", Carbon, 16, 1978. p47.

147

CHAPTER 6

TRANSPORT MECHANISMS

6.0 INTRODUCTION

The rate of physical adsorption at a surface is generally high so that in a porous adsorbent the overall rate of adsorption is always controlled by mass or heat transfer resistance, rather than by the intrinsic sorption kinetics. This is not always immediately obvious from first inspection of the kinetic data as a diffusion-controlled process may exhibit many of the characteristic features commonly associated with a slow activated surface rate process. There are several distinct resistances to mass and heat transfer which may limit the sorption rate. Without detailed analysis, coupled with designed experiments, it is not always obvious which resistance is rate controlling. Thus, although direct measurement of the transient uptake curve for a sample of adsorbent in principle provides a simple method of studying adsorption kinetics, the interpretation of such data presents more difficulties than might be expected. The basic theory required for the analysis and interpretation of transient uptake curves for batch systems is presented as well as examples of the results found while performing the experiments.

6.1 EXPERIMENTAL

The dynamic breakthrough test method was used. The three different textiles were evaluated. Different exposure conditions discussed/shown in Chapter 5 were used. Equation *(2.56)* was applied to the breakthrough results. Diffusion coefficients were calculated for the two gradients obtained with each breakthrough measurement.

6.2 RESULTS AND DISCUSSION

The results obtained for various experimental runs were analysed according to equation *(2.56)* and are illustrated in Figures 6.1, 6.2 and 6.3.
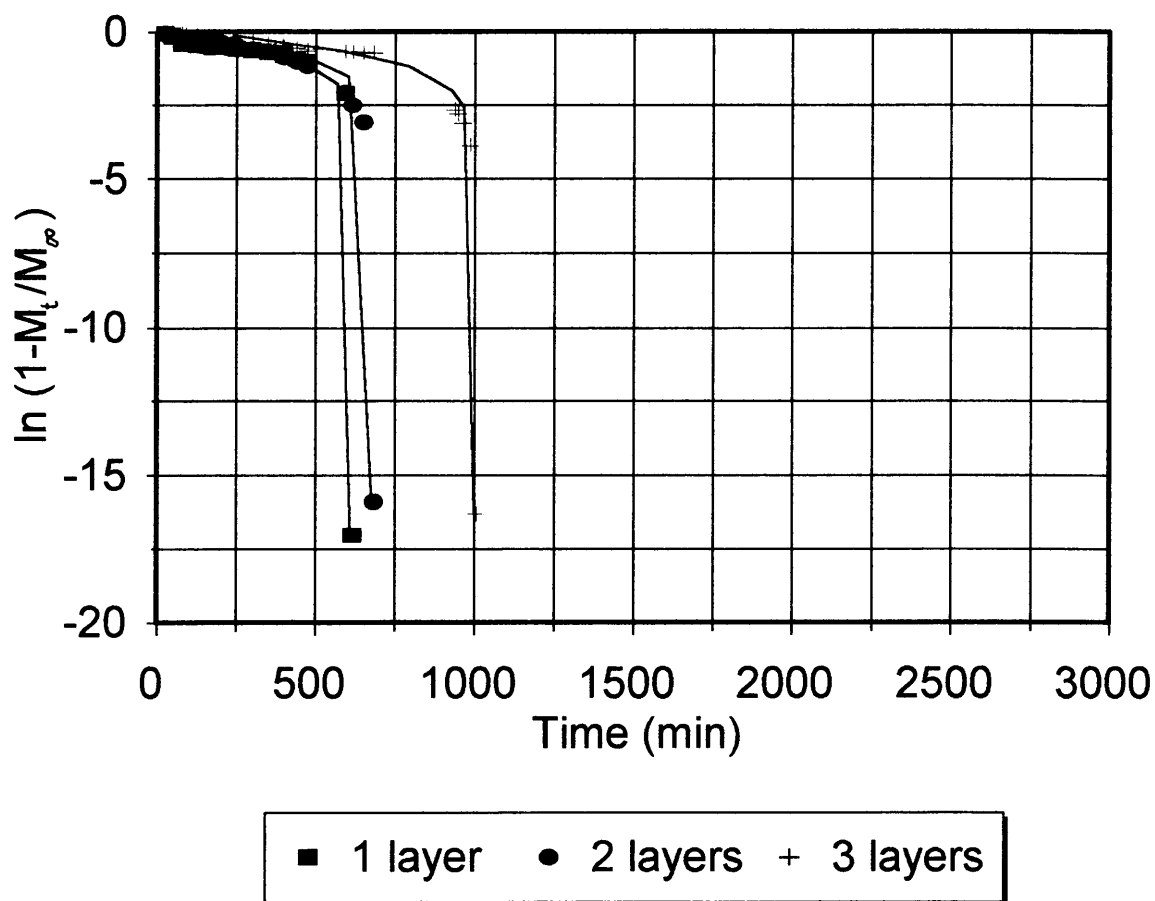
FIGURE 6.1:

Uptake curves for the PUCP textiles calculated with equation (2.56) at test conditions: 40 ° C, 124 μg HD/l, and an air velocity of 0.50 cm/s (1, 2 and 3 layers represent the number of the textile layers used).

149
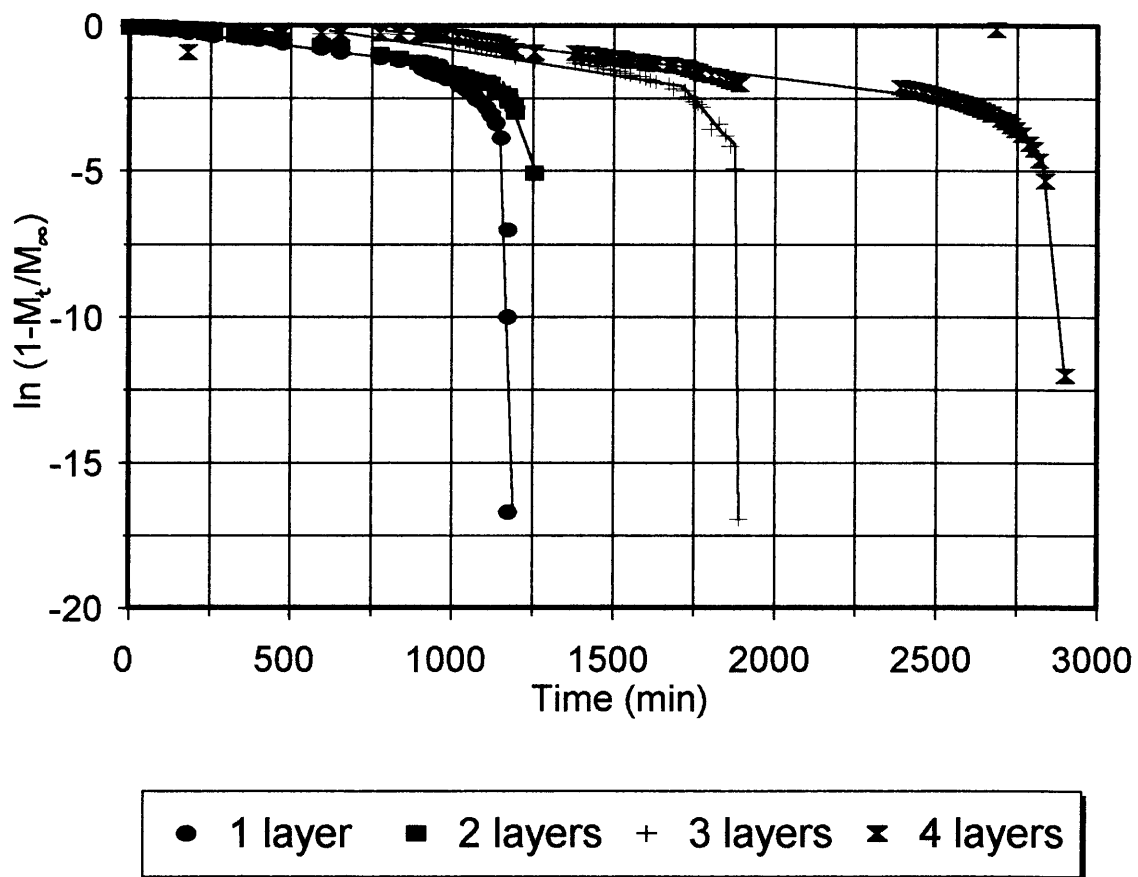
FIGURE 6.2:

Uptake curves for the C-spheres textiles calculated with equation (2.56) at test conditions: 40 ° C, 124 μg HD/l, and an air velocity of 0.50 cm/s (1, 2, 3 and 4 layers represent the number of the textile layers used).
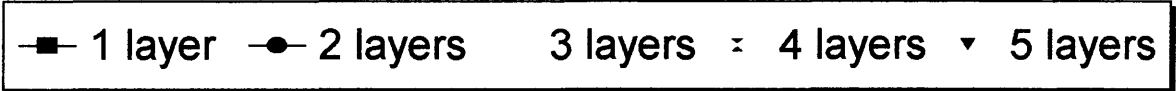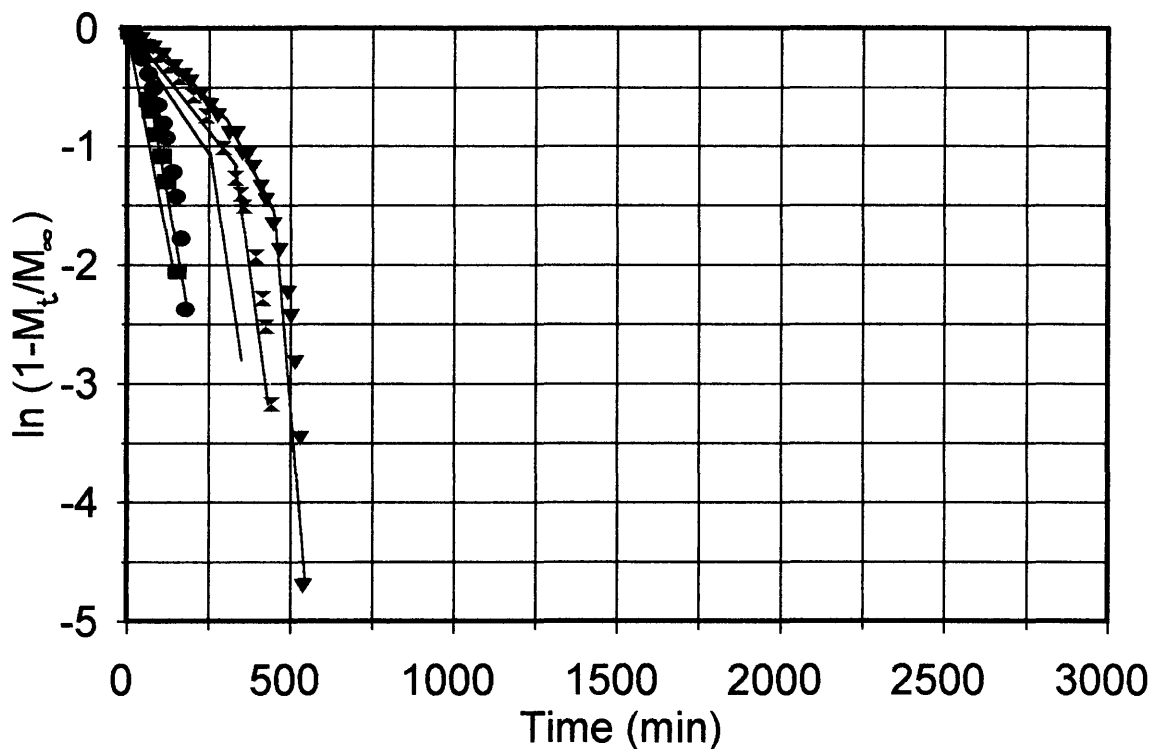
FIGURE 6.3:

Uptake curves for the CC textiles calculated with equation (2.56) at test conditions: 40 ° C, 124 μg HD/l, and an air velocity of 0.50 cm/s (1, 2, 3, 4 and 5 layers represent the number of the textile layers used).

A straight line with a distinct break in each set of results indicates that heat transfer might be controlling the adsorption process [1]. (In some instances the HD concentration (124 μg/ℓ) in the vapour phase was also sufficiently high, so that heat transfer could be the main controlling process of adsorption.) From the graphs the

151

diffusion coefficients D_1 and D_2 were calculated from the two gradients in each graph. The diffusion coefficients calculated for the first part of the uptake curve were very small $\approx 10^{-13}$ cm^2 / s, which indicated that the adsorption process was controlled by isothermal diffusion. However, the diffusion coefficient calculated from the second part of the uptake curve was larger $\approx 10^{-8}$ cm^2/s (especially for the C-spheres) which could be indicative of heat transfer and/or interparticle diffusion controlling the adsorption process.

Increased concentration of organic (HD) vapour on the surface and the slow dissipation of heat from the carbon surface could be responsible for the decrease in the heat transfer coefficient (h) [1].

The break in the results for the PUCP (Figure 6.1) and the C-spheres (Figure 6.2) appeared relatively late in the breakthrough curves. This is due to the higher loading of carbon impregnated on the textiles [2]. The carbon loading on the textiles was: 50 ± 10 g carbon/m^2 for the CC, 180 ± 20 g carbon/m^2 for the PUCP, and 200 ± 30 g carbon /m^2 for the C-spheres [3].

Increasing the number of textile layers in the bed increased the carbon mass and therefore the heat capacity and the heat transfer coefficient. This indicates that the adsorption process was controlled by isothermal diffusion [4]. The break in the curve occurred after the sorption process had progressed and the active surface area had been covered to a certain capacity, indicating the change in the adsorption process to heat transfer.

Figure 6.3, obtained for the CC, displayed the break earlier than in the case of the PUCP and the C-spheres. Owing to the small carbon mass the adsorption process was controlled by heat transfer almost from the start of the breakthrough determination [5].

Two distinct processes control the adsorption of HD on the carbon in the textiles, namely (a) isothermal diffusion and (b) heat transfer.

152

a. Isothermal diffusion

In the initial region, thermal effects are unimportant and the uptake is essentially independent of sample size [6]. In the later region the uptake curves diverge for different sample sizes.

Initially the adsorption process for all three textiles evaluated was controlled by isothermal diffusion. For the CC this was due to the pore distribution over a wide range of meso- and micropores (measured with the DFT method in Chapter 4). The adsorption in the larger pores is slow and takes place by isothermal diffusion.

However, the PUCP and the C-spheres have a high carbon loading (relative to the CC) which has a higher heat capacity and therefore the heat transfer coefficient is large, indicating isothermal diffusion [6]. Also, in the case of the C-spheres, due to the large particle diameter, i.e. 0.3 mm, adsorption of HD in large carbon particles is relatively slow and the uptake curves are essentially controlled by isothermal diffusion and are independent of the quantity of adsorbent used [7]. In smaller crystals heat effects become significant (PUCP and the CC) and in the later stages there is a significant deviation from the expected curve for isothermal diffusion.

b. Heat transfer

The adsorption of HD vapour in large pores is relatively slow and is controlled by isothermal diffusion. This should apply to the CC, which according to the average pore diameter analysis in Chapter 4 has a large average pore diameter of 24.4 Å. However, with the low capacity and small carbon loading (mass of the adsorbent bed) the CC has a small heat capacity and thus a small heat transfer coefficient, which causes the adsorption to be heat transfer controlled. A further factor that plays a role in the adsorption process being controlled by heat transfer, is the small diameter of the charcoal particle, i.e. 20 μm. Thus the adsorption rate constant is large.

153

6.3 DIFFUSION COEFFICIENTS AS A FUNCTION OF MASS OF CARBON IN THE BED

The transport model by de Boer and Gilliland, namely the migrations of adsorbed molecules along the internal surfaces of the microporous materials, was adopted for this study **[8,9]**.

De Boer describes surface migration as a process in which molecules hop between adjacent adsorption sites. *"A model of hopping molecules offers a reasonable description of surface transport in systems which display adsorption energies exceeding the thermal energy of translation. At low coverage, transport proceeds by the jumping of molecules between the adjacent surface sites. At high coverage neighbouring molecules interact and the process bears some similarity to liquid diffusion. However, a jumping mechanism still occurs but with a jump distance that is about the same as in the low coverage case. The variation in surface diffusivity with coverage is probably due to progressive filling of sites of decreasing energy.*

The heat of adsorption for gas-solid systems decrease with an increase in C_s, because of the progressive filling of sites of decreasing energy. Molecules which are more weakly bound to the surface would encounter smaller energy barriers and consequently would be more mobile. Surface heterogeneity may therefore result in an increase of surface diffusion D_s with C_s.

Surface transport measurements were presented in terms of a two-dimensional form of Fick's law:

$$N_s = -bD_s\frac{dC_s}{dx} \qquad (6.1)$$

where N_s - *is the flux in the x-direction across a line of width **b**, and*

154

dC_s/dx -   is the surface concentration gradient.

The jump distance and frequency may vary with C_s to give:

$$N_s = -\frac{1}{4}b\lambda_s^2 v(C_s)\frac{dC_s}{dx} \qquad (6.2)$$

The jump frequency of a single molecule can be given as:

$$v = v_0 e^{-E/RT} \qquad (6.3)$$

where v_0 -   is the frequency of vibration of the adsorbed molecule normal to the surface, and

     E -   is the size of the energy barrier which separates adjacent surface sites.

As the surface is filled up and lower energy sites are occupied, the energy barrier for migration can be expected to decrease. A useful measure of the binding energy is the differential heat of adsorption q, and can be approximated that *E* varies linearly with q:

$$E = aq \qquad (6.4)$$

Combining equations *(6.1)*, *(6.2)*, *(6.3)* and *(6.4)* give:

$$D_s = 1/4 v_0 \lambda_s^2 e^{-aq/RT} = D_0 e^{-aq/RT} \qquad (6.5)$$

Equation *(6.5)* describes surface transport as the jumping of adsorbed molecules between adjacent adsorption sites of different energy. Equation *(6.5)* is a quantitative statement that the more strongly adsorbed molecules are less

155

mobile".

From the foregoing it could be concluded that an increase in surface concentration would mean multi-layer adsorption at sites with a lower adsorption energy (E), thus a more mobile molecule with a higher diffusion coefficient. The same argument could be applied to an increase in temperature. Increase in temperature increases the jumping frequency and causes an increase in the diffusivity of the adsorbed molecule.

a. CC

The diffusion coefficients are summarised in Table 6.1. The diffusion coefficient D_1 for the CC decreased with an increase in mass. This could be explained by an increase in the surface area onto which the HD molecules could be strongly adsorbed as a monolayer. The low value for D_1 cannot be explained with the above theory. The increase in D_2 with an increase in mass shows that after a time a monolayer has already been formed and HD molecules are adsorbed as secondary (and higher) layers. The adsorption energy is therefore decreasing and consequently an increase in the diffusion coefficient is measured. The low value for D_2 for three textile layers could not be explained with the above theory.

b. PUCP

The diffusion coefficient D_1 increased with an increase in mass, which is contrary to the model of surface migration. The percentage increase in D_1 was small compared to the percentage increase in mass. This could not be explained by the present model, but could be due to pore filling. The diffusion coefficients are summarised in Table 6.1.

TABLE 6.1:

Diffusion coefficients as a function of mass

MASS (g)	D_1 (cm²/min x 10⁻¹¹)	D_2 (cm²/min x 10⁻¹¹)
CC		
0.0075	56.94	179.1
0.0150	66.97	331.4
0.0225	57.00	325.9
0.0300	27.26	390.0
0.0375	21.58	556.1
PUCP		
0.027	8.09	3 877
0.054	12.81	2 150
0.081	16.14	1 465
C-SPHERES		
0.03	25 330	2 162 000
0.06	5 699	107 800
0.09	3 673	1 065 000
0.12	2 216	133 200

D_2 decreased with an increase in mass. This could be due to a large micropore volume in which monolayer coverage was not completed, therefore causing a decrease in D_2.

c. C-spheres

The decrease in the diffusion coefficient D_1 with an increase in mass could be explained in the same way as for the CC, namely that due to an increase in the adsorption energy the molecules are strongly adsorbed and consequently D_1 decreases.

D_2 also decreased with an increase in mass. This could be due to a large

157

micropore volume in which monolayer coverage was not completed, therefore causing a decrease in D_2. The diffusion coefficients are summarised in Table 6.1. The high value for D_2 for three textile layers cannot be explained with the above theory.

6.4 DIFFUSION COEFFICIENTS AS A FUNCTION OF HD CONCENTRATION

a. CC

The diffusion coefficients are summarised in Table 6.2. The D_1 and D_2 showed an increasing tendency with an increase in the HD concentration. This could be explained by increased surface coverage and possibly the formation of multi-layers where adsorption energy is lower, making surface migration and diffusion faster. The low values for the fourth layer cannot be explained by the above theory.

TABLE 6.2:

Diffusion concentration as a function of HD concentration

HD CONCENTRATION (μg/ℓ)	D_1 (cm²/min x 10⁻¹¹)	D_2 (cm²/min x 10⁻¹¹)
CC		
20	42.25	114.5
60	54.51	218.8
94	160.40	513.5
124	56.94	179.1
PUCP		
20	0.41	42.29
49	6.95	1 509.00
77	5.96	2 292.90
124	8.09	3 877.00
C-SPHERES		
20	1 899	400 100
109	18 240	827 200
124	25 330	2 162 000

158

b. PUCP

The D_1 shows a weak function of HD concentration with a slight increase in the diffusion coefficient. This could be explained by the monolayer which was not fully reached and the adsorption energy is still high with lower surface migration and thus a smaller D_1.

D_2 shows a stronger increase at high HD concentration (77 μg/l and 124 μg/l), which indicates that monolayer coverage has been completed and that the adsorption sites and multi-layer adsorption energy are less strong and diffusion is thus also faster. The diffusion coefficients are summarised in Table 6.2.

c. C-spheres

The D_1 and D_2 show a large increase with an increase in the HD concentration, which indicates a high surface migration and low adsorption energy. This is contrary to the theory that the smaller the micropores, the higher the adsorption energy will be [10]. It could also be argued that the adsorption sites have low adsorption energy, due to deactivation of the -O and -OH groups on the surface to prevent water adsorption and thus perspiration poisoning of the carbon [11]. The diffusion coefficients are summarised in Table 6.2.

6.5 DIFFUSION COEFFICIENTS AS A FUNCTION OF TEMPERATURE

a. PUCP

The D_1 and D_2 increased with an increase in temperature due to an increased jump frequency [12]. The diffusion coefficients are summarised in Table 6.3. The low value for D_1 at 40 °C cannot be explained with the above theory.

159

TABLE 6.3:

Diffusion coefficient for PUCP as a function of temperature

TEMPERATURE (°C)	D_1 (cm²/min x 10^{-11})	D_2 (cm²/min x 10^{-11})
20	11.47	149.58
30	20.65	1 471.00
40	8.09	3 877.00
50	27.01	2 208.70

160

CONCLUSIONS

A method was developed which could be used to vary the test conditions (temperature, air velocity through the carbon bed, exposure concentration and adsorbent mass). The dynamic breakthrough method was used to differentiate between textiles containing activated carbon other than breakthrough time.

Adsorption isotherms, active surface area, pore volume and pore distribution of three different textile systems namely, charcoal cloth (CC), polyurethane foam rubber impregnated with charcoal powder (PUCP) and carbon spheres (C-spheres) were measured. The adsorption capacity (W_e) and rate constant (k_v) for HD adsorption on the textiles were measured and the results were interpreted in terms of the micropore volume and pore distribution. The influence of the exposure concentration on the W_e and k_v were investigated for the three textiles. The influence of temperature on the W_e and k_v of the PUCP were investigated. The diffusion coefficients for HD in the carbon of the three textiles at different exposure conditions were investigated and interpreted. The more relevant results are summarised in Table 6.4.

The isotherm displayed by the CC represented a Type II isotherm closer than a Type I, indicating micro- and mesoporosity. The PUCP and the C-spheres both displayed Type I isotherms indicating a microporous structure. The active surface area of the C-spheres was the highest, followed by the PUCP and the CC respectively. The micropore volumes measured were in agreement with the active surface areas measured. The C-spheres displayed the smallest average pore diameter. Pore size distributions measured with the DFT confirmed the results obtained for the isotherms namely, a narrow pore distribution was displayed by the PUCP and C-spheres with a farely wide distribution displayed by the CC, containing a large volume of mesopores.

161

TABLE 6.4:

Summary of results

PARAMETERS	CC	PUCP	C-SPHERES
thickness (cm)	0.0036	0.0127	0.0124
particle diameter (μm)	20	14	500
mass of carbon (g/m^2)	50	180	200
active surface area (m^2/g)	146	334	389
t-plot micropore volume (cm^3/g)	0.0577	0.1444	0.1716
mesopore volume (cm^3/g)	0.0293	0.0155	0.0094
aver. pore diameter (Å)	24.41	20.06	19.11
W_e at 124 μg/l, 40°C, 0.50 cm/s (g HD/g C)	0.087	0.086	0.155
k_v at 124 μg/l, 40°C, 0.50 cm/s (min^{-1})	93 531.9	22 742.9	18 527.1
W_c at 124 μg/l, 40°C, 0.50 cm/s (g C)	0.0032	0.0129	0.0179
% •т at 124 μg/l, 40°C, 0.50 cm/s (g C)	8.9	10.4	13.1
D_1 at 124 μg/l, 40°C, 0.50 cm/s (cm^2/min)	56.94	8.09	25 330
D_2 at 124 μg/l, 40°C, 0.50 cm/s (cm^2/min)	179.1	3 877	2 162 000

Three equations; Wheeler; Yoon and Nelson; and Ackley were used to calculate the W_e and k_v for HD vapour adsorption on the three textiles. The calculated W_e and k_v were used to calculate breakthrough times (t_b's) with the three equations. The t_b was considered as the time at which the outlet concentration (C_x) was equal to 1% of the inlet concentration (C_o). Comparison of the calculated t_b's with the experimentally measured t_b's showed that the deviation from the latter was the smallest for the t_b's

162

calculated with the Wheeler equation followed by the Ackley equation. The t_b's calculated with the Yoon and Nelson equation showed the largest deviation from the experimental values.

The W_e for HD vapour of the C-spheres was the largest, which confirmed the micropore volume measured for the textile. The W_e for HD vapour of the PUCP was the second largest confirming the micropore volume results. The W_e for HD vapour of the CC was the smallest confirming the micropore volume results. The k_v of the CC was the largest due to the small particle diameter. The critical mass (W_c) was the smallest and the critical residence time (τ_c) was the shortest for the CC. These results indicated that the ideal textile should have an open pore structure, with meso- and micropores and the carbon particles should have a small diameter (smaller than 20 μm).

The W_e of the PUCP stayed constant over the concentration range evaluated, due to the large micropore volume. The W_e of the PUCP did not increase with HD concentration due to the decreasing k_v and a constant residence time (τ) of the HD molecules in the adsorbent bed. These results were confirmed by the increase in the W_e at a slower air velocity through the bed. For CC the W_e increased with an increase in the HD concentration due to the high k_v. The τ was sufficient to adsorb the HD molecules over the concentration range investigated. The W_e of the C-spheres stayed constant over the HD concentration range tested. Although the micropore volume and the W_e are large, the k_v is not high enough to adsorb more HD molecules at the τ, due to a large particle diameter. These results indicated that the ideal textile should contain carbon with a large micropore volume to ensure a large capacity.

Sensitivity analyses on the W_e indicated that the increase in exposure temperature had a more negative effect on the W_e than an increase in the exposure concentration. This indicated that textiles to be used for the manufacturing of protective clothing in hot climates should be qualified at higher exposure temperatures.

The k_v of the PUCP decreased as a function of HD concentration due to the τ in the

163

textile bed being too short to adsorb an increasing number of HD molecules per bed volume. The same results were obtained for the CC and the C-spheres. The results indicated that the ideal protective textile should have a large k_v and thus a small carbon particle and open pore structure containing meso- and micropores.

The W_e and k_v of the PUCP showed a decrease at temperatures higher than 30 °C. The results showed that the protection offered by a textile against HD vapour decreases seriously at ambient temperatures higher than 30 °C.

A study of the % T of the HD molecule in the carbon bed used for adsorption showed that less than 20 % of the T is used for adsorption. Overall the %T used for adsorption increased with increased temperature, air velocity through the adsorbent bed and exposure concentration.

Drawing a graph of the breakthrough results for the PUCP, CC and C-spheres processed with Fick's diffusion equation gave straight lines with a distinct break indicating that heat transfer might be controlling the adsorption process. In the initial region thermal effects did not play an important role and adsorption was controlled by isothermal diffusion. Deviation from the isothermal process occurred first for the CC due to the small carbon mass and thus low heat capacity of the sorbent bed. The PUCP and C-spheres have a high carbon loading which has a high heat capacity and thus a high heat transfer coefficient. The thermal heat effects only played a role later in the adsorption process for these two textiles causing deviation from the isothermal diffusion.

Expressing the diffusion coefficient as function of mass indicated that the D_1 and D_2 increased as a function of the sorbent mass. This could not be explained by the de Boer and Gilliland theory of an increase in the active sites and therefore more high energy sites with stronger binding energy.

Expressing the diffusion coefficient as function of HD concentration indicated that the

164

D_1 and D_2 increased as a function of the concentration for all three the textiles. A high HD concentration could fill the high energy sites quickly followed by filling of lower energy sites which would result in low binding energy and high jump frequency and cause the D_1 and D_2 to increase.

Expressing the diffusion coefficient as function of temperature for the PUCP indicated that the D_1 and D_2 increased as a function of the temperature due to the increase in the jump frequency.

The selection criteria for chemical protective textiles can be summarized as:
-high chemical protection and therefore high capacity,
-thin and lightweight and therefore the chemical reaction/adsorption should be fast and,
-the layer should have a high physical strength for resistance against friction and abrasion.

The ideal textile could be identified as a textile impregnated with a high active surface area carbon (400 - 500 m²/g) to ensure a high adsorption capacity, a pore distribution which includes mesopores (20 - 24 Å) and a carbon particle with a diameter smaller than 30 μm to ensure a high sorption rate constant.

165

REFERENCES

1.   D.M. Ruthven, *"Principles of Adsorption and Adsorption Processes"*, John Wiley & Sons, NY, 1984. p192.

2.   J. Medema, *"Evaluation of the NBC Overgarments Manufactured by Seyntex Belgium C-Contract"*, Report no. PML 1980-33, Rijswijk, 1980.

3.   D. Griffiths, Unpublished work.

4.   D.M. Ruthven, *"Principles of Adsorption and Adsorption Processes"*, John Wiley & Sons, NY, 1984. p176.

5.   Ibid. p191.

6.   Ibid. p192.

7.   Ibid. p190.

8.   J. H. De Boer, *"The Dynamic Character of Adsorption"*, Clarenden Press, Oxford, UK, 1968. p34.

9.   E. R. Gilliland, R. F. Baddour, G. P. Perkinson and K. J. Sladek, *"Diffusion on Surfaces. I. Effect of Concentration on the Diffusivity of Physically Adsorbed Gases"*, Ind. Eng. Chem., Fundam., 13, $\underline{2}$, 1974. p95.

10.   M.M. Dubinin, *"Adsorption of Gases and Vapors in Micropores"*, Oxford Press, UK. 1967.

11.   E.E. Alexadroff, *"Saratoga: Carbon Pellet Technology in Chemical Warfare Protective Fabrics"*, Proc. 2nd Int. Symp. Protection Against Chemical Warfare Agents, Sweden, 1986. p67.

12.   K.J. Sladek, E.R. Gilliland and R.F. Baddour, *"Diffusion on Surfaces. II. Correlation of Diffusivity of Physically and Chemically Adsorbed Species"*, Ind. Eng. Chem., Fundam.. 13, $\underline{2}$, 1974. p100.

APPENDIX A

List of publications

1. C.C. Eloff, *"The Objective Comparison of the Merits of Textile Tests: HD Vapor Test Methods"*, The ASA Newsletter, 92-3, June 1992. p4.

2. C.C. Eloff, M. Papenfus and J.F. van Staden, *"Challenge Methods Affect the Protection Time of Chemical Protective Textiles Against Mustard (HD) Vapour"*, Proc. 5th Int. Symp. Prot. Against Chem. and Biol. Warfare Agents, Stockholm, Sweden, June 1995. p212.

3. C.C. Eloff, M. Papenfus and J.F. van Staden, *"Relative Humidity Affects Protection Times of Charcoal Containing Textiles Against Methyl Salicylate (MS) Vapour"*, European Carbon Conf., Newcastle, UK, July 1996. p56.

4. C.C. Eloff, M. Papenfus and J.F. van Staden, *"Evaluation of Physical Parameters for Protective Clothing in Hazardous Environments: Important Criteria for Hot Climates"*, SA J. Chem., in print.